Universidade do Minho
Escola de Engenharia

Ana Inês Campos Santos

Electrochemical Characterization of PDMAAp/PEDOT coated electrodes for DC Stimulation

November 2019

Universidade do Minho
Escola de Engenharia

Ana Inês Campos Santos

Electrochemical Charaterization of PDMAAp/PEDOT coated electrodes for DC Stimulation

Master Dissertation

Master's Degree In Biomedical Engineering

Dissertation supervised by

Prof. Dr. Stieglitz, Laboratory for Biomedical Microtechnology

Albert-Ludwigs Universität of Freiburg

November 2019

Acknowledgment

First of all, I would like to thank Prof. Dr. Thomas Stieglitz, head of the Laboratory for Biomedical Microtechnology (BMT), and Dr. Maria Asplund, group leader of the Electro-Active Coatings Group of the Laboratory BMT, for giving me the opportunity to work in this project and for the fantastic learning experience.

A special thanks to my supervisor, José Leal, for all the help and excellent ideas, patience, and positivity during the past year. Thank you very much for being always present.

I would like to also thank Nicole Jedrusik for helping and explaining so much about the cytotoxicity tests. Thank you to my colleagues in the SPEEDER group, Christian Böhler, Sebastian Shaner, Zaid Aqware, Marion Dürr, and Ute Riede for always being there to help, answering to my questions, and for the amazing environment in the FRIAS Lab.

Furthermore, I would like to thank the BMT colleagues and the RSC personnel for the excellent working environment and for helping and sharing their knowledge when I needed it.

I would also like to thank Maria Cruz and Maria João Sousa for giving the best advice since the beginning of this journey.

A special thanks to Mariana Rajado, Ioana Georgiana, and Ana Pasturel for always accompanying and listening to me throughout this year.

Ai miei amici italiani, Fede, Albi, Andrea e David, grazie mille per tutte le cene, i discorsi, le "serate cinematografiche" e per avermi rallegrato nei momenti più stressanti.

Um especial obrigada aos meus pais e à minha irmã por todo o apoio e motivação e, acima de tudo, por acreditarem e me ajudarem a alcançar novos desafios.

STATEMENT OF INTEGRITY

I hereby declare having conducted this academic work with integrity. I confirm that I have not used plagiarism or any form of undue use of information or falsification of results along the process leading to its elaboration.

I further declare that I have fully acknowledged the Code of Ethical Conduct of the University of Minho.

Abstract

Electrotaxis or Galvanotaxis is the directed migration of cells in an electric field and constitutes a fundamental phenomenon in many biological mechanisms, for instance, cell division, wound healing, and embryonal development. It is caused by spontaneous endogenous electrical fields (EFs) due to ionic gradients. Multiple studies and experimental research have proven that applying an external electrical field (direct current DC) can originate an electrotactic response on the cells, since it resembles an endogenous EF. Besides fundamental understanding in biology, this form of artificial electrotaxis appears to be a promising alternative for wound healing treatment. The cell's response and the mechanisms related to electrotaxis are still uncertain, and the properties of the electrode material hinder the advancements in cellular research and medical applications. A promising solution for this problem is the use of conductive polymer electrodes for DC stimulation.

In this work, electrodes of different materials, IrOx, PEDOT/PSS, and PDMAAp/PEDOT, were developed, fabricated, and tested. The materials of the electrodes had different thicknesses that were tested and compared with each other. These electrodes were electrochemically characterized and used for DC stimulation. Due to their supercapacitive behavior, the electrodes were able to go through several DC stimulation cycles with different currents applied, without observable damage.

A fluidic setup and an electronic readout system were designed and fabricated for pH measurements during different DC stimulations for all the electrodes materials. No changes in the pH value were observed in the medium surrounding the electrodes. Moreover, the electrodes materials were tested for cytotoxicity, and none could be observed.

This work concludes that PDMAAp/PEDOT coated electrodes show excellent electrochemical properties and DC stimulation capabilities similar to PEDOT/PSS.

Table of Contents

List of Figures

List of Tables

Nomenclature

Formula Symbols

Variable	Meaning	Unit
E	Electrical field	V/m
I	Electric current	A
σ	Conductivity	S/m
W	Width	m
h	Height	m
pH	Potential of hydrogen	1
C	Capacitance per surface area	F/cm^2
E	Energy density	J/cm^2
V	Potential operating window	V
C_d	Double-layer capacitance	F
E	Nernst potential	V
T	Temperature	K
C_{H+}	Hydrogen ion concentration	Mol/L
R	Electrical resistance	Ω
ρ	Resistivity	Ω/m
L	Length	m
A	Area	m^2

Constants

Constant	Meaning	Value
F	Faraday constant	96 485.33 As/mol
R	Ideal gas constant	8.3145 J/mol K

Abbreviations

Abbreviation	Meaning
EFs	Electrical Fields
Na^+	Sodium ion
K^+	Potassium ion
TEP	Trans Epidermal Potential
DC	Direct Current
EST	Electrical Stimulation therapy
Ag/AgCl	Silver/Silver-Chloride
Cl^-	Chloride ion
PDMS	Poly(dimethylsiloxane)
ES	Electrical Stimulation
H^+	Hydrogen ion
OPW	Potential operating window
ECP	Electrically conducting polymer
PEDOT	Poly(3,4-ethylenedioxythiophene)

CPs	Conductive polymers
CHs	Conductive hydrogels
HCl	Hydrochloric acid
LA	Lauric acid
PTSA	P-toluene sulphonic acid
PSS	Polystyrene sulfonate
PPy	Polypyrrole
PTh	Polythiophene
PANI	Polyaniline
PA	Polyacetylene
CPHs	Conductive polymer hydrogels
EMF	Electromotive force
PI	Polyimide
IrOx	Iridium Oxide
BMT	Laboratory for biomedical microengineering
Pt	Platinum
SIROF	Sputtered iridium oxide
PDMAAp	P(DMAA-co-MABP-co-SSNa)
TMAH	Tetramethylammonium hydroxide
DMSO	Dimethyl sulfoxide

RIE	Reactive Ion Etching
WTi	Tungsten-Titanium
OCP	Open-circuit potential
CV	Cyclic Voltammetry
EIS	Electrochemical Impedance Spectroscopy
RE	Reference Electrode
WE	Working Electrode
CE	Counter Electrode
PBS	Phosphate-buffered saline
CSC	Charge Storage Capacity
DMAA	Dimethylacrylamide
MABP	Methacryloyloxy benzophenone
NaPSS	Sodium 4-styrene sulfonate
3-EBP	4-(3-triethoxysilyl)propoxybenzophenone
PCB	Printed circuit board
IC	Integrated circuit
ADC	Analog to Digital Converter
PTFE	Polytetrafluoroethylene
PMMA	Plexiglas

1 Introduction

Electrotaxis or Galvanotaxis describes the directed cell migration in response to endogenous electrical fields (EFs). This phenomenon is present in many fundamental biological mechanisms, such as cell division, wound healing, and embryonal development [1]. Multiple studies and experimental research have demonstrated, that applying an external electrical field can generate an electrotactic response on cells by mimicking the spontaneous endogenous fields. The cell's response and the fundamental mechanisms related to sensing these electric fields are still uncertain, therefore electrotaxis research aims to study and understand these cellular reactions [1]–[3].

Electrotaxis experiments consist of applying a direct current (DC) with metal electrodes on a channel filled with cells and a conducting solution to generate an EF. This current is driven by faradaic redox reactions which lead to corrosion of the electrodes, to the release of cytotoxic materials and to changes in the pH of the medium. The use of agar salt bridges between the electrodes and the cell channel is necessary to overcome these problems since they are able to stop the toxic by-products from reaching the cells. This solution helps overcome this problem, for in vitro experiments, however, it also makes the electrotaxis setup bulky, difficult to reproduce and is not a suitable solution for future medical applications of DC stimulation [4], [5]. To address these challenges, new materials such as conductive polymers (CPs) and conductive hydrogels (CHs) emerge as an alternative to the standard metal electrodes. These electroactive coatings are capable of driving constant direct currents through ionic charge injection and have many other advantages such as biocompatibility, low electrical impedance, and easy fabrication and coating methods [6].

Poly(3,4-ethylene dioxythiophene) polystyrene sulfonate (PEDOT/PSS) is a conductive polymer that has been studied as a polymeric coating of electrodes and has demonstrated to be a suitable replacement of the metal electrodes due to its electrochemical stability and to its high charge injection without releasing toxic by-products. However, this polymer is very rigid, and after some cycles of DC stimulation, delamination can occur due to the stress provoked on the polymer coating [7], [8]. As an alternative to this polymer, a conductive polymer hydrogel (CPH), which consists of a conductive polymer within a hydrogel network will be tested. The conductive hydrogel P(DMAA-co-MABP-co-SSNa), PDMAAp, functionalized with PEDOT is a CPH capable of electrical stimulations and has excellent mechanical properties due to the hydrogel network [9], [10].

The conductive polymer hydrogel, PDMAAp/PEDOT, should be tested as a new coating of electrodes in order to replace the metal electrodes in electrotaxis experiments. The electrochemical stability of

the hydrogel-polymer electrodes should be tested, as well as their response to electrical stimulation and the effects these materials have on the medium and in cells.

The present work is subdivided into nine sections. The first section explains the fundamentals of the wound healing process as well as the cellular signaling and behavior during electrotaxis, followed by a brief overview of the state of the art of the most significant electrotaxis experiments. Conductive Polymers and their characteristics are introduced alongside the electrochemistry involved in electrical stimulation, as well as pH measurements. Chapter three presents the proposed ideas and approaches to achieve the goals set for this work. The following chapters describe thoroughly the used materials and methods to fabricate and prepare the electrodes for the electrochemical characterization, as well as the PDMS and pH channels, and pH sensors. The experimental setups for electrical and electrochemical characterization can be found in chapter five. Section six contains the results obtained during the characterization and testing of the electrodes, pH measurements, and cytotoxicity tests. The discussion of the results and the conclusion reached through them are present in chapter seven. A summary of the present work and an outlook of the following steps is written in sections eight and nine.

2 Fundamentals

2.1 Endogenous electrical fields in the body and their role in wound healing

The healing of a wound starts immediately after the tissue has been damaged or broken. Wound healing consists of various processes that involve different tissues, cells, and signaling mechanisms. Endogenous electrical fields (EFs) are an essential cue during wound healing since electrical signals have a considerable effect on how the cells behave [11], [12].

2.1.1 Endogenous electrical fields

Endogenous electrical fields are spontaneously generated due to ionic gradients across cellular membranes and play an essential role in several biological processes. Membrane potentials are present in cells, especially in areas where development processes that involve cell movement and cell division occur. The voltage gradients are used for transport functions and signaling. Endogenous Electric Fields have a functional role in cell growth and development, such as embryogenesis, tissue regeneration, and wound healing [13].

The epithelium is a membranous tissue characterized by small cells that cover the external and internal surfaces of the body and its organs. This tissue has Na^+/K^+ ATPase pumps that continuously maintain the flow of ions, originating an electric current and assuring an ionic gradient across the epithelial tissue. Consequently, a potential difference is generated, which create endogenous Electric Fields (EFs) [14]. This ion flow generates a transepidermal potential (TEP) ranging between 20 to 50 mV, and this transcutaneous voltage is known as “skin battery” [14]–[16].

When the epithelial barrier is damaged, the charge concentration at the wound site drops, which generates a negative electric pole and affects the ion flow. Positive charge flows towards the wound center, creating an electric current, and establishing a transversal EF (Figure 1). This change in the electric field triggers the migration of different cells directly involved in the wound healing process such as fibroblasts, keratinocytes, endothelial cells, macrophages, and platelets. Fibroblasts are the cells responsible for producing an extracellular matrix which functions as a scaffold for the endothelial cells in wound healing. The fibroblasts are crucial in injury responses since they contribute to both initiation and final phases. The keratinocytes in skin represent a constantly renewing cellular compartment and migrate towards the cathode (negative pole) under DC electric fields, which raises interest in a scientific and therapeutic point of view [17], [18].

The directed migration of cells as a response to an EF is denominated Electrotaxis or Galvanotaxis. One of the most critical processes in cells polarization and directional migration is the reorganization of the cytoskeleton of the fibroblasts and epithelial cells to improve the receptors on cell-surface and the adhesive molecules present at the front of the cell [19]. These receptors and molecules detect the EFs and follow them, directing the cells to migrate either towards or away from the wound [20]–[22].

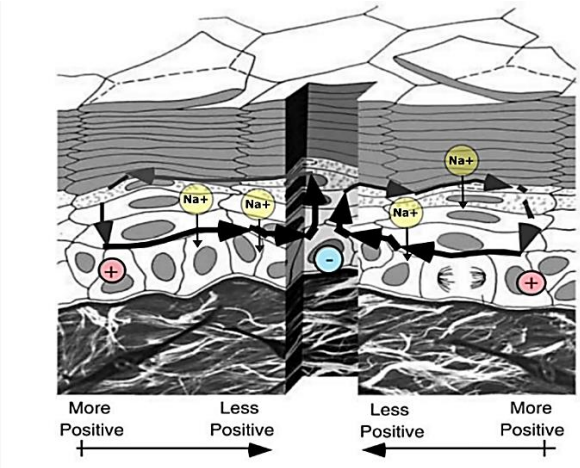

Figure 1: Endogenous electric field in a wound with ion transport and positive charge flowing towards the wound [23].

2.1.2 Wound healing

Wound healing is a complex process that requires the interaction amongst different types of cells, as well as their migration towards the injured site. The migration is directed by endogenous EFs, which generate spontaneously after the wound occurs. In some pathologies, the cells do not react normally, and the signaling is impaired, hindering the healing rate of the wounds. However, it has been proven that cells react directionally to externally applied EFs (created through electrical stimulation with direct current, DC), which could serve as a therapeutic solution for people with said conditions [14], [21].

The process of healing a wound consists of several phases, these being hemostasis, inflammation, re-epithelialization, and tissue remodeling. When the tissue is damaged, the hemostasis starts by preventing fluids, blood losses, and infections, which results in the formation of a clot, that consists of a fibrin net and a number of platelets aggregated together with embedded blood cells [20]. The exposed, injured tissue is susceptible to bacteria; therefore, inflammatory cells, which produce cytokines, growth factors, and degradative enzymes, are brought to the wound area so that bacteria

and dying cells can be eliminated in order to proceed with the healing process (Figure 2) [13], [24], [26].

In 2-10 days after the initial wound, the new tissue formation starts and is characterized by different cells migrating towards the wound site and cellular proliferation, as well as revascularization of the injured area. The re-epithelialization aims to recover the skin's barrier functions; however, the repaired tissue cannot reacquire all the properties that an uninjured tissue has. Approximately 21 days after the injury, the tissue starts remodeling and creating a scar; its strength is characterized by the quantity and quality of the deposited proteins [12], [21], [24].

In a healthy patient, the healing phases occur adequately, and the EFs are able to enhance the movement of cells towards the wound. However, when the patient suffers from diabetes, skin, or chronic diseases, there are many physiologic factors as well as a deficient endogenous EF. Amongst many of the physiological factors, some examples are the deficiency of growth factor production, misfunction of the macrophages, the quantity of granulation tissue, and accumulation of collagen [27]. In these cases, the healing process is affected, and the epithelium cannot be reorganized and reconstructed to be healthy and mature as it was previous to the wound [20], [28].

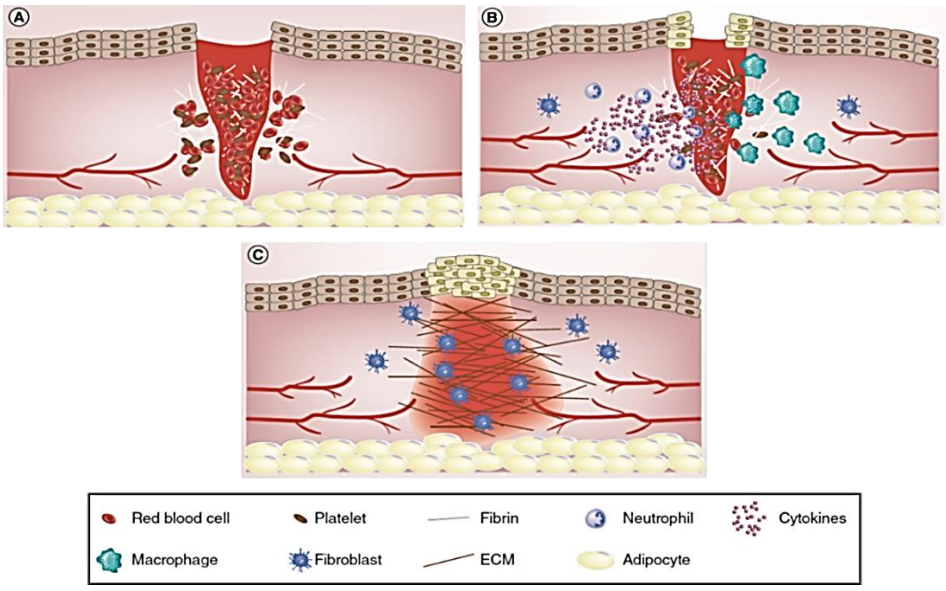

Figure 2: Wound healing pathophysiology. (A) Hemostasis. (B) Inflammation. (C) Tissue Remodeling and re-epithelization. Adapted from [29].

In order to ease the healing process, several wound intervention mechanisms have been developed in the last decades. Different invasive or non-invasive methods to treat chronic wounds have been

proposed, being the invasive ones skin substitute therapy and wound debridement (removal of dead or infected skin). Among non-invasive methods, oxygen therapy, negative pressure therapy, use of ultrasound, and electrostimulation therapy (EST) are well known [20]. The application of electrical currents, EST, has been applied by many researchers as a technique to induce and improve the treating of wounds, showing benefits on wound closure and faster healing *in vivo* models and clinical studies [30]–[34].

Electrostimulation therapy is a natural, painless, and cost-effective method that improves the healing process by simulating the natural current of the injury. It has been shown that the cells involved in the wound healing process change in migration, proliferation, and orientation. Not only that, but they also demonstrate antibacterial effects and an increase in proteins or DNA synthesis. However, there is still no therapy approved for skin wounds, due to discrepancy of different stimulations used in clinical studies [35], [36].

2.2 Electrotaxis

Electrotaxis or galvanotaxis consists of the movement of an organism or system of cells in an electric field. This field can be generated by applying a direct current (DC) (exogenous) or spontaneously within the biological system (endogenous) to induce the movement of cells either towards the cathode or the anode, depending on the polarity of the electric field and cell type [37].

2.2.1 Cellular Behavior

Experimental research is contributing to improving the knowledge of how cells react and how sensitive they are to physical or chemical stimuli that can originate a directional motion [2]. Multiple studies and experiments have investigated the mobility of cells influenced by external cues such as electrotaxis or galvanotaxis (electrostatic potential), haptotaxis (variation of surface-attached chemicals) and chemotaxis (chemical gradients in solution) [38], [39].

Research has demonstrated that chemical guidance loses its influence on cells migration when an external electrical stimulus is applied; some cells changed their initial migration according to the electrical stimulus, and when the polarity of the electric field was reversed, the direction of the cells migration changed [40]. Most cells exhibit electrotaxis alongside the electric field lines (towards the cathode), including human keratinocytes. However, there are some cells like the epidermal fibroblasts, which demonstrate anodal electrotaxis, making the understanding of this process more complex [41].

The observed cell effects to an applied electrical stimulus can be understood through how the applied field is distributed within the cell. Considering the cell as a sphere with a radius R placed between two electrodes, when an electrical field is applied, the cell response is similar to a RC circuit. The capacitor is charged with a charge flow through the resistor, and when the capacitor is fully charged, no more charge drives through the resistor and an induced transmembrane voltage (TMVi) is established. This TMVi achieves a value that is higher than the natural transmembrane voltage (TMVo), which is generated through the channels and ion pumps present in the membrane. When the electrical field is applied, the channels and pores in the membrane allow for the molecules in the surrounding medium to go into the cell, achieving a TMVi [42].

The increase of ions inside the cell causes cell contraction on one part of the cell, and cell protrusion on the other, generating the "push-pull" movement, which consists on adaptor proteins connected to cortical actin filaments that "push" the membrane of the cell towards the cathode or anode (Figure 3) [13].

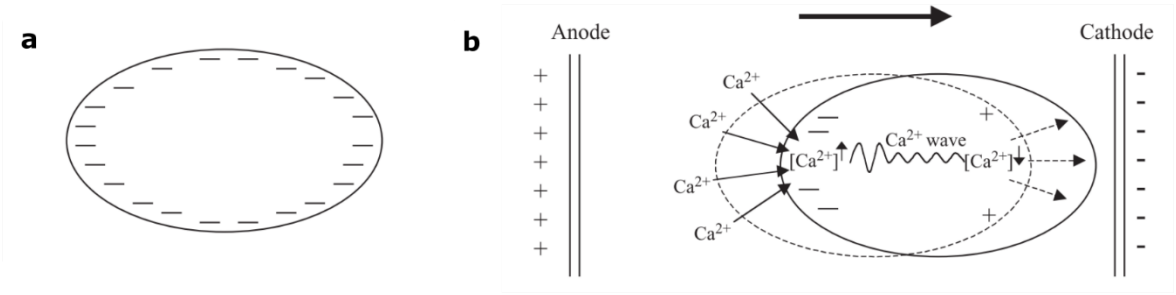

Figure 3: Response of cell to an applied electrical field. (**a**) The cell is in a resting state with negative membrane potential. (**b**) Cell exposed to an electrical field; the membrane near the anode attracts Ca^{2+}, contracting that side of the cell, and moving the cell towards the cathode. Adapted from [13].

Cells prosper in a controlled, balanced environment, which is why homeostasis is so vital for their proper function. Cell migration can be hindered or disturbed if the surroundings of the cells are not ideal. In wound healing, a pH change from 6.2 to 5.8 can stop the migration of keratinocytes, affecting the following phases of the wound healing process [43].

2.2.2 State of the art for Electrotaxis experiments

Studying electrotaxis allows a better understanding of cell migration during biological processes. For experiments to be accurate, a precise electric field needs to be applied to the cells, which requires the use of microfluidic devices with exact dimensions. Therefore, several devices for cell migration experiments have been developed to analyze this phenomenon [43], [44].

An electrotaxis experiment consists of applying EFs to cell culture and, as a result, observe cell migration. One of the most straightforward experimental setups consists of a cell culture chamber in contact with Ag/AgCl electrodes through agar salt bridges. When a voltage is applied, the electrochemical dissolution of the electrodes is initiated, providing an ionic current to the cell culture. However, the ion flow into the channel generates an electrode potential drift in the Ag/AgCl electrodes, and the medium might have changes in its conductivity as well as in the pH, that are prejudicial to the cells. Furthermore, silver ions, which are cytotoxic, are released during DC stimulation as part of faradaic reactions at the electrode surface. Therefore, agar salt bridges are used to prevent any dangerous reaction by-product from reaching the medium while sustaining the ionic flow of Na^+ and Cl^- [1], [4], [5].

Initially, the setups for electrotaxis experiments were simple, consisting of a culture dish with two glass slides placed side-to-side that create a channel for cell culture with the advantages of being easy to operate and allowing for the visualization of migratory cells (Figure 4) [44]. However, it is not possible to obtain a homogeneous, well-defined EF in such a device and the necessity of agar bridges leads to a large system, which requires long preparation time before experimenting [5].

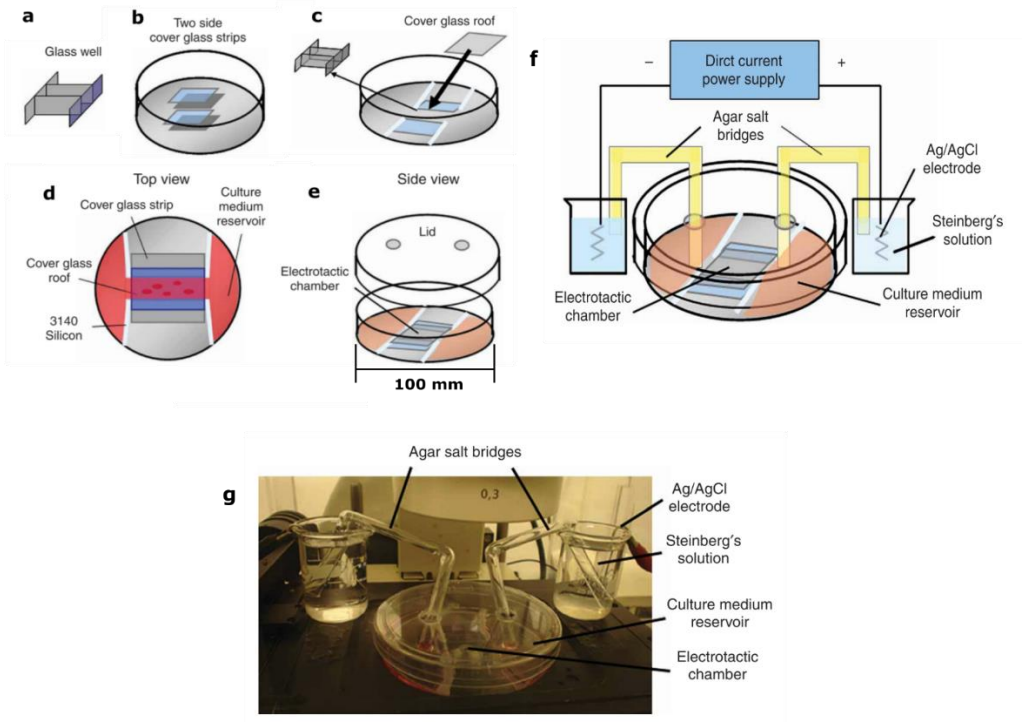

Figure 4: Electrotactic chamber. (**a**) Glass well. (**b**) Two side cover glass strips fixed in parallel onto the petri dish as the electrotactic chamber base. (**c**) The glass well is used to seed the cells in the well and then is removed. A coverslip roof is glued to the strips completing the electrotactic chamber. (**d**) Top view of the electrotactic chamber. (**e**) Chamber ready for the experiment. (**f**) Schematic of electrotactic chamber setup with agar salt bridges. (**g**) Electrotactic chamber setup [1].

Due to the fabrication strategy of the system, a very high current needs to be applied to achieve a biologically relevant EF strength. Furthermore, the system is limited to a single experiment each time, which increases the time between each possible experiment and iteration of the system [45]. The EF strength can be determined based on Ohm's law, through the following equation:

$$E = \frac{I}{\sigma \cdot w \cdot h} \tag{1}$$

where I corresponds to the electric current, σ represents the conductivity of the solution, and w and h are, respectively, the width and the height of the channel. The EF can be drastically influenced by the geometry of the channel. Careful fabrication and miniaturization of the cell channel can lead to a higher and homogeneous EF [45].

An alternative conventional device is one based on transwell assay which consists of two compartments, a lower and an upper one, each with an electrode in. When the electric field is applied, the cells migrate from the upper compartment to the bottom one, allowing to quantify how many cells reacted to the EFs applied. In comparison to the previous conventional devices, the transwell assay is more advantageous since it has a higher experimental throughput; thus, several runs can be done in one single experiment [5], [44]. Other types of microfluidic devices, such as plastic, PDMS or glass can generate more than one EF strength per experiment, reduce the experiment time and the Joule heating effect; this last one is decreased as a result of the miniaturization of the microfluidic devices [5]. Furthermore, with these microfluidic systems, it is possible to include microsensors in the experimental setups, allowing the control of cell populations, temperature, and pH [43]. However, all of these approaches remain to be limited by the use of Ag/AgCl electrodes and agar bridges to generate the desired electric fields, which hinders the translation from research into medical application.

2.2.3 Electrical stimulation for Wound Healing

Focusing on the applications regarding wound healing, ES directs the migration of epithelial cells as well as immune cells. It also promotes angiogenesis, which is characterized by the formation of new capillaries and regulates protein synthesis during the different phases of wound healing [46].

It has been proven that the use of ES can either speed up the healing process or slow it down based on the enhancement or reduction of induced ionic currents, respectively [21]. This can happen due to the influence that external EFs have on cells since they are able to change the direction of the migration of cell types, or even reverse the current direction when the polarity of the EFs is also reversed [5]. Moreover, by analyzing the results of experiments with ES in patients with an abnormal healing capacity, it was detected an increase of the blood flow in cutaneous wounds compared to patients that did not receive the same treatment. Hence, the wounds treated with ES showed an adjustment of angiogenesis and reduced the inflammation, resulting in a more effective curing process and wound closure [46].

Electrostimulation has been tested in several clinical trials to improve the wound healing rate in both healthy and unhealthy patients. Different stimulation paradigms have been employed to generate exogenous EFs such as direct current (DC), pulsed current (PC), and alternating current (AC) [47]. Direct current stimulation showed the most promising results amongst the different trials; however,

sustained stimulation is not possible due to the electrodes employed during testing. Metals, as well as metal-salt electrodes, corrode under prolonged DC stimulation, releasing toxic by-products, which could be more detrimental for wounds.

2.3 Fundamentals of Electrical Stimulation

Electrical stimulation (ES) has seen a widespread of applications such as deep brain stimulation for epilepsy, Parkinson's disease or depression; prostheses for bladder control, upper and lower limb movement, retinal/cortical visual or cochlear implants; and much more [48]–[52]. In electrical stimulation, an alternating current or voltage is applied to an electrode that is in contact with an electrolyte, which can be a cell medium, skin, or an extracellular fluid [48]. There is a charge transfer between the electrodes and the electrolyte, resulting in a flow of ions, such as potassium (K^+), sodium (Na^+), chlorine (Cl^-) and hydrogen (H^+) in the electrolyte. The charge transfer can occur through different mechanisms, such as Faradaic charge injection, Capacitive charge injection, and Super Capacitive or Ionic charge injection [48].

2.3.1 Faradaic Charge injection

In this type of injection, the chemical species in the electrolyte are subjected to reduction or oxidation reactions, resulting in the transfer of electrons between the electrodes and the electrolyte. Reduction occurs at the cathode (negative electrode), which consists of receiving an electron. On the other hand, there is an electron removal (oxidation) in the anode (positive electrode). These Faradaic reactions can either be reversible or irreversible depending on mass transport and on the rates of electrons transfer at the interface (kinetics). A reversible Faradaic reaction is characterized by fast kinetics relative to mass transport rate. If the direction of the current is reversed, since the electrochemical product remains close to the surface, the same product can be reversed into its original form. The reactions are irreversible if the process cannot be undone whenever the direction of the current is reversed. Irreversible reactions have slower kinetics than the rate of mass transport, enabling the diffusion of by-products in the solution, which cannot be recovered when the electrode's polarity is reversed.

The interface between the electrode and the electrolyte can be modeled as an electrical circuit with a double layer capacitor, C_{dl}, in parallel with the Faradaic impedance, $Z_{Faradaic}$ (Figure 5, a). The capacitor represents the charge flow brought by the electrode without any electron transfer in the electrolyte.

The Faradaic impedance represents the Faradaic processes where electrons are transferred from the electrode to the electrolyte due to the reduction and oxidation reactions (Figure 5, b) [48].

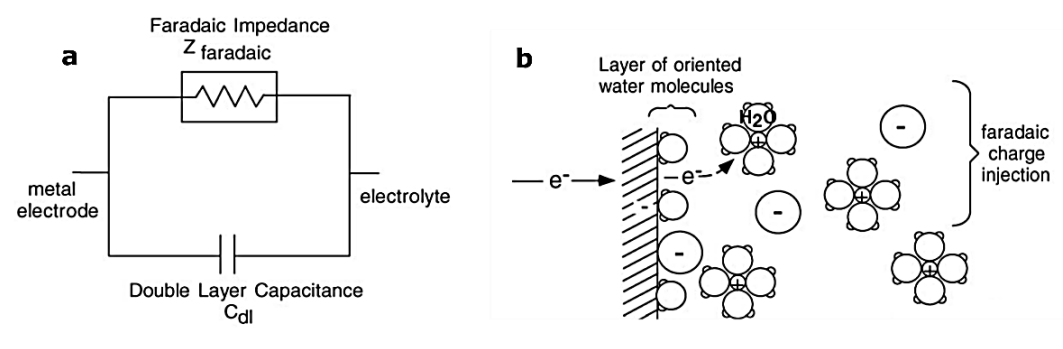

Figure 5: Electrical model of the electrode/electrolyte interface (a); Faradaic charge transfer at the electrode/electrolyte interface (b). Adapted from [48].

Reversible reactions are desired whenever electrostimulation is employed in the human body or with cells. The reactions can be reversed by switching the polarity of the stimulation pulse with AC stimulation. Utilizing pulses with the same amount of charge should lead to both charge and chemical balancing at the electrode interface. Typical materials employed for stimulation are Platinum or Iridium Oxide since their electrochemical reactions can be controlled by staying underneath the electrolysis potential of water (water window). Silver-Silver chloride electrodes also work utilizing reversible reactions by dissolving and reducing silver in the electrolyte:

$$2IrO_2 + 2H^+ + 2e^- \rightarrow Ir_2O_3 + H_2O \quad (2)$$

$$Ag^+ + e^- \rightarrow Ag\ (reduction\ of\ silver\ ions) \quad (3)$$

$$AgCl \leftrightarrow Ag^+ + Cl^-\ (dissolution) \quad (4)$$

Exceeding the water window or stimulating without charge balance, as would be the case for DC stimulation, leads to irreversible reactions. These reactions should be prevented during electrostimulation since they lead to pH changes in the solution, the release of toxic by-products and corrosion of the electrodes. Said reactions and changes are hazardous for the biological tissue and can lead to cellular apoptosis and irreversible damage.

$$2H_2O + 2e^- \rightarrow H_2 + 2OH^- \ (reduction\ of\ water) \quad (5)$$

$$\mathrm{Pt} + H_2O \rightarrow \mathrm{PtO} + 2H^+ + 2e^- \ (oxide\ formation) \quad (6)$$

$$\mathrm{PtO} + 2H^+ \rightarrow \mathrm{Pt}^{2+} + H_2O \quad (7)$$

2.3.2 Capacitive Charge injection

Non-Faradaic or capacitive charge injection is characterized by the redistribution of charged chemical species present in the electrolyte. Variation of the electrode potential leads to charge redistribution on its surface due to the attraction and repulsion of ions in the solution (Figure 6). This movement of charge does not involve the transfer of electrons across the boundary and can be seen as the charging/discharging of a capacitor. The current density achieved by this type of charge injection is lower than the injection involving electron transfer at around 20 $\mu C/cm^2$ [48]. The fact that no species are consumed nor new ones are created during a stimulation pulse on this type of injection makes this process safer than the faradaic charge injection for both the electrode and the tissue [52]. However, the lower charge injection capabilities make the use of this mechanism during functional electrostimulation extremely challenging.

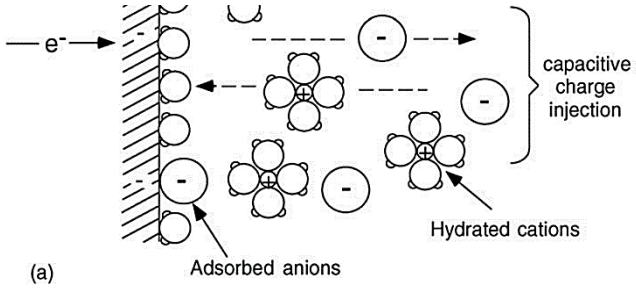

Figure 6: Physical response of the capacitive charge transfer in the electrode/electrolyte interface. Adapted from [48].

2.3.3 Ionic Charge injection

Ionic or super capacitive charge injection consists of the physical adsorption of ionic species on porous electrodes made out of conducting polymers or hydrogels, as well as certain forms of carbon. These electrodes can be represented as supercapacitors, which are able to store much more electrical energy, with the following advantages: longer cycling lifespans, faster-charging kinetics, and higher power densities [53].

For the charge-injection to occur, it is necessary to acquire high electronic conductivity, which is possible by doping anions of the polymer. In this way, a charge-transfer complex is formed as a result of the polymer oxidation resulting in high electronic conductivity. Whenever the electrode potential is changed, the electronic conductivity of the polymer leads to the intake or release of ions or dopant into the solution. These reactions allow for higher charge injection due to the larger active area without the necessity of faradaic reactions.

$$P^0 + M^+X^- \leftrightarrow P^+X^- + M^+ + e^- \quad (8)$$

$$P^0 + M^+X^- + e^- \leftrightarrow P^-M^+ + X^- \quad (9)$$

In the equations (8) and (9), P^0 represents the polymer, M^+ the metal, and X^- a doping anion, resulting in polymer oxidation, P^+X^-. One of the most important electrically conducting polymer (ECP) is PEDOT, poly(3,4-ethylenedioxythiophene), which demonstrates electronic and ionic conductivity [53]. The ionic conductivity of conducting polymers and hydrogels is described in further detail in the following section.

2.4 Conducting Polymers and Hydrogels

Electroactive coatings such as conductive polymers (CPs) and conductive hydrogels (CHs) have established themselves over the years as a suitable material for electrostimulation due to their high charge storage capacity, ionic charge injection, ease of fabrication, low price, and drug release capabilities [6]. This subsection focuses on the properties of CPs and CHs, as well as their application as electrode material for electrostimulation.

2.4.1 Conductive Polymers

Conductive polymers are electroactive coatings that are distinguished by their electrical and optical properties and high conductivity to weight ratio. This type of materials are biocompatible, porous, and have a vast active surface area that enables a lower electrical impedance [53]. Moreover, some of the advantages are the ease to synthesize, their low price, and the possibility of changing CPs' chemical, electrical or physical properties to meet the needs of their application even after they have been synthesized [6]. These select properties are possible because CPs have a delocalized π-system

backbone along the polymeric chains that allows influencing the properties of the polymer (chemical, physical and electrochemical) through a process of doping and de-doping [54]. The polymers have a conjugated carbon-hydrogen backbone which consists of a chain containing single (σ-bond) and double bonds (π-bond) between adjacent carbon atoms (Figure 7). In the π-system, the electrons can move freely due to the overlapping of the π-bonds, which provides these polymers with high electronic conductivity [6], [55].

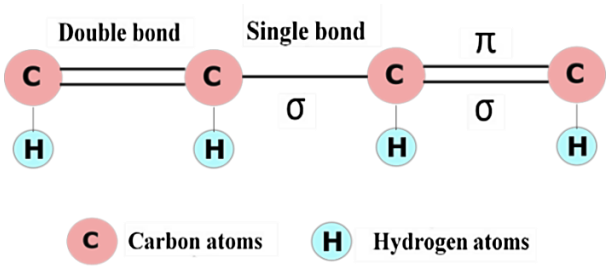

Figure 7: Schematic of a conjugated backbonewith alternating single and double bonds. Adapted from [6].

Furthermore, charge carriers are always introduced in the polymer during synthesis to improve their electrical properties and stabilize the polymer backbone. This process is denominated doping; when a positive charge is added, it is called p-doping and when it has a negative charge corresponds to n-doping [56]. The removed or added electrons from/to the polymer chain disrupt the conjugated backbone, creating a delocalized charge. This disruption allows for the charge to go through the polymer in the form of polarons or bipolarons. The polaron moves along the polymer chain, hence increasing electrical conductivity (Figure 8) [6], [57]. This process requires that the polymer has dopants which will initiate redox reactions, and, therefore, the electrons move in the polymers chain. Dopants can be inorganic compounds such as hydrochloric acid (HCl), or organic such as lauric acid (LA), p-toluene sulphonic acid (PTSA) and sodium poly(styrene sulfonate) (PSS). The dopants and doping level have a great influence on how the surface energy of the conducting polymers change, as well as the polymers swelling behavior and stability [58], [59].

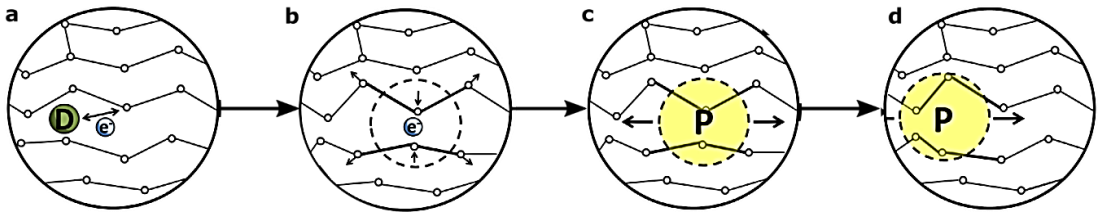

Figure 8: Electrical conductivity of conducting polymers.Dopant removes or adds an electron resulting on a delocalized charge. (**b**) Charge localized and surrounded by a local distortion. (**c**) Polaron is a charge surrounded by a distortion. (**d**) Polaron moves along the polymer chain. Adapted from [6].

There are different ways in which the conductive polymers can be synthesized (chemically, electrochemically, vapor-deposited, etc.). Chemical synthesis consists of mixing a monomer solution with an oxidizing agent, resulting in a thick film or powder of the polymer. This method enables the production of all kinds of polymers and bulk production, being the chosen method for commercial applications. However, the polymers synthesized through the chemical process have lower conductivity than the electrochemically synthesized ones, and it is not possible to produce thin films [60], [61]. Electrochemical polymerization consists of applying an electrical current using electrodes, which are into a solution that has the doping agent, solvent, and the monomer of the polymer. The monomer is deposited and oxidized on the positively charged working electrode, resulting in insoluble polymer chains. The properties of the film obtained can be defined by the time and deposition charge, the solvent, the doping agent, and the electrode system. This method is only applicable if the monomer that is being used is able to oxidize with an electrical potential [58], [62].

Electrochemical techniques can be used through three different methods, such as potentiostatic, galvanostatic, and potentiodynamic polymerization. In the potentiostatic method, the potential is fixed, and the current changes, enabling the protection of the integrity of the component to be coated; the galvanostatic polymerization consists of controlling the current, and the potential varies, allowing for the deposition rate to be carefully controlled. In the potentiodynamic method, the potential varies from a low to a high potential limit in cycles, enabling deposition in layers and for each layer to be activated electrically before the next one is synthesized [61].

Some of the most studied CPs are polypyrrole (PPy), polythiophene (PTh), ply-aniline (PAn), their copolymers, and derivatives (Table 1) [61]. These polymers have numerous applications, from electrical conductors to chemical and biologic sensors, photoresists, superconductors, electromagnetic shielding materials, etc. [63], [64].

Table 1: Some examples of CPs, their conductivity, and molecular structure [65]

Conductive Polymers	**Conductivity (S cm^{-1})**	**Molecular Structure**
Polypyrrole (PPy)	40-200	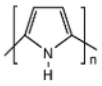
Polythiophene (PTh)	10-100	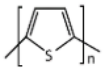
Polyaniline (PANI)	1-100	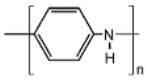
Poly(3,4-ethylenedioxythiophene) (PEDOT)	10-100	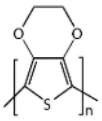

It is essential that the electrode materials demonstrate good adherence to the CPs and also that the polymers present high conductance and stability. For functionalization of electrodes employed in electrostimulation, these electrodes are coated with CPs through electro-polymerization; however, it is not possible to form a strong bond between the polymer structure and the electrodes' materials. The physical and mechanical interactions are essential for proper adhesion of the polymer. During electrical stimulation, the CPs expand and contract due to the release and uptake of ions into the polymeric matrix and hydration-dehydration, making the bond of the polymer with the electrode material even weaker. Consequently, delamination can occur due to the stress that the polymer-metal interface is under. This is the limiting factor for the long-term usability of CP-coated electrodes for electro stimulation. An improvement of the adhesion between metal and polymer can be achieved by modifying the surface of the electrode prior to polymerization. Rougher surfaces serve as an anchor point for the polymer to attach, which reduces the rate of delamination during stimulation cycles. Two promising materials are nanostructured platinum and iridium oxide. The latter has demonstrated to be the superior material due to its ease of fabrication (e.g., through sputtering in a reactive oxygen atmosphere) and its inherent roughness and porosity [9].

2.4.2 Conductive Hydrogels

Conductive hydrogels are a derivative of CPs and consist of cross-linked hydrophilic hydrogel networks with a conductive polymer matrix embedded within. Research has been done in order to synthesize scaffold materials that are conductive, biocompatible, and biodegradable by combining conductive polymers with highly hydrated hydrogels. These resulting electroactive hydrogels present excellent properties. The hydrogel guarantees a high degree of hydration, swellability, biocompatibility, and diffusion of ions, as well as soft mechanical properties. On the other hand, the electroconductive polymer implies high electrical conductivity, electrical and optical switching, and electrochemical redox properties [66], [67].

Hydrogels can be divided into two categories accordingly to the type of cross-linking: chemical cross-linked and physically cross-linked hydrogels. Chemical hydrogels are formed by covalent networks and only dissolve in water when the covalent bonds break, while physical hydrogels are created by dynamic cross-linking of synthetic or natural building blocks based on non-covalent interactions. Exposure to some physical, chemical or biochemical stimuli causes reversible changes in swelling of the network, which depends on the hydrogel composition, cross-linking type and on the degree of cross-linking [56], [68].

Conductive hydrogels can be tailored to reach some specific properties to be used in implantable biosensors, drug release devices or deep-brain stimulators. Besides these applications, they are known for their great potential in electrochemical systems, which are characterized by ionic and electronic transport processes. Therefore, electrodes coated with CPHs can be used as energy storage devices, more specifically as supercapacitors, lithium-ion batteries, and biofuel cells. Moreover, the CHs network facilitates fast charge transport, favoring the transport of molecules and ions. This assures continuous conduction and enables the creation of high power density electrochemical capacitors [6], [66], [69].

The electrical properties of the hydrogels can be defined via blending, doping, or chemical modification with electroactive materials. The hydrogels' electroconductive behavior is characterized by the charge transfer in the polymer matrix. The charge transfer can occur as a reduction (by n-type), or as oxidation (p-type), resulting in the creation of unbound charge carriers. The type of dopant and the efficiency to abstract or induce an electron within the matrix can define the conductivity of these electroactive hydrogels. The conductivity also depends on the mobility of the charge carriers within or between

chains. One way of enhancing the electronic and ionic transporting capacities of the hydrogels is by fabricating them into large surface areas and porous microstructures [9].

2.5 pH measurement

The pH value distinguishes between an acidic and a basic solution and is defined as:

$$pH = -\log\{aH^+\} \tag{10}$$

where $\{aH^+\}$ represents the activity of hydrogen ion, which is given by the activity coefficient (γ_{H^+}) and concentration (m_{H^+}) of the hydrogen ion to be measured in the solution divided by the hydrogen ion's standard state molality [70].

$$pH = -\log\left\{\frac{\gamma_{H^+}\, m_{H^+}}{m_{H^+}{}^\circ}\right\} \tag{11}$$

Since the pH is the activity of a single ion, determining the *pH* values requires an approximation method, which generally, consists of using standard buffer solutions that work as references [71].

The pH value is determined according to the methods used to measure it. The most accurate process to measure the pH is electrochemically way, which is based on an electrochemical cell that consists of a reference and a solution with transference.

$$Pt|H_{2(g)}|reference\ ||KCl(aq, concentrated)||unknown|H_{2(g)}|Pt \tag{12}$$

The pH changes occur through the Nernst potential, with electromotive force (EMF) E of the cell as defined in the following equation:

$$E = \frac{RT}{F} ln \frac{C_{H^+}(solution)}{C_{H^+}\,(reference)} \tag{13}$$

where *R* represents the ideal gas constant, *T* the temperature, *F* the Faraday constant, C_{H^+} (*solution*) is the unknown hydrogen ion concentration in the solution and C_{H^+} (*reference*) in the reference solution [72]–[74].

Moreover, there are alternative methods to measure pH changes besides electrochemical measurements, such as colorimetric determination of pH. This method consists of the change of color intensity accordingly to the changes in the concentration of the solution. The colorimetric measurement can be done using pH indicators, which are organic acids or bases that change color when the solutions become more acidic or basic; or, pH test papers, which shows different colors according to the degree of acidity and basicity of the solution [75], [76].

3 Aim and Own Approach

3.1 Aim

The main goal of the thesis is to characterize and test the Electrochemical stability of supercapacitive hydrogel-polymer electrodes and its suitability for Electrotaxis experiments. To determine if the electrodes can be used in cellular research and wound healing applications, its response to direct current stimulation as well as the changes these materials provoke in the environment need to be carefully observed. With this in mind, the aim is to:

- Develop different electrode designs which will allow for the mechanical stabilization and improvement of the electrical properties of the coatings without changing the electrical properties.
- Fabrication of a PI electrodes batch, with precise control of metallization and activation of the electrodes surfaces at wafer level through short-circuiting all electrodes.
- Use of a fabrication process that enables homogeneous coating of hydrogel on several electrodes simultaneously with an electrochemical cleaning step before coating.
- The electrodes should be flexible to allow testing of mechanical, electrical, and electrochemical stability.
- The electrodes should be easy to handle and easy to coat with hydrogel or a conductive polymer.
- The characterization of the material during DC stimulation should be carried under the same circumstances expected in a live-cell electrotaxis experiment (microfluidic channel).
- Different coating thicknesses and polymer concentrations within the hydrogel should be tested to determine a relationship between the physical and the electrical characteristics of the material.
- Implementation of pH sensors to determine possible pH changes during DC stimulation with different currents and electrode materials.
- pH measurements should be done as close as possible to the electrodes and within a fluidic channel to carefully monitor the changes in the electrode's surroundings.
- The cytotoxicity of the polymers on the electrodes with different thicknesses should be tested to analyze their effects on cells.

3.2 Own approach

To achieve all the previously mentioned points is necessary to find the best method to fabricate the electrodes, which will serve as a base for the electroactive coating. The electrodes should be flexible and biocompatible and should allow for batch fabrication with high reproducibility. Therefore, thin-film polyimide-based electrodes are chosen for this work. Polyimide (PI) has established itself as one of the best materials for electrode fabrication in neural engineering, and the thin-film processing of this material is one of the standard processes developed at the Laboratory for Biomedical Microengineering (BMT). The wafer level processing of the electrodes allows the integration of different electrode designs within one single wafer and the simultaneous fabrication of various electrodes with precise control over the electrode geometry and layer thicknesses. Furthermore, with careful placing, a trace connecting all electrodes in one row with a contact pad on the edges of the wafer can be implemented to allow for electrochemical cleaning of the electrode surface before the wafer-level coating with hydrogel.

The PI electrodes will be fabricated using platinum (Pt) as a material for all tracks and contacts and sputtered iridium oxide (SIROF) as the active electrode site to improve the adhesion of the electroactive coatings to the electrodes. Different designs will be tested with a surface area of 0.20 cm^2. The distribution of the area will be different amongst the designs by utilizing several smaller circular active sites. The designs will vary based on the number of active areas and their corresponding diameter (Figure 9). A larger surface area leads to a higher charge and current delivery, however, it also contributes to higher stress once the electrodes are coated with the CPs. The distribution amongst smaller areas should improve the mechanical stability of the coatings as well as the current they are capable of delivering due to a higher edge effect, without requiring a larger electrode size [77], [78].

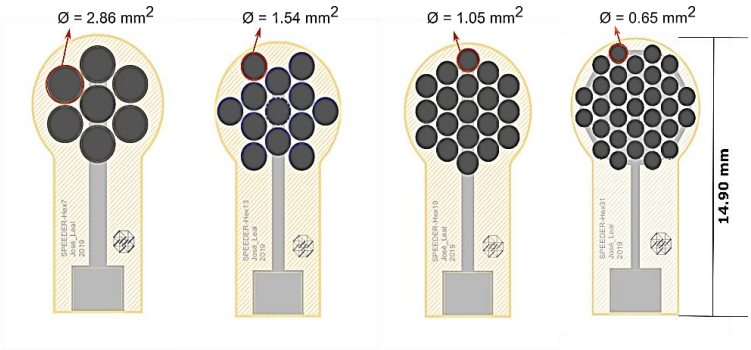

Figure 9: Different electrodes designs with a total area of 0.2 cm^2.From left to right: Hexagonal 7, Hexagonal 13, Hexagonal 19, and Hexagonal 31.

Different electroactive coatings based on PEDOT/PSS will be tested on the different electrode designs, and its electrochemical stability, as well as their influence on the electrolyte during DC stimulation. It has been demonstrated that PEDOT/PSS is capable of DC stimulation and can be implemented in electrotaxis experiments with the successful directed movement of cells [8], [79]. Electrodes coated with PEDOT/PSS have shown stable currents in an experimental environment during short and long-term experiments. However, delamination and damage to the coatings have been observed, when driven to voltages beyond the water window of platinum, drying of the electrodes, movement of the probes, and repetitive cycling. The hydrogel P(DMAA-co-5%MABP-co-2,5%SSNa), PDMAAp, allows PEDOT chains to be grown within the hydrogel matrix which could improve its mechanical stability and biocompatibility due to its better mechanical matching to biological tissue (Figure 10). The influence of the hydrogel thickness as well as the amount of PEDOT grown within it will be tested and compared against electrodes coated only with PEDOT/PSS.

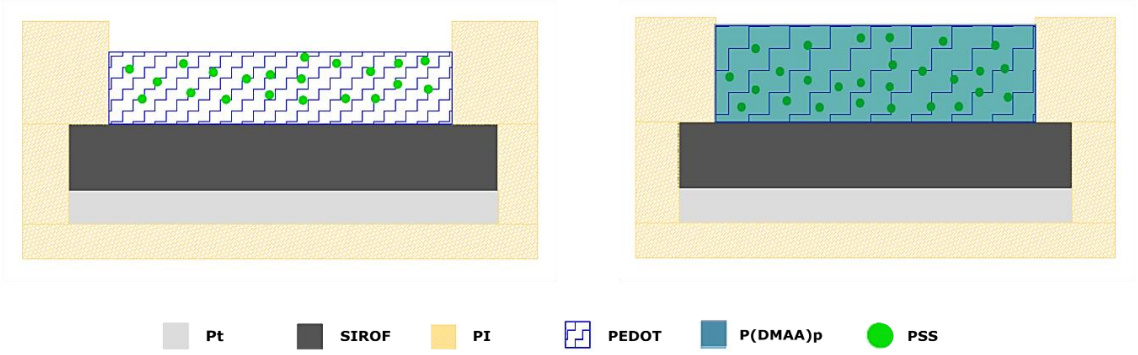

Figure 10: Schematic of PEDOT/PSS and Hydrogel electrodes.

The electrodes will be interconnected to a Pyrex carrier with a metallic track and pad for easier handling and interconnection to the stimulation electronics. The stimulation of the electrodes will be carried in a microfluidic channel made out of polydimethylsiloxane (PDMS) structured through a soft lithography process. The channels consist of two medium reservoirs connected by a 3 mm long microchannel with a cross-section of 100 x 300 μm^2 (Figure 11, b). The microfluidic channel allows for precise application of a homogeneous electric field to the cells during electrotaxis experiments. To facilitate testing of several electrodes, a compression system out of laser cut acrylic with magnets is utilized. The PDMS channel system is placed on a glass coverslip, then the electrodes are positioned in the corresponding well, and the whole setup is kept in place by the acrylic holder (Figure 11, a and c). Electrical stimulation is done by applying a constant current in a two-electrode setup in both anodic and cathodic direction while measuring the electrodes potential.

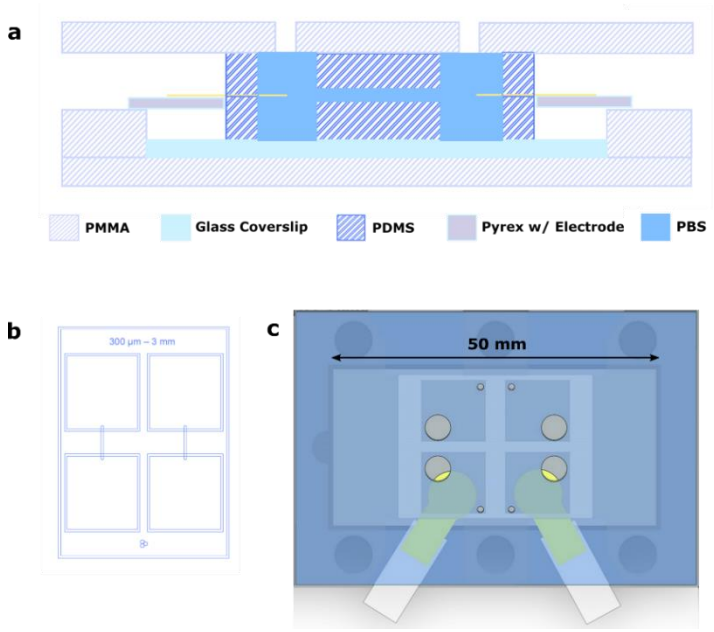

Figure 11: Schematic of the setup for DC stimulation(**a**) using a PDMS channel (**b**). (**c**) Schematic of setup for DC stimulation top-view.

After the first tests in a microfluidic channel, the most stable electrode design will be chosen for the pH measurements. Electrochemical pH sensors out of SIROF with integrated guard rails will be used to determine the effect of the DC stimulation with different coatings on the cells. A particular setup milled in Teflon with two reservoirs and a channel connecting them will be utilized for the pH testing (Figure 12, a). After calibration of the sensors, one of these will be placed close to each of the stimulating electrodes, and one will be placed in the middle of the channel (Figure 12, b). Changes in the electrochemical potential of the SIROF sensors will be measured with dedicated electronics against a silver-silver chloride reference electrode. The experiments will be performed in a buffered and a not buffered solution to determine if the changes measured with the electrodes are due to changes in the hydrogen ion concentration or the ionic concentration of the electrolyte. Alongside the electrical testing and the pH measurements, different electrochemical characterization methods will be employed to quantify the stability of the coatings utilizing cyclic voltammetry to determine the changes in the charge storage capacity of the electrodes and electrochemical impedance spectroscopy. Furthermore, cytotoxicity of the coatings will be tested on different skin cells to prove the biocompatibility of the fabrication process before any electrotaxis experiments.

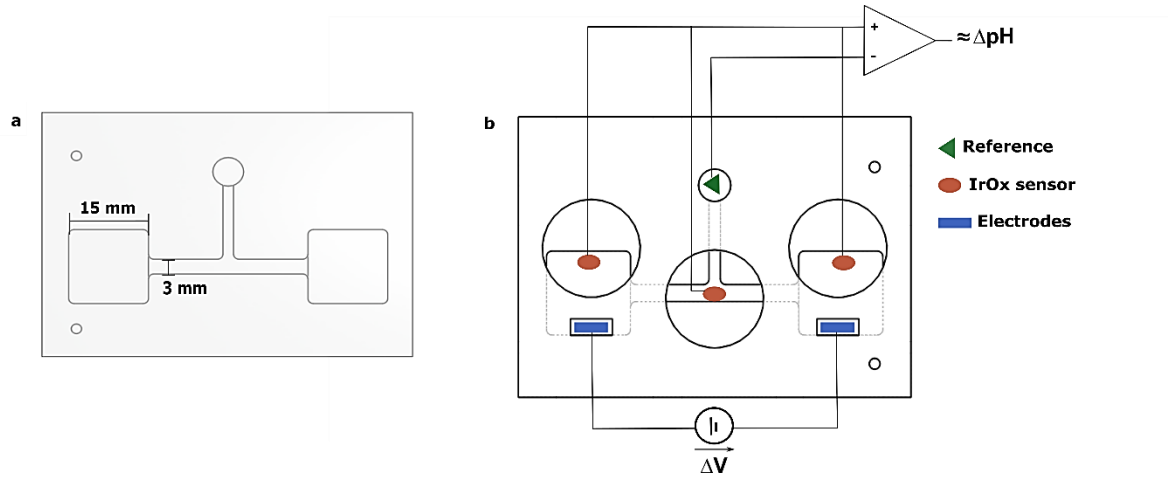

Figure 12: Schematic of the pH channel setup for DC stimulationand pH measurement: (a) pH channel, (b) pH channel with electrodes holder on top.

4 Materials and Methods

All procedures used for the preparation of the electrodes, including the fabrication processes, electrochemical characterization, and the coatings of the conductive polymers are described in this section. Moreover, an explanation of how the setups for DC stimulation, pH measurements, and cytotoxicity tests were designed and fabricated as well as the preparation of the pH sensors is given. Lastly, the software programs used to obtain the data and analyze it are briefly explained.

4.1 Fabrication of Polyimide electrodes

The polyimide (PI) electrodes are fabricated in the cleanroom of the Faculty of Engineering of the University of Freiburg (IMTEK). The electrodes are produced on a silicon wafer, which is used as a carrier substrate. The first layer of PI (U-Varnish-S) (UBE INDUSTRIES, LTD) with a thickness of 6 µm is spin-coated on the substrate and cured utilizing a YES furnace (Yield Engineering Systems YES-PB-HV, USA) (Figure 13, a). The metallization is done through a bi-layer process. A layer of 1.4 µm LOR 5A (MicroChem, Westborough, MA, USA) and approximately 1.8 µm of the photoresist AZ1518 (Microchemicals Gmbh, Ulm, Germany) are spin-coated on the polyimide and structured through exposure with UV-light (Figure 13, b) and development with tetramethylammonium hydroxide (TMAH). This process dissolves the photoresist as well as the LOR 5A layer creating an undercut, which facilitates the lift-off process (Figure 13, c). The metallization for the tracks, contact pads and active sites is done through sputtering of a 300 nm layer of platinum with a Leybold-Univex 500 (Leybold Vacuum GmbH, Cologne, Germany) (Figure 13, d). The lift-off of the excess metal is done with dimethyl sulfoxide, DMSO (TechniStrip® Micro D350, Microchemicals GmbH, Ulm, Germany) (Figure 13, e). These last steps are repeated for the layer of IrOx deposited at the active sites of the electrodes. A 100 nm layer of Ir is sputtered first to improve adhesion to the Pt layer, followed by an 800 nm IrOx layer deposited through reactive sputtering in an oxygen atmosphere (Figure 13, f). Lastly, a second PI layer is spin-coated and cured (Figure 13, g) before the etching of the openings for the electrode sites, contacts, and contours through Reactive Ion Etching (RIE) (STS Multiplex ICP, SPTS Technologies, United Kingdom). A 20 µm thick layer of AZ9260 (Microchemicals Gmbh, Ulm, Germany) was used as a mask for this last processing step (Figure 13, h). The RIE step is done with oxygen plasma until the active sites, and contact pads are free of PI, and the contour of the electrodes is completely etched (Figure 13, i). The electrodes are then removed from the wafer and prepared for future experiments (Figure 13, j). The relevant parameters for the process of fabrication are described in Annex 11.1.

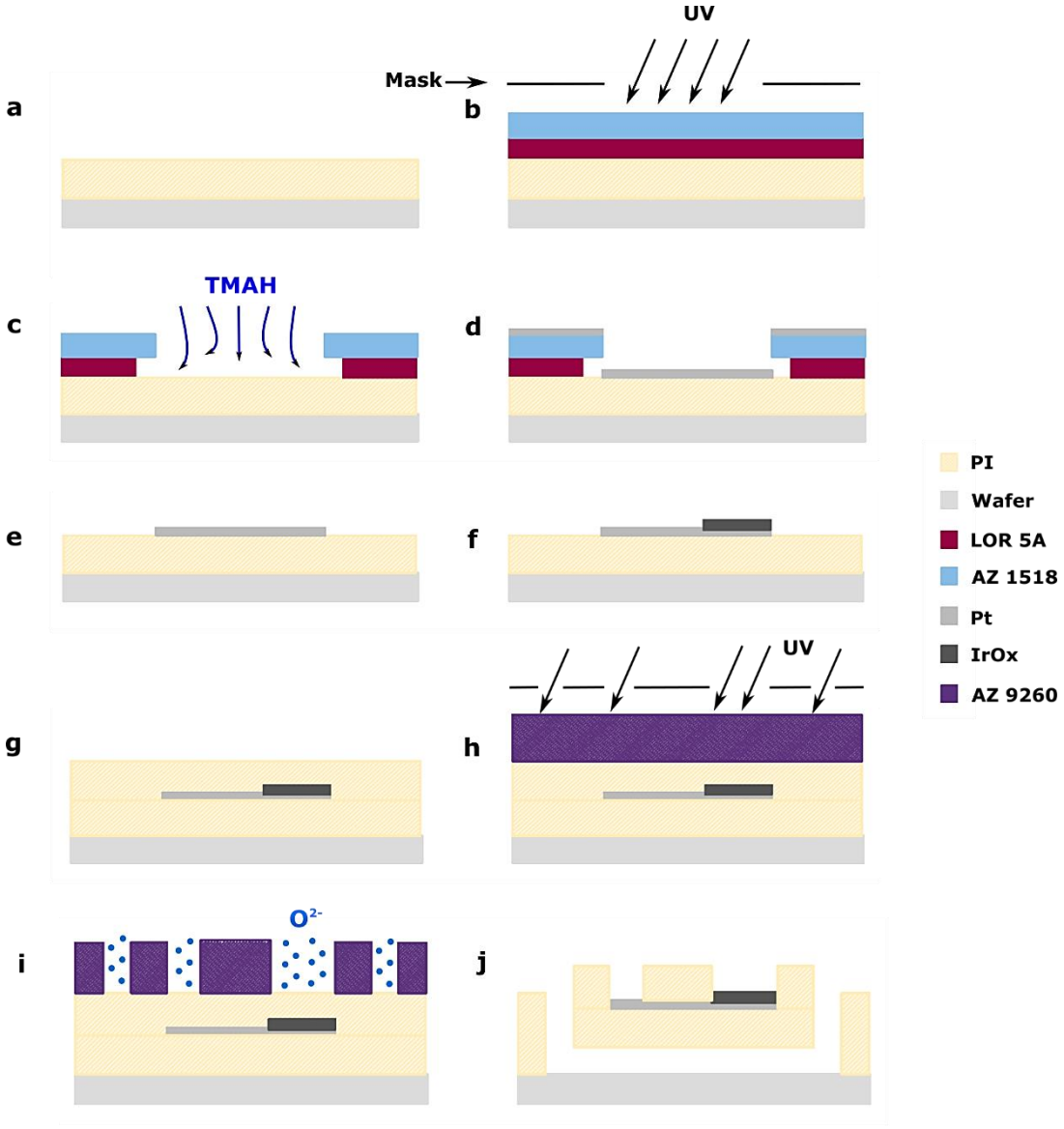

Figure 13: Schematic of electrode fabrication. (**a**) substrate structuring with PI layer; (**b**) bi-layer processing; (**c**) development with TMAH; (**d**) sputtering of platinum; (**e**) lift-off with DMSO; (**f**) repetition of the first 5 steps with metal IrOx; (**g**) deposition of the second layer of PI; (**h**) deposition of AZ9260 for RIE; (**i**) RIE with oxygen plasma; (**j**) electrode removed from wafer.

After fabrication, the electrodes are peeled off from the wafer very carefully with a flat tweezer. The contacts of the electrodes are soldered to the contacts of the Pyrex holders, which are also fabricated in the cleanroom. The holders have contact pads for the electrodes and clamps as well as tracks made out of 100 nm sputtered Platinum (Pt) with a 50 nm Tungsten-Titanium (WTi) layer as an adhesion promoter between glass and Pt. Tin-Copper-Lead (S-Sn60Pb39Cu1) is used for soldering the electrodes onto the pyrex carriers (Figure 14). Afterward, the electrodes are cleaned with isopropanol

and DI water and dried before insulating the contacts with a liquid plastic insulator (Plastik 70 Super, Kontakt chemie®). This prevents corrosion of the solder during the characterization and electrostimulation of the electrode and prevents leaching of toxic materials.

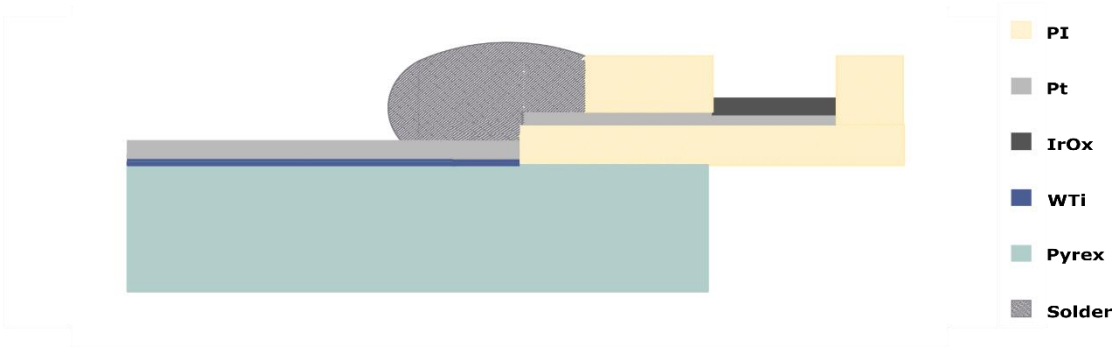

Figure 14: Electrode soldered to pyrex holder.

4.2 Electrochemical characterization

The cleaning and characterization of the electrodes are done through the open-circuit potential (OCP), cyclic voltammetry (CV) and electrochemical impedance spectroscopy (EIS), with an Autolab PGSTAT potentiostat (Metrohm Autolab BV, Netherlands) in a three-electrode setup. The reference (RE) for the measurements of the PI-electrodes (working electrodes, WE) is a Silver-Silver Chloride (Ag|AgCl) electrode, and the counter electrode (CE) is a piece of stainless-steel. The electrolyte used for all characterization and cleaning steps is phosphate-buffered saline (PBS, 0.01 M, Sigma Aldrich Life-Science), with a pH = 7.4.

A triangle-shaped potential is applied between the WE and the RE, with values ranging from -0.6 V to 0.9 V and the current flow between WE and CE is then measured. These values arise from the water window of Platinum, which is, in turn, the base for IrOx and subsequent PEDOT coatings. The electrodes are cleaned by subjecting them to 100 CV cycles at 250 mV/s in order to preserve the oxide layer and remove remaining impurities from the manufacturing. The characterization of the electrodes is achieved through 5 CV scans at 100 mV/s. Afterward, the charge storage capacity (CSC) is determined for each electrode by calculating the area of the CV curve during a full sweep. The Electrochemical Impedance Spectroscopy, EIS, is measured by applying a sinus signal with 10 mV of amplitude that is swept over a frequency range from 0.125 Hz to 10 kHz. After cleaning all the electrodes, it is possible to proceed to the deposition of CPs on them.

4.3 Hydrogel coating

4.3.1 P(DMAA-co-MABP-co-SSNa)

The hydrogel component chosen to coat the electrodes was P(DMAA-co-MABP-co-SSNa), P(DMAA)p, which is a copolymer composed by dimethylacrylamide (DMAA) (92.5 %), 4-methacryloyloxy benzophenone (MABP) (5 %) and sodium 4-styrene sulfonate (NaPss) (2.5 %). The chemical structure of the hydrogel is shown in Figure 15.

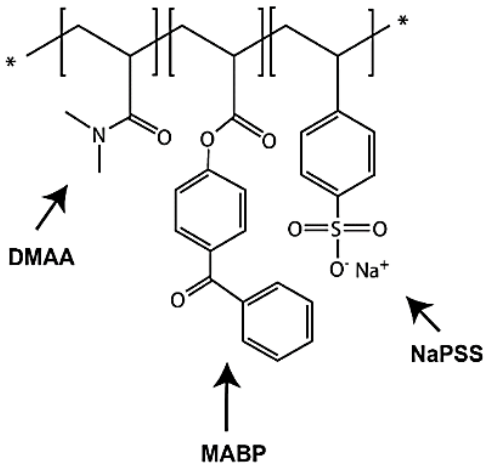

Figure 15: Chemical structure of PDMAAp. Adapted from [54].

The blocks that integrate P(DMAA)p have different functions: the DMAA is the backbone of the hydrogel and eases the swellability and solubility in aqueous solutions. The block MABP allow for the photocrosslinking, and micropatterning mechanisms and the NaPSS acts as the countering dopant in the polymerization of the CP [58].

4.3.2 Electroactive coating

Hydrogel functionalization consists of several steps, such as the cleaning of the electrodes, the functionalization with 4-(3-triethoxysilyl)propoxybenzophenone (3-EBP) silane, and the coating and crosslinking of the Hydrogel. Before coating electrodes on a wafer with Hydrogel, it is necessary to clean the electrodes. The wafer was designed with four rows of ten electrodes shorted through a platinum track and contacts to said tracks at the edges of the wafer (Figure 16), so it is possible to

clean ten electrodes at a time utilizing the methods described in 4.2. A wafer-sized reservoir with an embedded stainless-steel mesh counter electrode is employed for this process. The wafer is submerged until the active site of one row of electrodes is under the water level, and the contacts are not. After every row has been electrochemically activated, the wafer is dried and prepared for the next step.

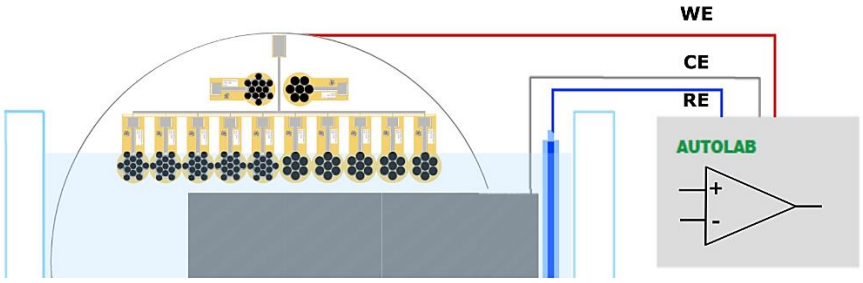

Figure 16: Schematic representation of the wafer-level electrochemical cleaningof the electrodes through cyclic voltammetry.

The IrOx electrodes have to be chemically functionalized for the hydrogel to bind covalently to the substrate (Figure 17, a). Therefore, the crosslinking agent 3-EBP silane provided by the Laboratory for Surface Chemistry at the Faculty of Engineering of the University of Freiburg is used (Figure 17, b) [80]. First, 2 mL of the 3-EBP silane solution are spin-coated onto the wafer at 1000 rpm for 120 seconds. Then the wafer is placed on a hot plate for 30 min at 120 °C followed by a washing step with toluene and dried with nitrogen. At the end of the functionalization process, the samples are kept in the dark at room temperature.

The Hydrogel P(DMAA)p, synthesized at the Laboratory for Chemistry and Physics of Interfaces (IMTEK, University of Freiburg) is dissolved in 90% Ethanol to obtain a concentration of 30 mg/mL [81]. The hydrogel is deposited on the previously functionalized wafer through dip-coating (ND-R Rotary Dip Coater, Nadetech Innovations, Spain) with a withdrawal speed of 300 mm/min and a down holding time of 10 s, which leaves a homogeneous layer after drying on a flat surface. The hydrogel is cross-linked and patterned on the active sites of the electrodes through UV radiation. A foil mask and a mask aligner (MA-6/BA6 Suss, Carl Zeiss AG, Jena, Germany) are utilized to ensure the coating of the IrOx active sites only (Figure 17, c). The UV exposure is carried out using an I-line filter with a dosage of 2 J/cm^2 at 365 nm for 400 s. The remaining hydrogel is removed by washing the wafers in a Petri dish with 99 % ethanol for 5 min (Figure 17, d).

The number of dips establishes how thick the hydrogel is on the samples. Therefore, the process was repeated three times for a wafer and six times for another to vary the thickness of the hydrogel layers. The photocrosslinking needs to be done in between each dip, as well as the cleaning of the unreacted hydrogel. When the hydrogel coating is finished, the electrodes can be released from the wafer and prepared for the PEDOT coating.

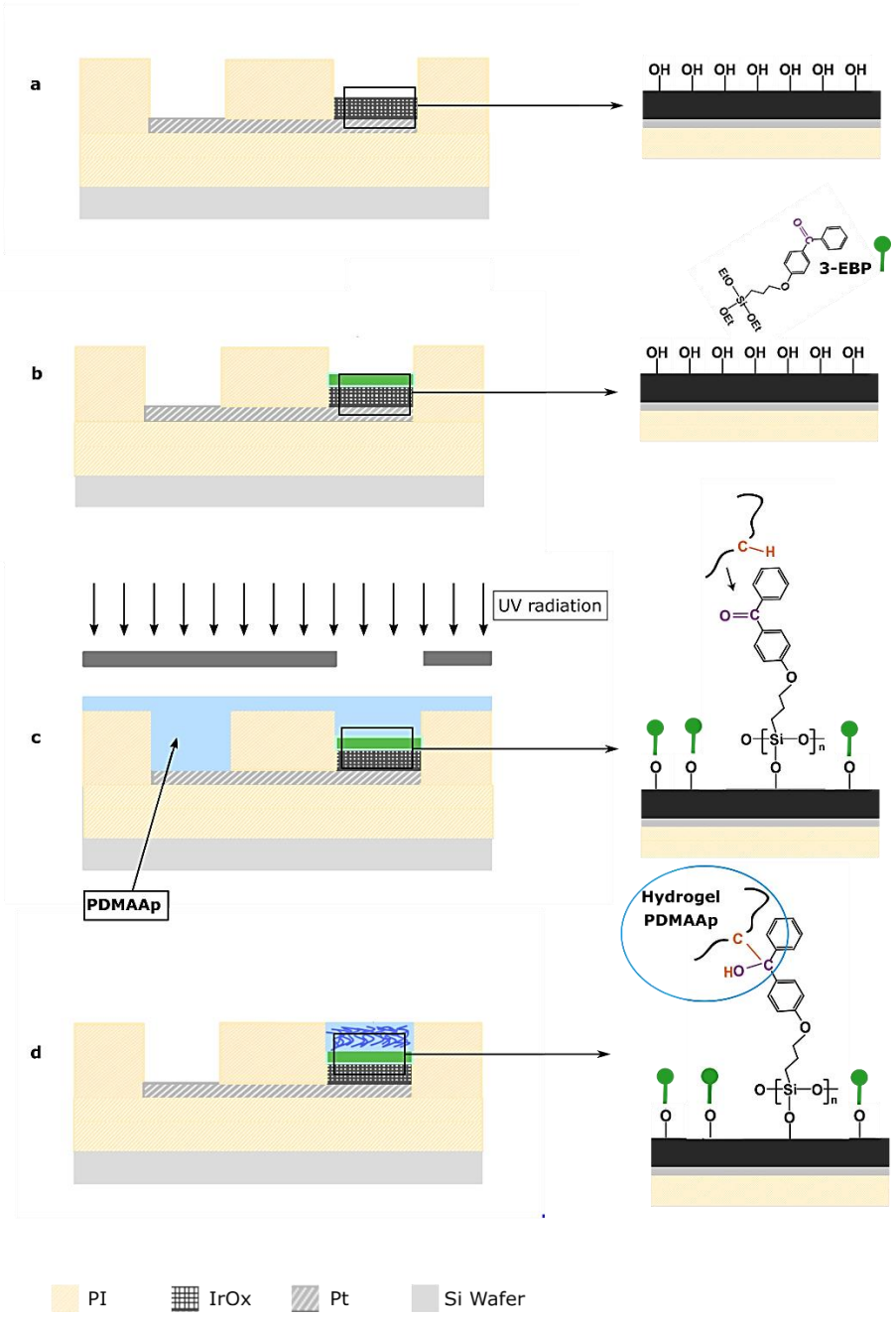

Figure 17: Schematic of the hydrogel coating.The electrodes on the wafer (a) are functionalized with 3-EBP silane (b). PDMAA is deposited into the wafer (c), and through UV-light, the hydrogel is formed on top of the IrOx (electrode site) (d).

4.4 PEDOT/PSS coating

4.4.1 Poly(3,4-ethylenedioxythiophene)

Poly(3,4-ethylenedioxythiphene), PEDOT, is a class of conducting polymer (CP) that presents characteristics such as extremely fast ion diffusion, optical transparency, and very high stability. Its constitution includes the 3,4-ethylene dioxythiophene (EDOT) monomer. When associated with polystyrene sulfonate (PSS) by allocation, it forms PEDOT/PSS, which makes the PEDOT electrically conductive and has the advantage of being a cheap chemical compound [82]. Given that this polymer is biocompatible with epithelial, neural and neuroblastoma cells, it has found many biomedical uses mostly in biosensing and bioengineering fields, for instance, for neural electrodes and heart muscle patches [7], [56], [59].

The polymer PEDOT doped with the counter ion and charge compensator poly(styrene sulfonate), PSS, has vast advantages comparing to other conducting polymers, such as long-term and thermal stability, high mechanical flexibility, solution processability, high transparency in the visible range and high conductivity. The film PEDOT/PSS, consists on a large dopant (PSS) incorporated into the PEDOT network (Figure 18), after the polymerization the dopants are trapped in the polymers network, disabling the PSS from leaving the polymer when the film is subjected to discharges and recharges [58], [67], [83], [84].

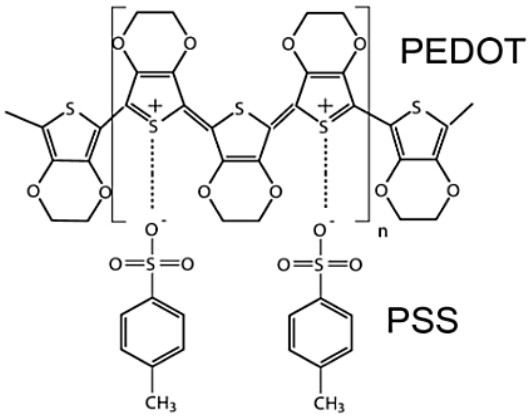

Figure 18: Chemical Structure of PEDOT/PSS. Adapted from [58]

The charge storage capacity of PEDOT/PSS, as well as the impedance, are proportional to the thickness of the deposited layers (Figure 19, a), while the impedance of the coatings correlates non-linearly (Figure 19, b). The effect of the PEDOT/PSS coatings on electrodes employed for electrostimulation has been studied, and it was shown that there is a higher charge injection for coated electrodes when compared to in simple Pt or IrOx electrodes [8], [67].

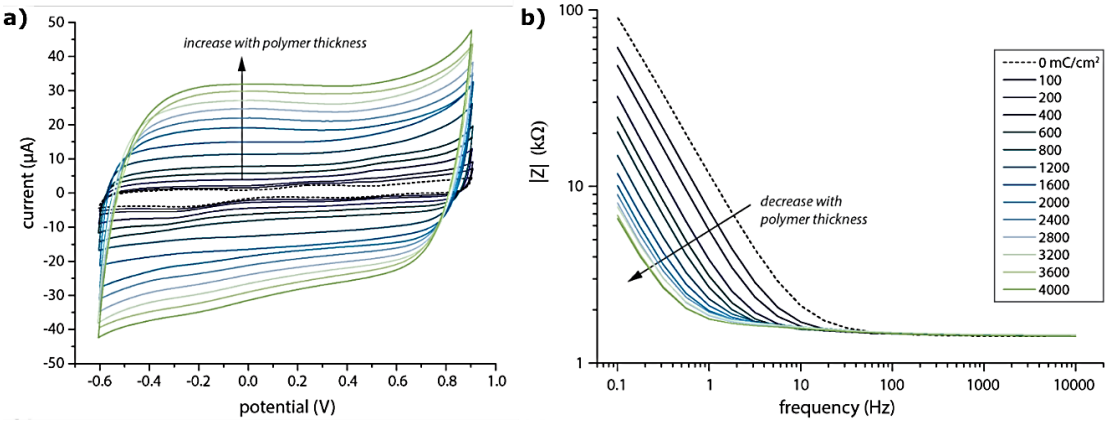

Figure 19: CV-diagram (a) and Impedance spectrum (b) of PEDOT/PSS. Adapted from [8].

4.4.2 Electropolymerization of PEDOT/PSS

The electropolymerization of PEDOT is done in a three-electrode setup where the electrodes are placed in a solution containing the EDOT monomer and the counterion PSS. For the hydrogel coated electrodes, the counterion is already embedded into the hydrogel matrix and is no longer required in the solution. However, the hydrogel electrodes need to be soaked in the EDOT solution for at least one hour before the polymerization to allow the monomer to diffuse into the hydrogel matrix and create homogenous PEDOT/PSS chains from the surface of the IrOx (Figure 20).

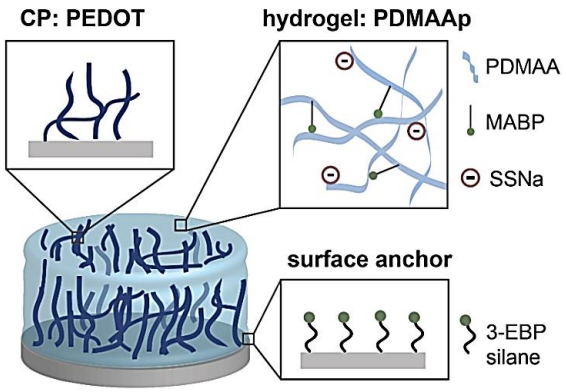

Figure 20: Schematic of CP Hydrogel and PEDOT compositionafter coating and functionalization [58].

The parameters for the different solutions are listed in Table 2. The EDOT solution for the hydrogel electrodes is composed of 10 ml of DI water and 21.4 µl of EDOT (Sigma Aldrich: 483028).

Table 2: Composition of the EDOT:NaPSS electrolyte for PEDOT functionalization

Hydrogel	**NO**	**YES**	
Composite	Quantity		Supplier
DI Water	10 mL	10 mL	-
NaPSS	50 mg	-	Sigma Aldrich: 434574
EDOT	10.7 µL	21.4 µL	Sigma Aldrich: 483028

An Ag/AgCl electrode acts as RE, a stainless-steel foil is used as CE, and the IrOx electrodes work as the WE onto which the deposition takes place. For the electrodes without hydrogel, a constant voltage of -0.9 V is applied (vs. Ag/AgCl) in order for the electropolymerization to be achieved potentiostatically on IrOx, whereas a galvanostatic deposition with a current density of 0.125 mA/cm^2 is required for the hydrogel electrodes. For these electrodes with a surface of 0.2 cm^2, a constant current of 25 µA needs to be applied for deposition into the hydrogel. The current and charge are measured at the same time during the deposition process. The charge density establishes the thickness of the PEDOT layers; therefore, the measured charge is used as the cut-off parameter during the polymerization. This can be calculated based on the electrode's geometry and the desired thickness. The PEDOT thickness and respectively cut off values are listed in Table 3. The coated electrodes are characterized electrochemically after the polymerization process through CV and EIS measurements, as described

in 4.2. To prevent the PEDOT layers on the electrodes from breaking or drying, these are always stored in 8 mL glass beakers with PBS.

Table 3: Cut off charge for PEDOT deposition for electrodes with area 0.2 cm^2

Charge density in mC/cm^2	**200**	**400**	**600**	**800**
Cut off charge in mC	40	80	120	160

4.5 PDMS channels

Polydimethylsiloxane (PDMS) is the most commonly used silicone elastomer in biomedical engineering due to its biocompatibility, biostability, non-toxicity, and low Young's modulus. Furthermore, it is easy to prepare and can be bonded irreversibly to glass through plasma activation. Therefore, it is the chosen material to fabricate the chambers with the microchannels for the DC stimulation testing.

Two-component PDMS Sylgard 184 (Sigma Aldrich, St. Louis, USA) is prepared by mixing the curing agent and the elastomer at a 1:10 ratio. Both compounds are mixed thoroughly until the mixture is foaming. A vacuum pump and a vortexer are used to remove bubbles from the mixture. When all the air is removed, the PDMS is poured on a silicon wafer with SU-8 structures coated with C_4F_8 (Figure 21, a), which prevents adhesion of the PDMS to the silicon. The SU-8 structures work as a stamp for the PDMS defining the microfluidic channels and the medium reservoirs (Figure 21, b). The curing process is accelerated by putting the casted PDMS in a furnace (Memmert, Germany) at 80 °C for 1 h (Figure 21, c). When cured and cooled down, the silicone can be easily detached from the wafer mold. The last step is the opening of the medium reservoirs by cutting off the PDMS with a scalpel (Figure 21, d).

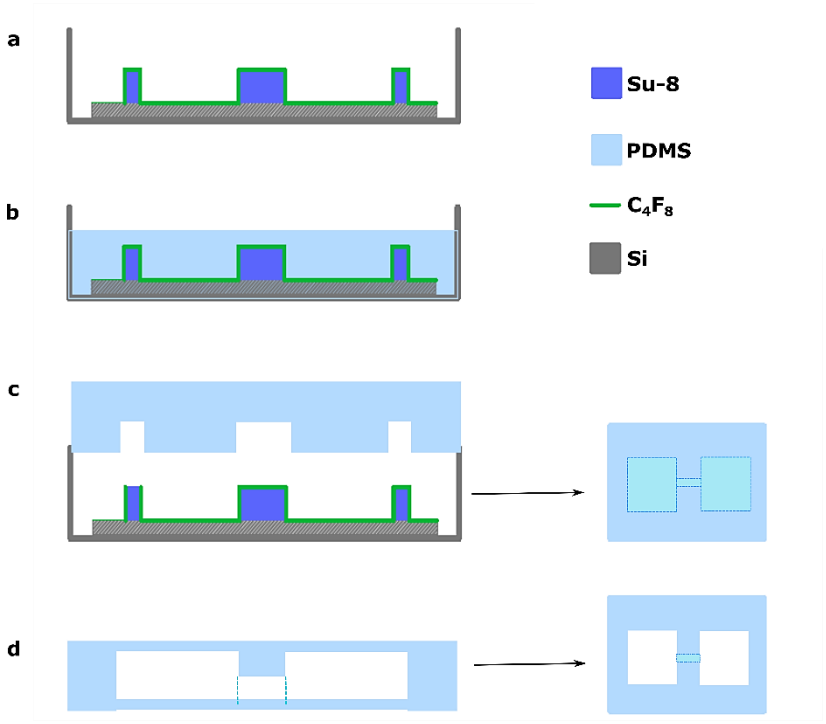

Figure 21: Schematic of fabrication of PDMS channel.Wafer with SU-8 structures (a). PDMS poured onto the wafer (b) and when cured, peeled off and cut following the stamp structure (c). Channels cut with a scalpel (d).

4.6 SIROF electrodes for pH measurement

One of the most stable and researched material for electrochemical pH sensors is IrOx thanks to its stability over a wide range of temperature and pressure in aqueous solutions, its low impedance, fast response times biocompatibility. Iridium oxide can be obtained through different methods: electrochemically (EIROF, AIROF) through sputtering (SIROF) or thermally (TIROF). The fabrication and preparation of the IrOx layers determine the pH response and sensitivity. Sputtered iridium oxide (SIROF) electrodes (Figure 22) have been established to be adequate for pH measurements since IrOx is the best material compared with other metal oxides based on electrochemical studies [85], [86]. The electrodes used were fabricated by José Leal for his master thesis project and consist of two different sensing IrOx areas surrounded by guard rails as well as two platinum electrodes, which are not going to be employed during this thesis [86].

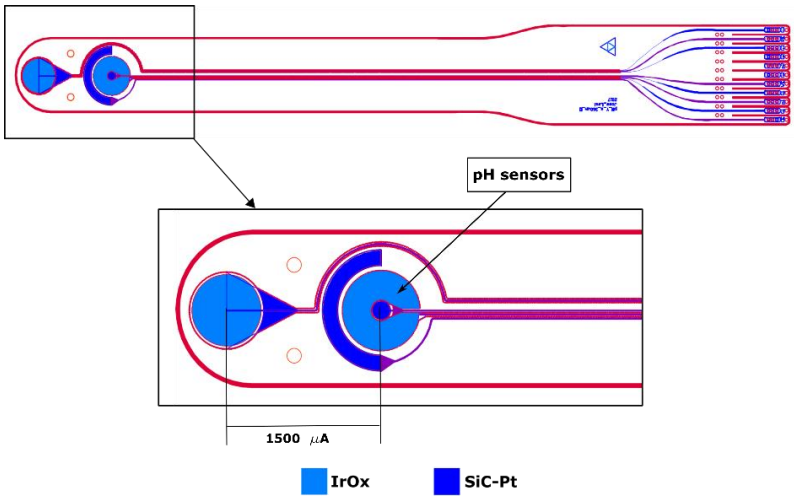

Figure 22:Schematic of the SIROF pH sensor. Adapted from [78].

Iridium oxide electrodes (or any metal oxide) react to pH variations in a solution by creating equilibrium through valency changes within the oxide. In response to pH changes. Sputtered IrOx (SIROF) electrodes have a linear Nernstian response with a slope of approximately -59 mV/pH due to the nonstoichiometric formation of the oxide as well as the hydration due to the redox equilibrium:

$$IrO_{\frac{x+n}{2}}(H_2O)_{y+m} + ne^- + nH^+ \leftrightarrow IrO_x(H_2O)_y + \left(\frac{n}{2} + m\right)H_2O \qquad (14)$$

The polyimide sensors are connected to a PCB through a Microflex process to allow for an easier connection to the measurement electronics [87]. The connection is made with a gold wire bonder (Digital Ball Bonder 452A, Kulicke & Soffa, Nuremberg, Germany) and protected with a small layer of two-component epoxy (UHU Plus Endfest 300, UHU GmbH &Co. KG, Bühl, Germany). Metal pins are soldered to the top part of the adapter for a simpler connection of the sensors to the measuring electronics. The electrodes are cleaned and characterized before any pH measurements by the processes described in chapter 4.2..

4.7 pH-readout

The design of the circuit for the pH readout was based on the work done by S. Rieger and J. Leal and was implemented on a PCB allowing the calibration and measurement of several sensors at the same time (Figure 23) [37], [86].

To determine pH changes in a solution, the open circuit potential of the SIROF sensors needs to be measured against an unreactive reference electrode (Ag/AgCl). One of the biggest concerns is to avoid polarizing effects on the sensing electrode. That can be achieved by implementing an amplifier with a high input impedance and low current compliance, such as the INA116 differential instrumentation amplifier. This integrated circuit (IC) is characterized by its low input bias currents, high impedance to a high voltage headroom (18 V) and integrated guard rails that avoid the leakage of input currents to the amplifier. The high voltage mid supply reference voltage (9.25 V) of the amplifier INA116 is provided by a reference OP2177 operational amplifier with a voltage divider at the input. The measured voltage is then shifted to a low voltage by a level shifter (INA826), enabling the signal to be scaled down. The signal is also inverted without amplification by the reference op-amp, (OP2177). To buffer the signal, an LTC6081 op-amp is used before the output. The signal is then ready to be recorded by a NI-DAQ USB 6008 Analog-to-Digital Converter (National Instruments, Austin, Texas) (ADC) since it is down-scaled not to exceed the ADC input voltage. This circuit is implemented four times on a PCB board (Multi Leiterplatten GmbH) (Annex 11.3), allowing for the calibration of several sensors simultaneously.

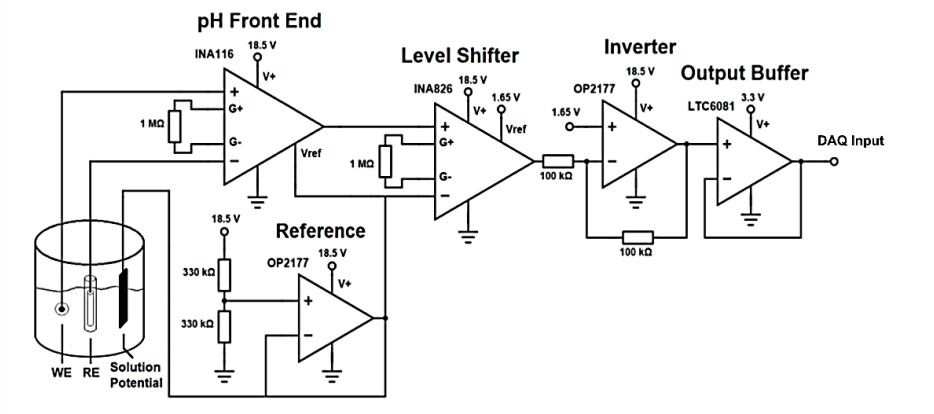

Figure 23: Schematic of the circuit of the PH readout system developed. Adapted from [88].

4.8 pH channel

A dedicated fluidic channel was designed with the purpose of measuring possible pH changes during DC stimulation. The setup consists of two medium reservoirs where the WE and CE are placed alongside its respective pH sensor. These reservoirs are interconnected by a 30 mm long channel with a cross-section of 3 x 3 mm^2, where a third sensor is placed (Figure 13, chapter 3.2.). A

perpendicular channel with a circular reservoir is connected to the first channel to allow placement of a reference electrode required for the OCP measurement of the sensors. The fluidic channel was designed in SolidWorks (Dassault Systemes, CAD, 2014) and milled in Polytetrafluoroethylene, PTFE, using CNC milling machine ICP 3020 (isel®, Eichenzell, Germany). A dedicated holder out of Plexiglas (PMMA) was designed in AutoCAD (Autodesk®, Munich, Germany) and laser cut with a CO^2 laser (VersaLASER®, Universal Laser Systems Inc., USA) to allow for secure handling of the sensors and electrodes without damaging them between electrode switching or solution changing. The electrical resistance R of the channel is calculated through the following equation:

$$R = \frac{1}{\sigma} \times \frac{L}{A} \tag{15}$$

where σ is the conductivity of the electrolyte, L the length of the channel and A the cross-section area of the channel. This equation enables to determine the voltage drop across the pH channel and determine the potential changes of the electrodes during DC stimulation.

4.9 Measurement software

4.9.1 NOVA

The electrochemical characterization data of the different types of electrodes are recorded through the software NOVA 1.11 (Metrohm AG, Germany). The data of the various measurements are then generated into Excel (Microsoft, USA) files utilizing the software NOVA 2.1 (Metrohm AG, Germany).

4.9.2 MATLAB

The obtained data is processed and analyzed through the MATLAB R2018b software (MathWorks, Natick, MA, USA). With this software, several codes were implemented in order to visualize and store the data for the different experiments and electrodes/sensors.

4.9.3 LabVIEW

The data obtained during the calibration and characterization of the pH sensors are processed using the software LabVIEW (National Instruments, 2019). A program, previously designed by José Leal, was used to convert the potential values acquired through the pH-readout into digital values. These are then processed by the software program and recorded in an Excel file.

4.10 Cytotoxicity tests

Cell viability is described as the ability of a cell to maintain homeostasis, i.e., proliferation, differentiation, and apoptosis. The cytotoxicity of the deposited CP is tested by verifying the membrane leakage (cytolysis tests by live/dead stainings), with RedOx assays (AlamarBlue Assay) according to DIN ISO 10993-5 and by Phase Contrast Microscopy to see changes in the cell morphology. The preparation of these tests is described in the section Supplementary materials 12.1. For the cytotoxicity tests, it was prepared sets of electrodes (Table 4); the PEDOT/PSS and the PDMAAp/PEDOT electrodes are prepared as previously explained. The electrodes coated with PEDOT are kept in PBS for at least 24 h after an electrochemical characterization (CV and EIS). The hydrogel electrodes are kept in distilled (DI) water as well for at least 24 h, and then, after the same electrodes characterization, the electrodes are saved in PBS. The hydrogel electrodes, without PEDOT deposition, are directly peeled off from the wafer coated with 3 layers of Hydrogel.

Table 4: Type of electrodes prepared for each test of cytotoxicity

	PEDOT	*Hydrogel*	*Hydrogel + PEDOT*
Number of samples	-	4	8
	4	4	4
	4	4	4
	6	6	6

The tracks and contact pads of the electrodes are cut off; each electrode is placed on top of a square micro slide of glass coated with PDMS. For some sets of electrodes, falcon rings are placed as well on top of the glass with the electrode on the center and fixed with Silicone Rubber Compound (Flowable

Fluid, RS 692-542) (Figure 24). The falcon rings are prepared by cutting falcon tubes of 15 mL in 6 pieces. Each micro slide is put in a well from a 6 Well Tissue Culture Plate (Falcon Sterile R, Ref 353046).

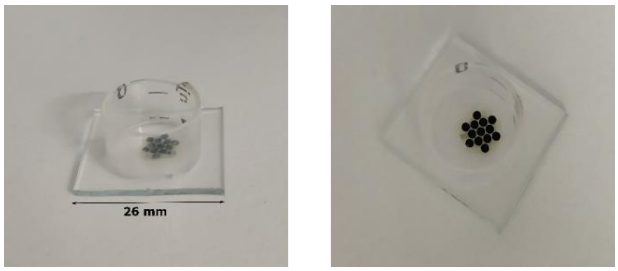

Figure 24: Micro glass slide with electrode centered inside a plastic reservoir.

5 Experimental

This chapter is divided into three main sections; the first section explains the experiments implemented for the characterization of the electrodes. The second part describes the pH calibrations and pH measurements during DC stimulation, and the last section explains how to perform the cytotoxicity tests by verifying the viability of the cells.

5.1 Electrodes characterization

Prior to testing the electrodes under DC stimulation with cells, it is necessary to characterize the electrodes under the same conditions as in an electrotaxis experiment. The main goal is to compare the conductive polymers, PEDOT and PDMAAp, in order to find the best material to coat the electrodes as well as testing the optimal electrode design.

5.1.1 DC stimulation setup

For the DC stimulation, a magnetic holder was designed and developed by Sebastian Shaner based on the work of Abhyankar et al., with the purpose of holding the electrodes on the PDMS channels in place [89]. The PDMS layer was peeled off a silicon wafer with SU-8 structures stamped on it and cut following the layouts of the structure. The magnetic holder and the glass coverslips were cleaned with Isopropanol and DI water before placing the first PDMS channel on it. The electrodes were placed into the reservoirs of the PDMS channel, and a second PDMS structure was placed on top of the first one. Due to the fact that the glass holders were getting between the two PDMS channels and preventing proper pressing of the electrodes, they were broken until the soldered contact to prevent any leakage. The magnetic lid was placed on top of both channels with the electrodes correctly placed, and each reservoir was filled with PBS through the openings on the top piece using a pipette (Eppendorf, Research plus, Germany). The openings of the magnetic lid were covered with PDMS pieces to prevent the evaporation of the PBS during the DC stimulation. The electrode on the left chamber was connected to the WE of the *Autolab PGSTAT* potentiostat while the other was connected to the CE and the RE shorted (Figure 25).

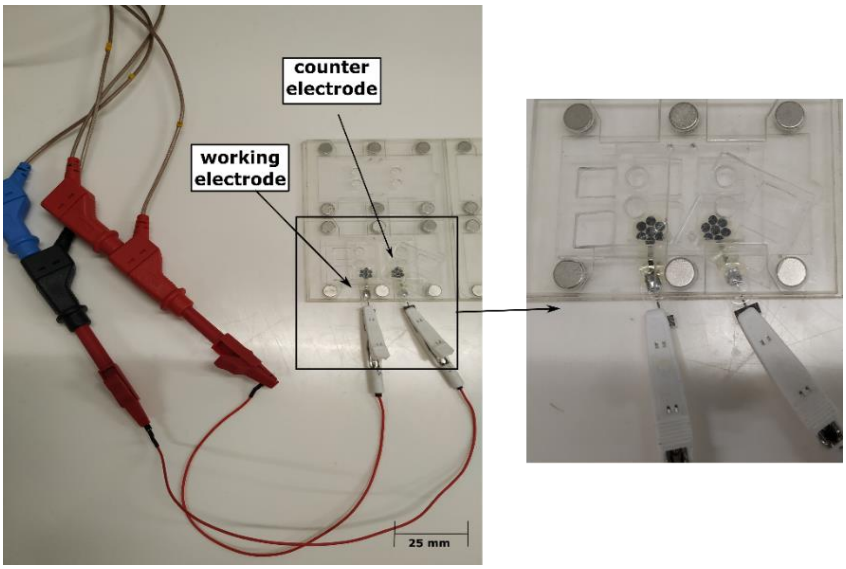

Figure 25: Setup for DC stimulation in microfluidic PDMS channel with PMMA magnetic holder.

5.1.2 Electrodes stability during DC stimulation

The setup used for the DC stimulation was based on a two-electrode setup, where the counter electrode also works as the reference electrode. Both electrodes had the same design and were coated with the same thickness of CP. As previously described in sections 4.1 to 4.3, the electrodes were prepared, characterized, and kept in PBS until the DC stimulation was done. A constant current of ±20 µA was driven for 1 h in each phase between the electrodes with a pause of 15 min between changes starting with the cathodic current (Figure 26). The OCP value was measured before each current was set, and at the end of the stimulation.

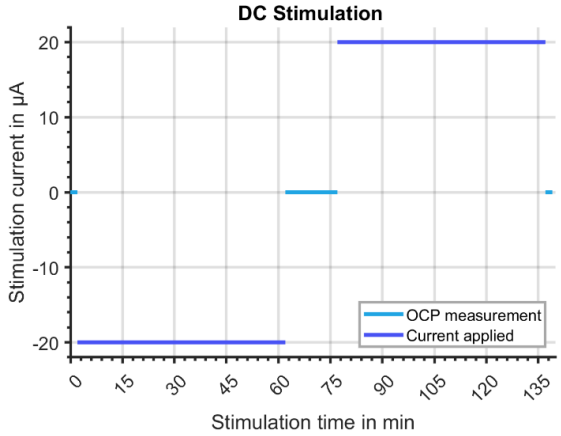

Figure 26: Schematic of the applied current during DC stimulation and the OCP measurements.

After the stimulation, the OCP, CV, and EIS of each electrode were measured individually to verify their stability after 2 h of stimulation. The electrodes were then kept in PBS again until further tests were performed. The surface of the electrodes was observed under a microscope (Leica Microsystems, Germany) before and after the DC stimulation to check for possible alterations.

5.2 pH measurements

The following section describes how the pH electrodes were calibrated before being used to detect any pH changes during DC stimulation. In the second part of this chapter, the setup for the pH measurements with DC stimulation is explained.

5.2.1 Calibration of the pH sensors

The setup for the calibration consists of three PCB adapters connected to the three pH electrodes an Ag/AgCl RE and a piece of stainless-steel to set the solution potential at 9.25 V. The pH electrodes were activated before any calibration or pH measurements, through OCP, CV and EIS measurements as described in section 4.2. The sensors were kept in the 8 mL beakers with PBS, held by a slit in the lid, and stored in a dry place at room temperature (Figure 27).

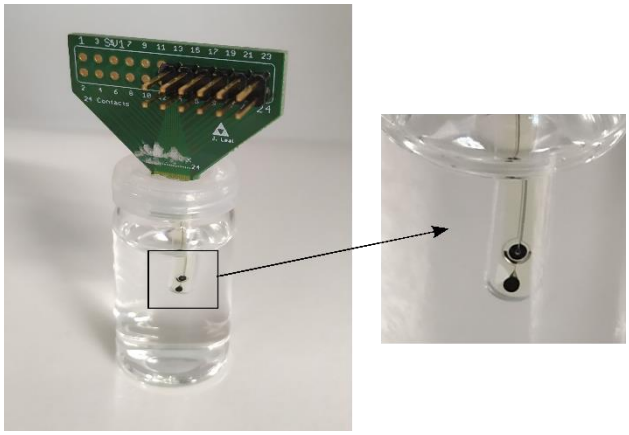

Figure 27: pH sensor kept in a beaker with PBS.

The sensor's response to pH changes was determined using several buffers with different pH values. The buffers were prepared with a pH range from 2 to 12 (cf. Annex 11.2 for buffer composition). The buffers were poured in 80 mL beakers, and the exact pH value of each solution was measured with a pH meter (Qph 70, VWR International GmbH, Darmstadt, Germany).

Each SIROF pH electrode was connected to the pH readout electronics, and the RE was connected to all three inputs simultaneously. Afterward, the electrodes were submerged in the first buffer, and the measurement of the SIROF potential was done (Figure 28). The sensors were in the solution for 1 min to stabilize the SIROF layers followed by 10 s of measurement at 1000 samples/s. Upon completion of the measurement, the electrodes were moved to the next buffer from the lowest pH value to the highest and then back to the lowest. After the first and the second round of measurements, the sensors were left for 2 min in PBS to wash off the residues of the buffer solutions.

At the end of the measurements, the average potential for each pH value was calculated, and the sensitivity of the sensors was determined through a linear approximation. The pH calibration procedure was done before every DC stimulation in the pH channel.

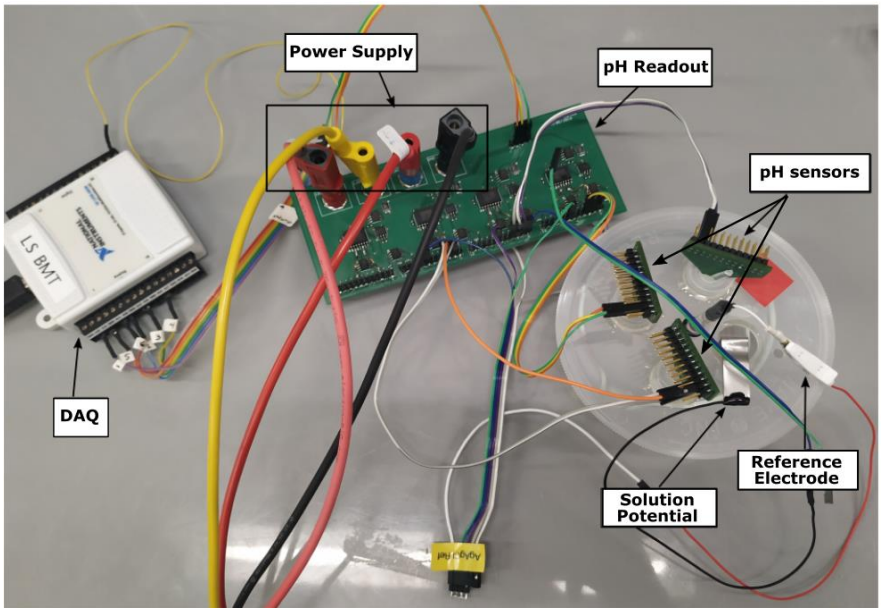

Figure 28: Measurement setup for pH calibration.

5.2.2 DC stimulation in pH channel

Measurement of transient pH changes during DC stimulation was done utilizing the pH channel described in section 4.8. After calibration of the pH sensors, these and the RE electrode were connected to the pH measurement hardware in the same way as they were connected for the calibration. The electrodes used for the DC stimulation were connected to the *Autolab PGSTAT* potentiostat, as explained in section 5.1.1.

The pH measurement was done over a time period of 45 min. Five minutes were measured before the stimulation took place to establish a baseline for the pH changes. Afterward, the constant current stimulation was done for periods of 15 min with 5 min pause in between each polarity starting with the anodic phase. The measurements were done in PBS and 0.9 % NaCl to distinguish between the potential changes elicited by the pH and by the changes in the concentration of ions in the solution (Figure 29).

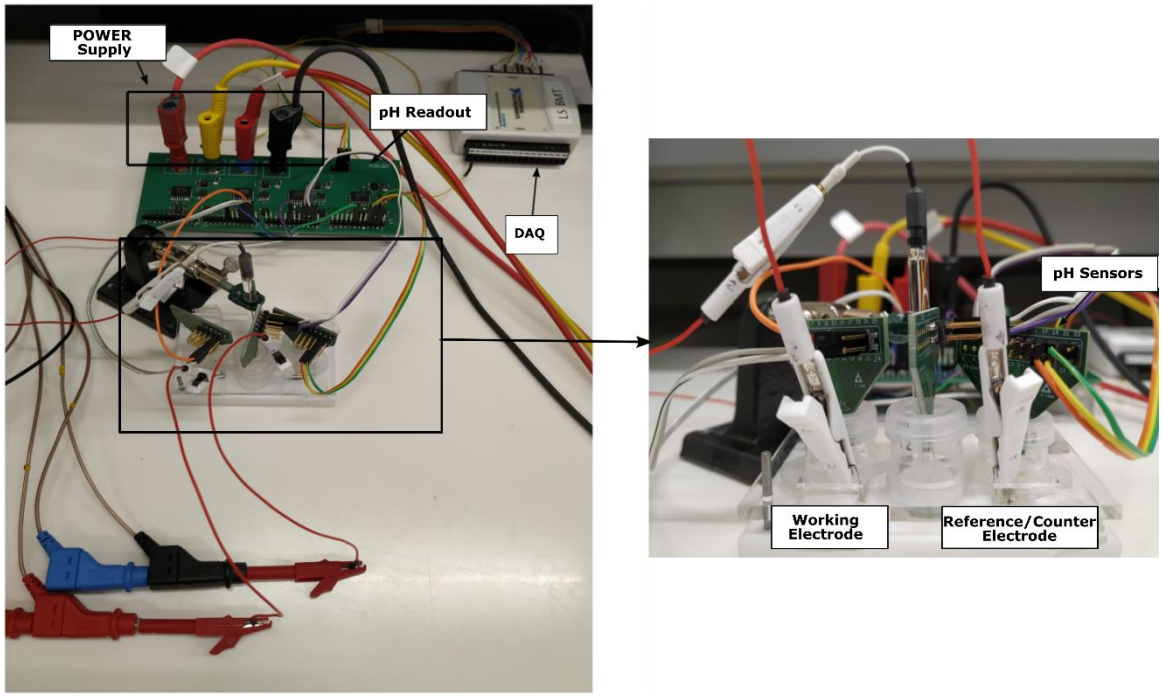

Figure 29: Setup for pH measurement during DC stimulation.

Different experiments were performed with different electrode coatings (IrOx, PEDOT/PSS, and PDMAAp/PEDOT) and varying currents to determine the pH changes of the employed solution. Initially, the current applied was of ±6 µA (Figure 30), and then it was increased to ±10 µA. The anodic and cathodic phases were inverted for a second stimulation.

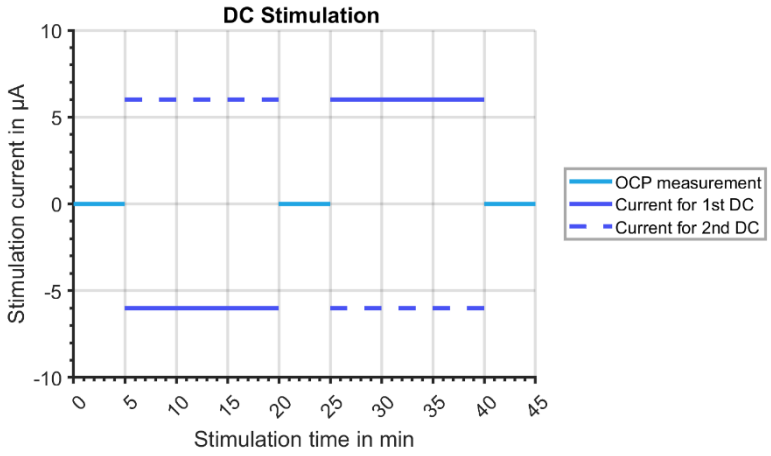

Figure 30: Applied current during DC stimulation for pH measurement.

The electrochemical pH measurements were verified in a separate experiment with the help of pH reactive paper (EMD Merck Millipore, Germany). Based on the diffusion properties of the electrodes it could be assumed that a small volume of solution in close proximity to the stimulating electrodes would show a different pH than the solution in the rest of the channel. The diffusion zone where pH changes were happening was calculated based on the distance r between the stimulating electrodes and the pH sensors. Due to the size of the electrodes, radial diffusion was assumed, which led to a volume of the diffusion zone of $V = 261$ mm^3 for a distance of $r = 5$ mm. Based on this result, it was safe to assume that taking a sample of the solution close to the stimulation electrode would allow for verification of the pH within the diffusion zone.

Small pieces of pH paper were placed in a Petri dish, and a small droplet (15 µL) of each buffer was applied to each paper to determine the reactivity of the paper to small volumes. Afterward, Petri dishes were prepared with 10 small pH papers to perform measurements every 5 min during the DC stimulation (Figure 31, a). Two Petri dishes with pH paper were prepared for each electrode (WE, CE) for each solution (Figure 31, b). After the stimulation was finished pictures of the results were taken and compared to the electrochemical measurements.

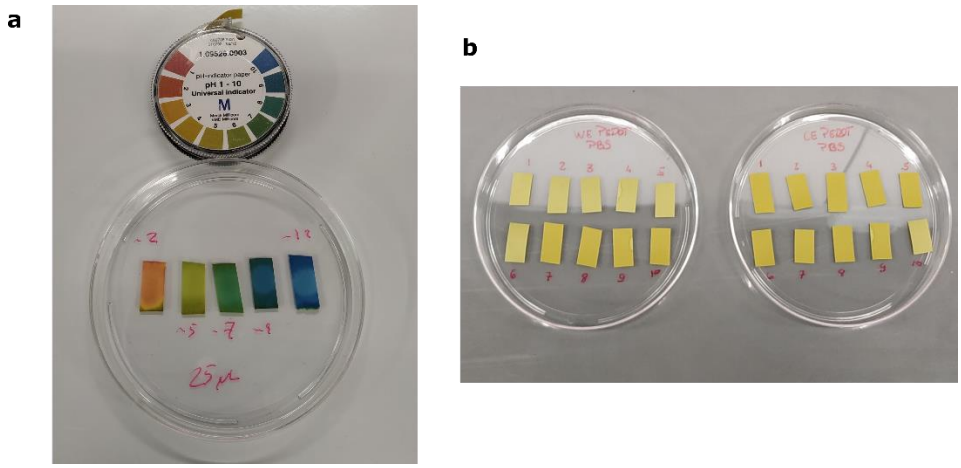

Figure 31: pH measurement with a colorimetric method:calibration with buffered solutions (25 µL) (**a**) and Petri dishes with pH paper for measurement during stimulation (**b**).

5.3 Cytotoxicity tests

The cytotoxicity experiments were performed by Nicole Jedrusik and are described in Supplementary materials 12.2.

6 Results

This chapter contains the results from the electrochemical characterization before and after the DC stimulations as well as the results from the calibration of the pH sensors. The results of the pH changes under electrical stimulation are also studied.

6.1 Fabrication of the Electrodes

The electrodes were fabricated on six wafers, where each wafer has four rows of electrodes, which are connected through a platinum shortcut. There are four designs per wafer, and each design contains a total of 10 electrodes (Figure 32). Two wafers were coated with hydrogel, one wafer with 3 layers and the other with 6 layers. The third wafer was used to prepare the PEDOT/PSS electrodes and the fourth wafer to prepare SIROF electrodes.

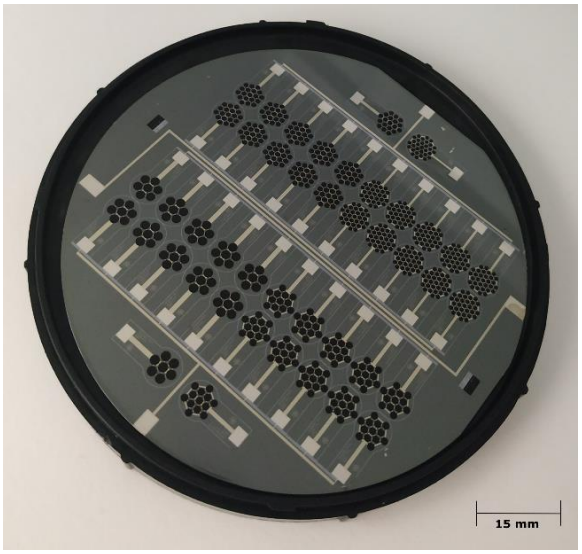

Figure 32: Fabricated wafer with different electrode designs.

After the fabrication of the electrodes, these were electrochemically activated and cleaned on a wafer level. The CV curves between the different rows on the wafer (W-1, W-2, W-3, and W-4) shown some slight differences and the current for all electrodes was high, reaching above 5000 µA (Figure 33).

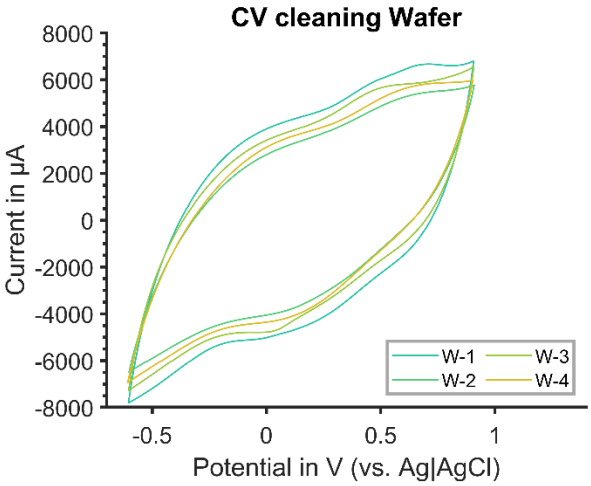

Figure 33: CV on wafer level, for 10 electrodes at the same time.

6.2 Electrode characterization

One of the first steps for the electrodes to be functional and stable for the electrotaxis experiments is a correct deposition of PEDOT and Hydrogel. The stability of the electrodes was studied through electrochemical characterization before and after the deposition of the conductive polymers.

6.2.1 PEDOT/PSS electrodes

In the graph before deposition are represented electrodes of IrOx, where two pairs of them were then coated with a thickness of 200 and 400 mC/cm^2 as well as one electrode of 600 and 800 mC/cm^2. Previous to the PEDOT deposition, all of the electrodes have similar CV curves and current values (Figure 34, a). The peak values of the current in these electrodes are ± 600 µA respectively, with slight variations amongst the different electrodes. After the deposition, the CV shows distinct curves with fewer peaks in between the maximum and minimum potential for each PEDOT thickness. An increase in the measured current was observed after coating, with higher currents corresponding to thicker layers. The curves showed no unexpected peaks or variations regardless of the electrode design (Figure 34, b).

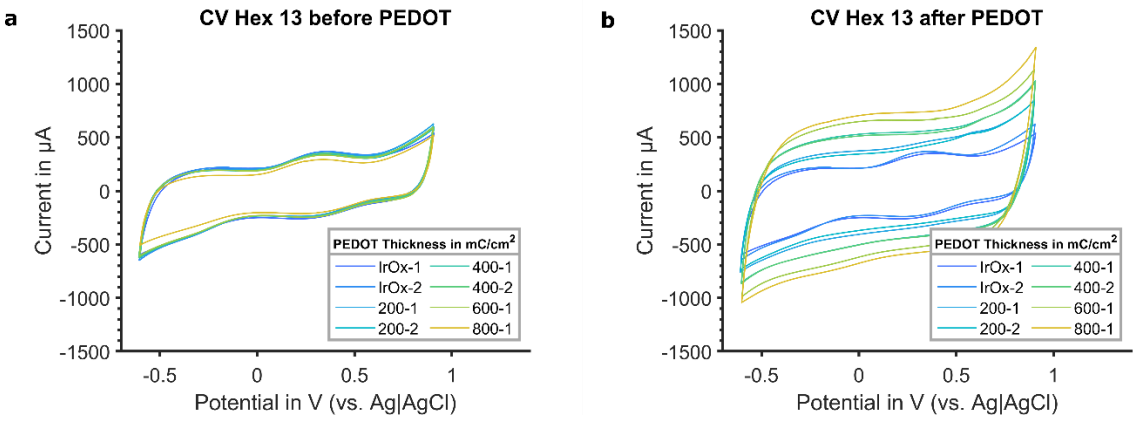

Figure 34: CV curves before (**a**) and after (**b**) PEDOT deposition for the Hex13 electrodes.

The impedance magnitude of the IrOx electrodes previous to PEDOT deposition is higher than the electrodes coated with the polymer (Figure 35, a). It can be seen that thicker coatings of the electrodes exhibit lower impedance, decreasing substantially from the bare metal electrodes to the PEDOT electrode with a thickness of 800 mC/cm² (Figure 35, b).

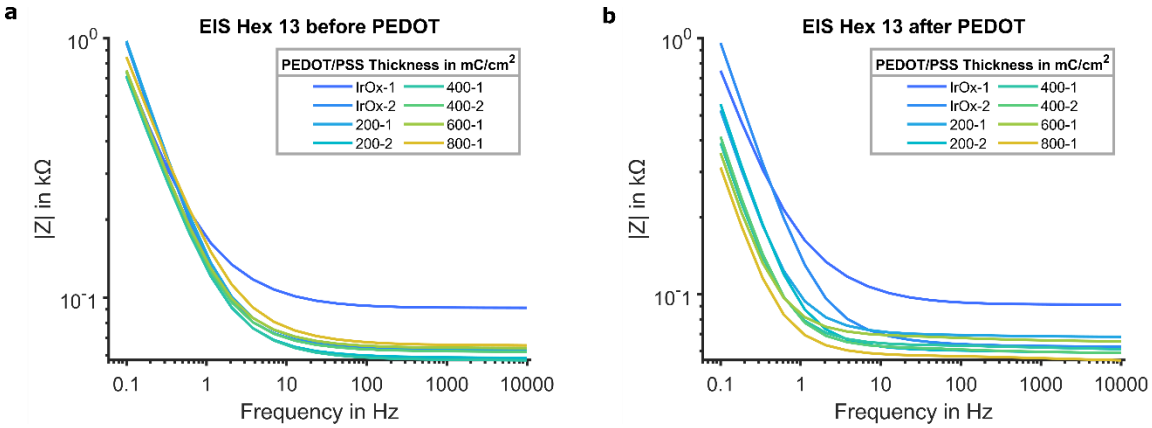

Figure 35: EIS curves before (**a**) and after (**b**) PEDOT deposition for the Hex13 electrodes.

An increase of the charge storage capacity could be observed after PEDOT deposition, as shown by the CV curves. The values of the CSC for the IrOx electrodes (Figure 36, a) were very similar amongst all different designs, with values ranging between 34 mC and 37 mC, with only two outliers. The electrodes coated with a thickness of 200 mC/cm² improved their CSC from around 35 mC to around 55 mC while the 400 mC/cm² almost doubled their CSC values to 70 mC/cm² (Figure 36, b). Small variations could be observed amongst the different designs, but no clear trend could be identified.

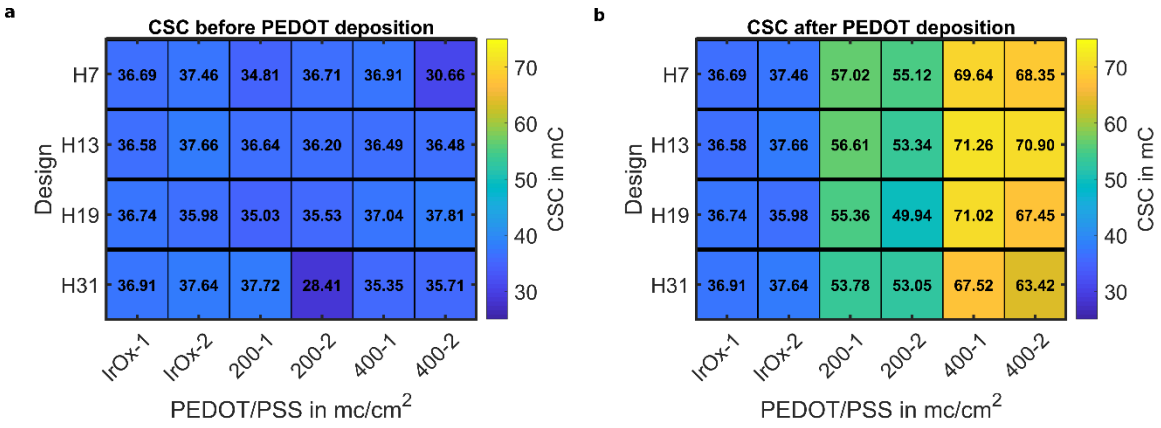

Figure 36: Charge storage capacity before and after PEDOT deposition.

6.2.2 (PDMAA)p electrodes

The electrodes coated with 3 and 6 layers of hydrogel (PDMAA)p and 200 – 400 mC/cm² of PEDOT show similar CV curves for all the different designs. The CV of the 6-layer electrodes shows a smaller area in comparison to the 3-layer electrodes with the same PEDOT concentration. Furthermore, the 3-layer electrodes with 400 mC/cm² thickness of PEDOT show more variations amongst the different designs than the 6-layer ones and the 3-layer with 200 mC/cm² thickness (Figure 37).

The impedance magnitude increased for electrodes with more layers of Hydrogel. It is similar through the electrode designs coated with 200 mC/cm² thickness of PEDOT, showing bigger differences for the thicker PEDOT coating (Figure 38). The 6-layer electrodes with 400 mC/cm² thickness showed a small distinction between the electrodes designs. For the 6-layer electrodes with 400 thickness, it can be seen that electrodes with smaller circumferences exhibited higher impedance than the ones with bigger circumferences (Figure 38, d).

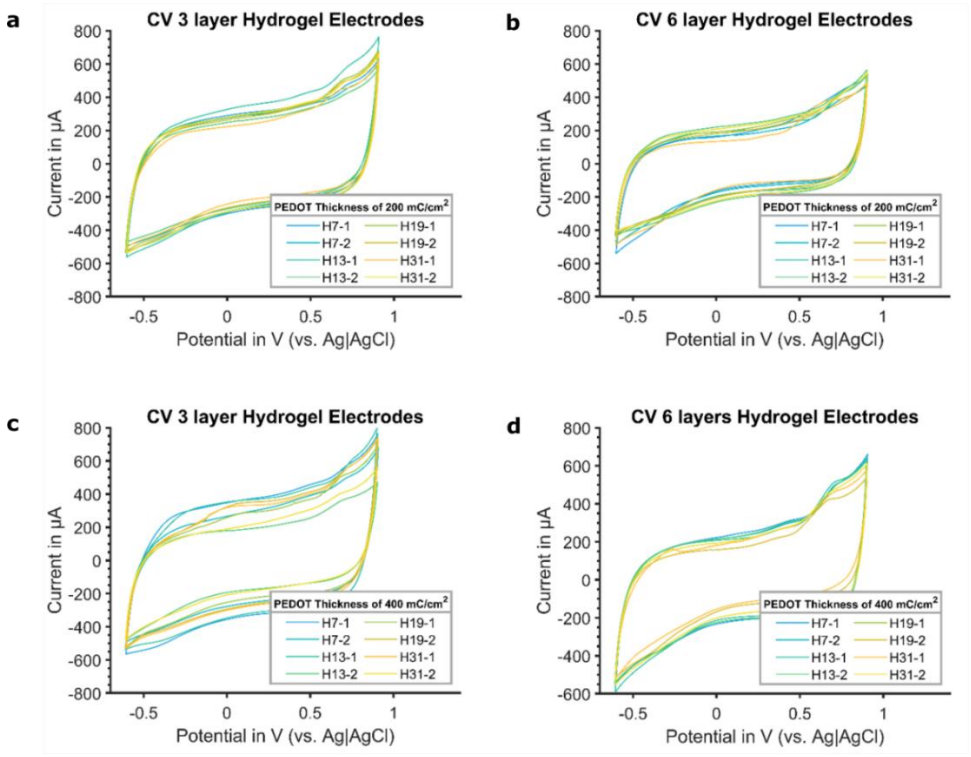

Figure 37: CV curve after PEDOT deposition for Hydrogel electrodeswith PEDOT thickness 200 mC/cm² and 3 layers (**a**) and 6 layers (**b**) of PDMAAp; and PEDOT thickness 400 mC/cm² and 3 layers (**c**) and 6 layers (**d**) of PDMAAp.

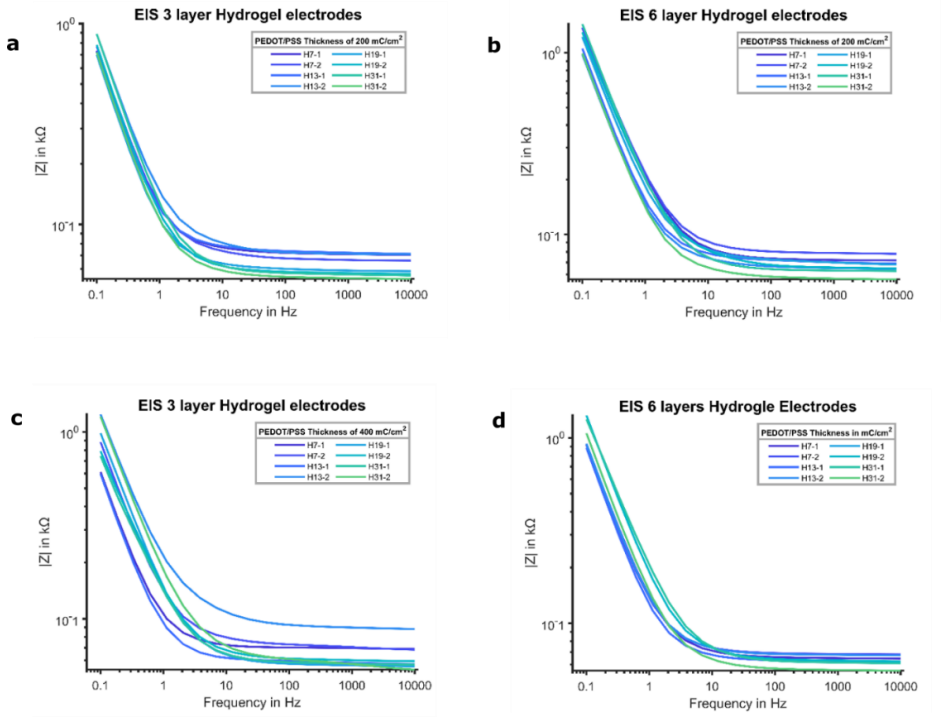

Figure 38: EIS curve after PEDOT deposition for Hydrogel electrodeswith PEDOT thickness 200 mC/cm² and 3 layers (**a**) and 6 layers (**b**) of PDMAAp; and PEDOT thickness 400 mC/cm² and 3 layers (**c**) and 6 layers (**d**) of PDMAAp.

Comparing the CSC values of the electrodes coated with PEDOT (Figure 37) and the PDMAAp:PEDOT electrodes (Figure 39), it is notable that the CSC of the Hydrogel electrodes is significantly lower. There is more variation amongst the different electrode and designs in comparison to PEDOT electrodes, however, no clear trend can be observed from these measurements. The 6-layer electrodes show less variation amongst designs and lower CSC than the 3-layer ones for the same PEDOT content.

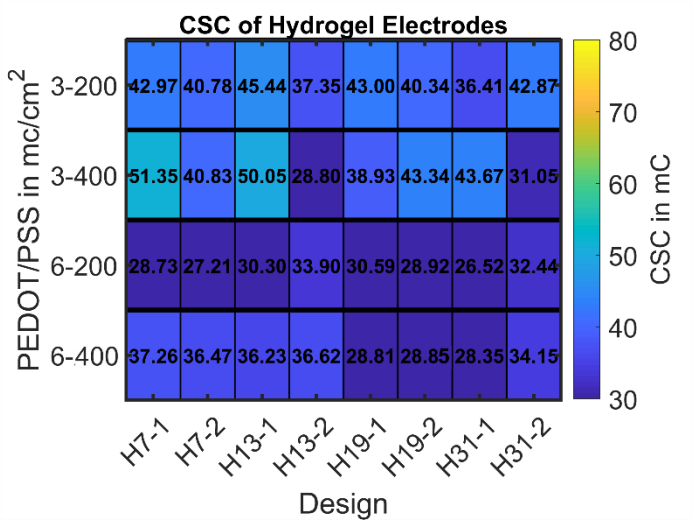

Figure 39: Charge storage capacity of Hydrogel electrodes.

6.3 DC Stimulation

After studying the stability of the electrodes, the different pairs of electrodes were stimulated, and the results are presented in the following sections.

6.3.1 PEDOT/PSS electrodes

The results of the PEDOT electrodes during the biphasic DC stimulation with a constant current of ±20 µA for 60 min (each phase) through all the stimulations show that most electrodes were stable through the stimulation (Figure 40). The pair of electrodes H7 with PEDOT thickness of 200 mC/cm^2 exhibit a stimulation potential extremely inconstant, reaching approximately 8 V in the last 30 min of the stimulation. There is no difference between the design of the electrodes in the potential. In the first 60 min of the stimulation (cathodic phase), the potentials vary more between the pairs of the electrodes, comparing with the anodic phase.

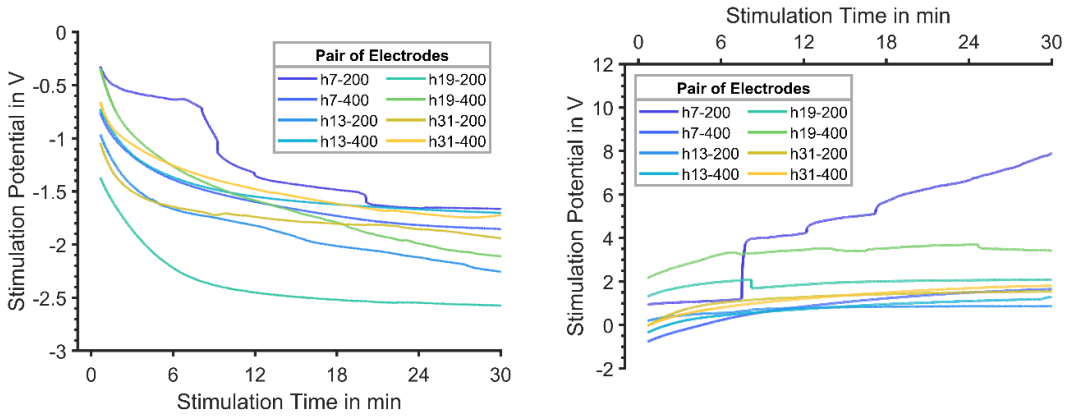

Figure 40: Stimulation potential of PEDOT electrodes for the last 30 min.

The absolute average potentials for the different pairs of electrodes was determined and is represented in Figure 41. The pair of electrodes H7-200 reached the highest value (≈ 8 V). The absolute value of the average potential for the last 30 min of stimulation was mainly between 1 and 3 V, with minimal differences between the stimulation polarities. A relationship between the potential and the different designs was not found. The pairs of electrodes coated with a PEDOT thickness of 400 mC/cm² have similar average potential in both phases of the DC stimulation. The electrodes coated with 200 mC/cm² show a more significant average potential difference between the cathodic and anodic phases; however, this difference decreases as the number of electrodes per design increases.

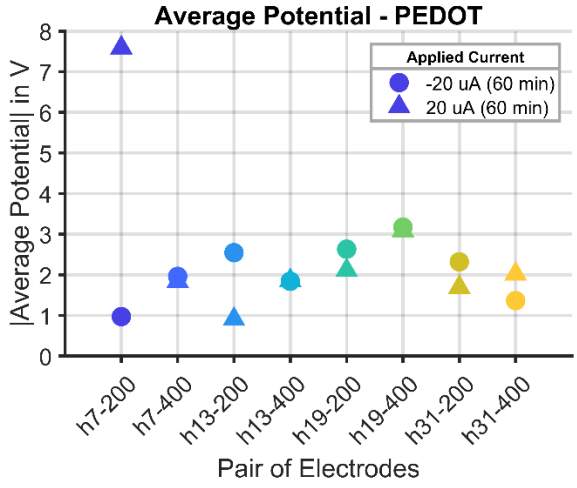

Figure 41: Average absolute potential of the different designpairs determined for the last 30 min of biphasic DC stimulation.

An apparent increase of the CSC values is visible for the different designs with a thickness of 200 mC/cm² before and after stimulation (Figure 42); however, for the design H7, the CSC value decreased for the WE (200-1). For the 400 mC/cm² thickness, there is an evident increase in the values of CSC after the stimulation for most electrodes; the CE (400-2) of the designs H13 and H19 show a smaller CSC value.

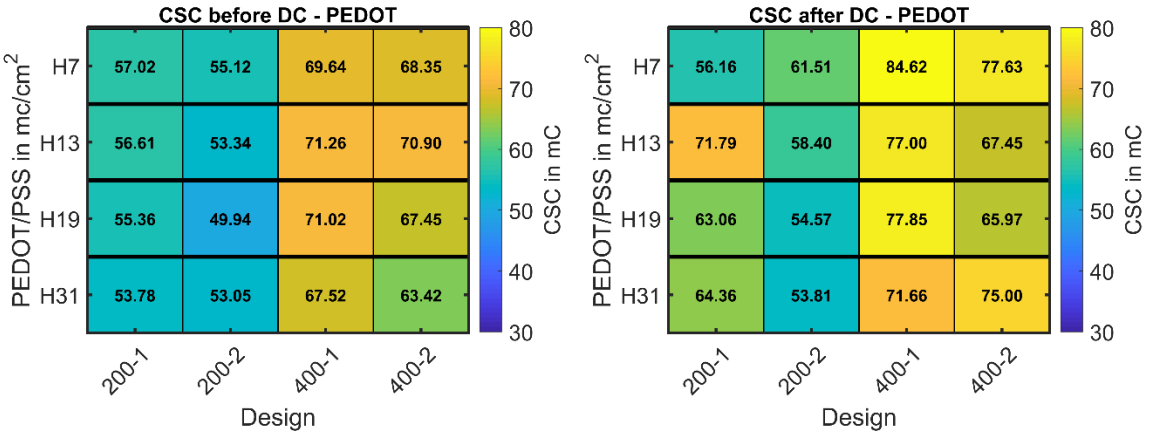

Figure 42: Charge storage capacity before and after DC stimulation.

6.3.2 PDMAAp/PEDOT electrodes

The current applied to the electrodes remained stable for all stimulations. The stimulation potential for the different pairs of electrodes is very constant for the hydrogel-3 electrodes. The measurement of the pair H7-200 in the cathodic phase and H31-400 are missing due to errors that occurred on the measurement software and in the files imported not allowing to export all the data. Furthermore, the stimulation potential for the hydrogel-6 electrodes was also quite stable. On the cathodic and anodic phase, it can be seen some instability on the electrodes H31-200 and H31-400, respectively (Figure 43). The stimulation potential was slightly higher for the electrodes with 6 layers than the 3-layer ones.

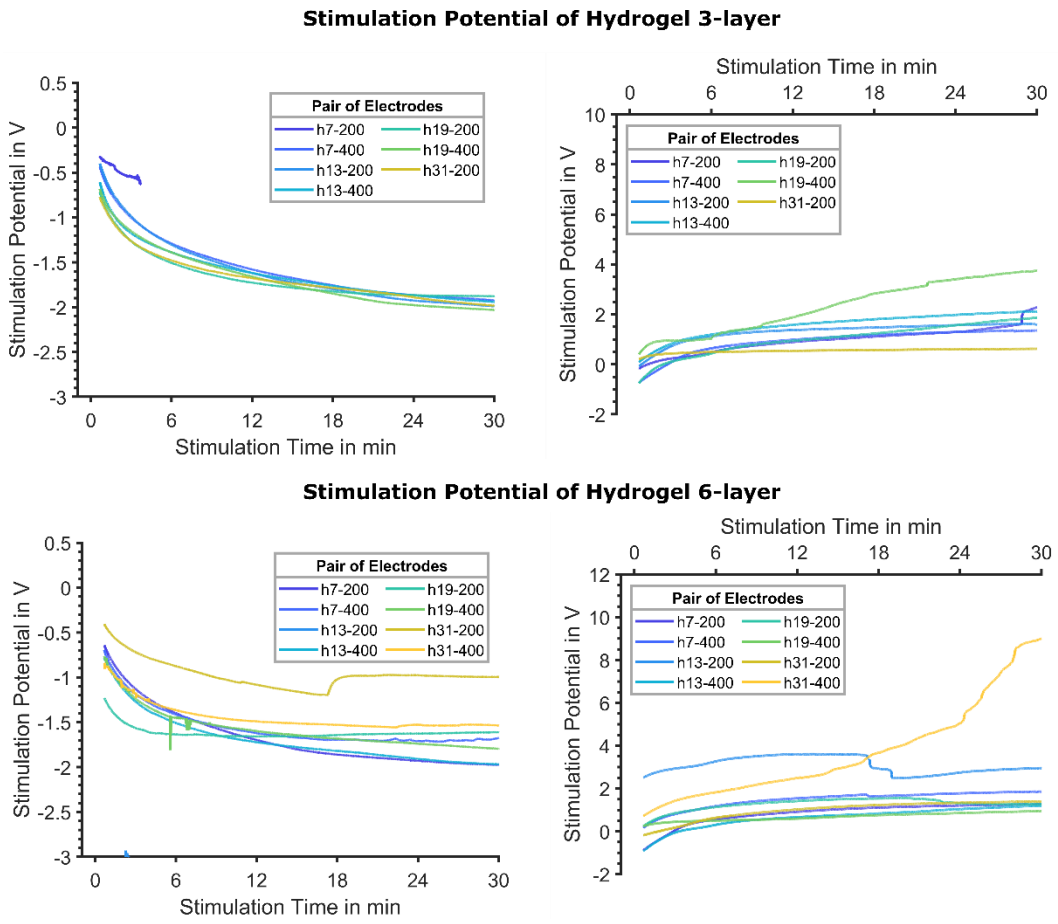

Figure 43: Stimulation Potential of hydrogel electrodes.

There is not an evident difference in the Average Potential between the different number of layers and the different designs of electrodes; however, for the 6 layer electrodes, the overall average potential is lower compared to the 3 layer electrodes (Figure 44). The pair of 3 layer electrodes H7-200 and H19-200 and the pair of 6 layers H31-400 were the least stables during the anodic phase of the stimulation, and the potential reached the highest values (≈ 8 V). The average potential was mainly between 0.5 and 3 V for the 3 layer electrodes and between 1 and 2.2 V for the majority of 6 layer electrodes. A relationship between the average potential and the design of the electrodes or the phase of the DC stimulation is not visible for this test.

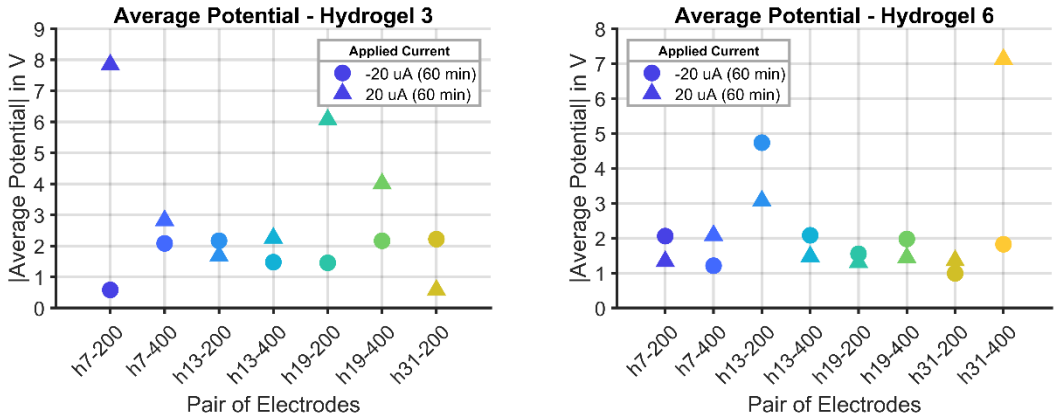

Figure 44: Average potential of the different designs during the biphasic DCstimulation for the 3 layer and 6 layer Hydrogel electrodes.

The CSC after the DC stimulation values were determined, and it can be seen an increase in these values compared with the ones previous to stimulation (Figure 45). Two exceptions to this increase are the electrodes H7-1 and H31-2 with PEDOT thickness of 200 mC/cm^2 and 3 layers (200-3), where a slight decrease on the charge storage capacity was detected. The CSC values for the electrodes with PEDOT thickness of 200 mC/cm^2 and 6 layers (200-6) are more similar throughout the different designs except for the electrode H19-2. For the electrodes with 6 layers of Hydrogel and 400 mC/cm^2 of PEDOT thickness, the similarity of the CSC between them before DC stimulation was no longer seen after the stimulation. Overall, the higher CSC values were obtained with the 3 layer Hydrogel electrodes and the lower ones with the 6 layer Hydrogel electrodes both coated with 200 mC/cm^2 of PEDOT thickness. There is no apparent difference between the WE and the CE, however, for the 3-layer electrodes before stimulation, the CSC of the CE was lower than the WE. After stimulation, the CSC kept being lower for the CE for the 400 thickness, and the same was not seen for all the 200 thickness electrodes. It is visible that the CSC values for hydrogel 6 are more similar between the designs than for hydrogel 3.

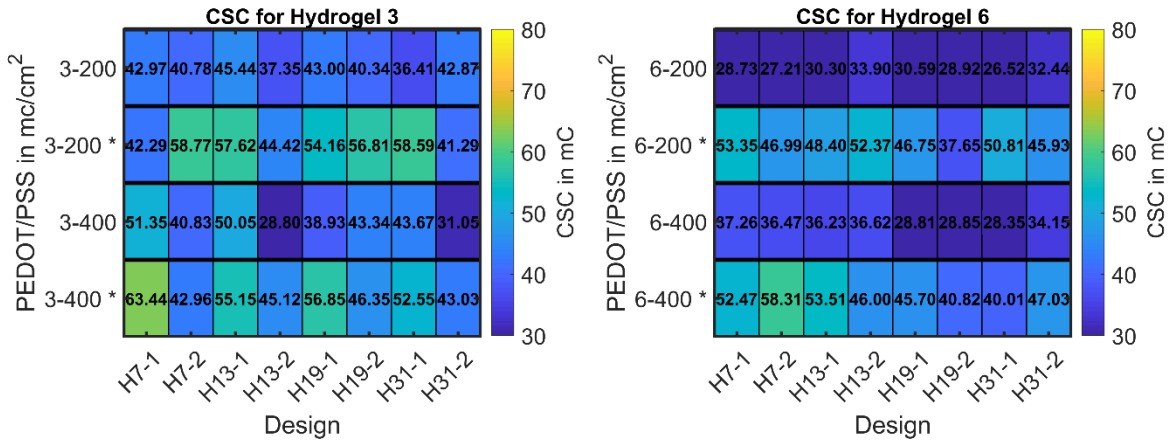

Figure 45: CSC values for the electrodes before and after (*) DC stimulation.

6.4 pH sensor calibration

The calibration of the three pH sensors was performed for 5 days before using them during DC stimulation. For every pH sensor, there were slight changes in the sensitivity through the different days of calibration, especially for the pH1 sensor, whose sensitivity decreased about 5 mV/pH within 5 days. The other two sensors, pH2 and pH3, varied slightly but did not show a constant decrease on sensitivity. None of the sensors showed significant drift over the calibration days, and all of them remained linear (Figure 46). The mean sensitivity of the sensors was determined and is represented in Table 5. All the sensors showed responses above the expected Nernstian behavior (≈ -59 mV/pH).

Table 5: Average Sensitivity of the pH sensors

Sensor	Average Sensitivity
pH1	-62.66 mV/pH
pH2	-64.50 mV/pH
pH3	-63.13 mV/pH

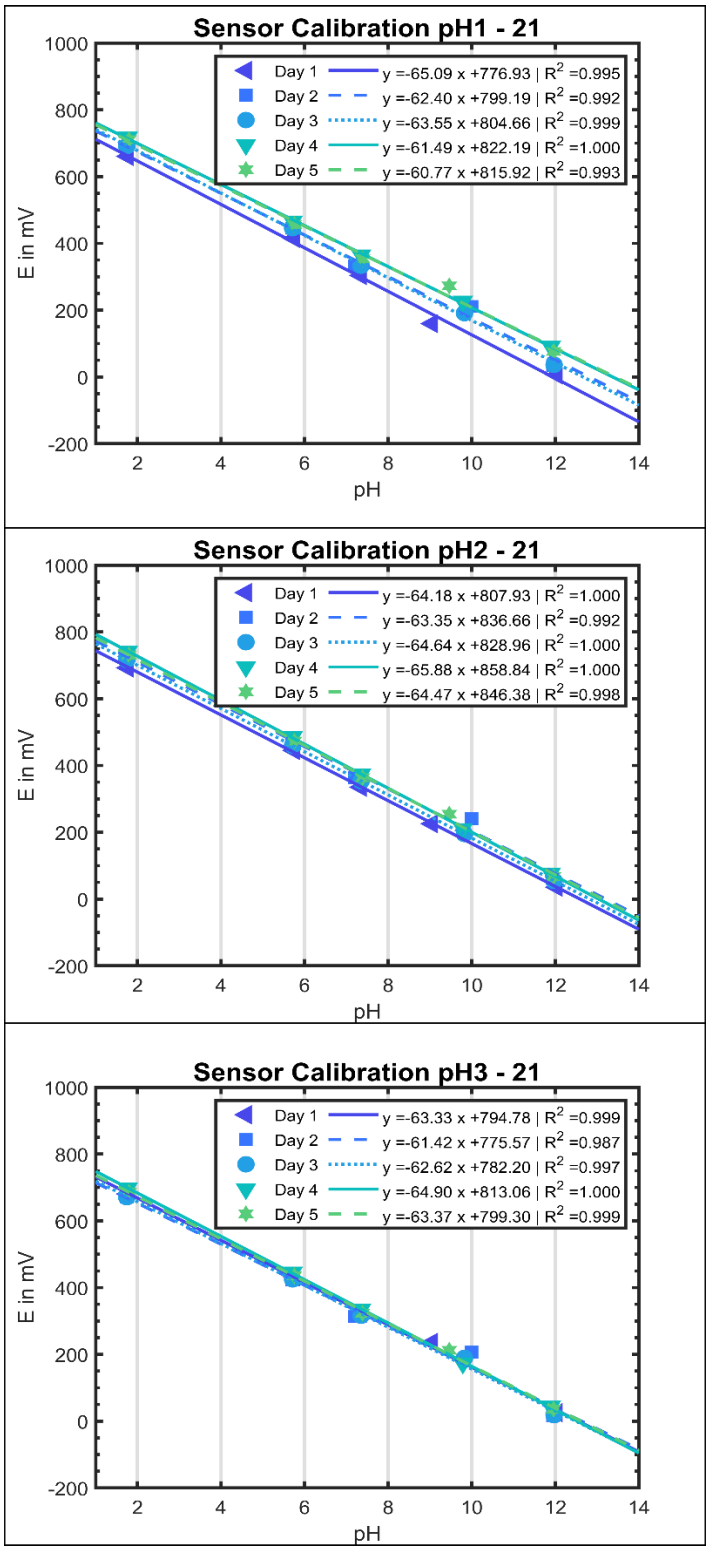

Figure 46: pH response of the sensor vs. Ag|AgClconnected to pin 21 during the sensor calibration period.

6.5 pH measurement during DC stimulation

6.5.1 Comparison of Stimulation Potential

Determination of the applied electric field and the achieved stimulation potential was done to correlate the pH changes that could happen inside a microfluidic channel to the macro channel where the measurements were conducted. The conductivity of the different solutions was measured at room temperature: the PBS conductivity is 15.43 mS/cm, and the NaCl is 17.40 mS/cm. The electric field strength E was calculated for the PDMS channels, and the pH channel using formula (1), and the values are indicated in Table 6.

Table 6: Values to determine the EF strength

	PDMS channel	*pH channel*
Current (I)	±20 µA	±10 µA
Width (W)	300 µm	3 mm
Height (h)	200 µm	3 mm
Conductivity (σ)	15.43 mS/cm	15.43 mS/cm
E	±216.03 mV/mm	±0.72 mV/mm

The electrical field strength of the PDMS channel is higher by a factor of 600 compared to the pH channel as expected for the different geometries. The average potential during stimulation in the PDMS channel and the pH channel (*) using different pairs of electrodes, H7, H13, and H19, was determined (Figure 47). The average potential is higher when the stimulation occurred in the PDMS channel during the anodic phase; the outliers (higher potentials) observed in the stimulation using the PDMS channel were excluded for the comparison between channels. In the pH channel, the average potential is very similar for both pairs of electrodes, in both cathodic and anodic phases. The average potential in the PDMS channel, considering the voltage drop across the channel, is very similar to the average potentials of the stimulation in the pH channel.

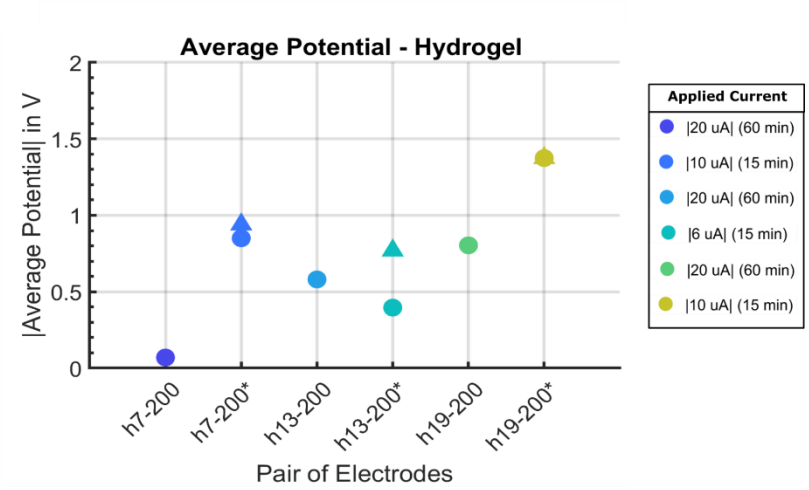

Figure 47: Average Potential on the PDMS channel and pH channel.

Afterward, the voltage drop (ΔV) on the different channels was determined considering the different conductivity of each medium, PBS and NaCl (Table 7). At first, it was determined the Resistance, R, of the channel using formula (15) and then, accordingly with the current applied, the ΔV was calculated.

Table 7: Values to determine the Voltage drop in the channels

channel	*pH*	*pH*	*PDMS*
R	2.16 kΩ	1.92 kΩ	32.41 kΩ
I	6 µA	10 µA	20 µA
ΔV_{PBS}	12.96 mV	21.60 mV	0.65 V
ΔV_{NaCl}	11.49 mV	19.16 mV	-

6.5.2 pH measurements

The average potential measured across the electrodes is slightly higher for the stimulation in PBS than in NaCl for all electrodes. The hydrogel electrodes had higher values than the other tested materials and less difference between the cathodic and anodic phases in PBS. The IrOx electrodes showed the second-highest average potential, whereas the PEDOT electrodes showed the most significant difference between the positive and negative phases (Figure 48). The potential for the stimulation with ±6 µA remained within the water window of platinum, except for IrOx electrodes, while the values for

±10 µA were clearly outside of it for the stimulation in PBS. However, no damage could be observed on the surface of the electrodes.

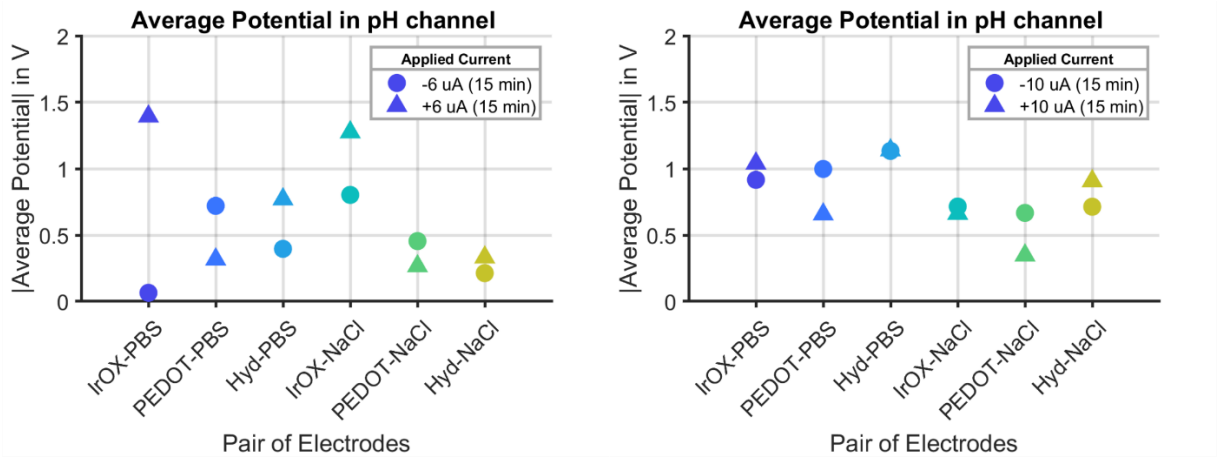

Figure 48: Average potential of DC stimulation in pH channel in PBS and NaCl.

The changes in pH measured during stimulation were only visible during the negative current and were more prominent near the CE (Figure 49). The only exception can be seen for the PEDOT electrodes in NaCl, where the pH sensors were affected by the accumulation of salt on its surface. The changes were always higher for the stimulation in PBS, most likely due to the differences in potential between both solutions. The changes in sensor potential at the RE were always in between the changes at the CE and WE in magnitude and started to change one to five minutes after the CE. The pH changes at the CE started immediately after the DC stimulation and reversed back once the stimulation stopped, with slower settling times for larger shifts in sensor potential (Δ pH). The pH shift curves have some oscillations for all the electrodes, due to the data processing since the sampling rate is lower than the velocity of pH change. The most significant pH changes were observed during the stimulation in PBS, reaching a value superior to -3. The changes in NaCl were smaller, reaching values around -2.

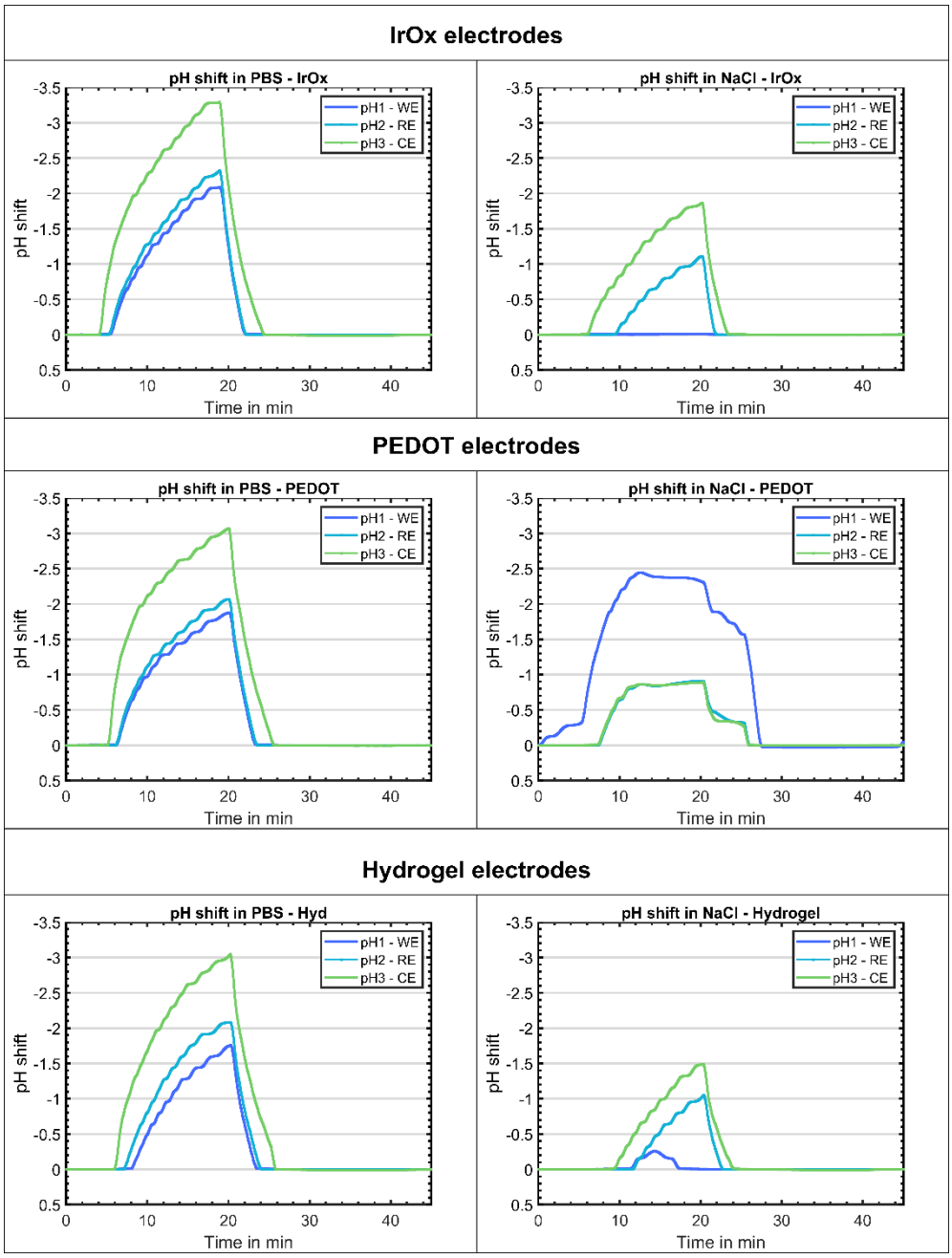

Figure 49: pH shifts for IrOx, PEDOT, and Hydrogel electrodesin PBS and NaCl.

During these experiments, the measured pH changes and the sensors were extremely large and without apparent reason as to why they were only happening during the anodic phase. Therefore, the same experiment was repeated, with chemical pH measurements. The average potential during the DC stimulation in PBS is very similar for both cathodic and anodic phases, while a larger difference and a decrease in potential can be observed in NaCl. The pH changes measured with the sensors were of approximately -2 pH values in PBS and -1 in NaCl. The measurements using the pH tape did not show any pH change for both electrodes and solutions (Figure 50). Slight alterations to the

measurement can be seen as a result of the manual extraction of solution for the chemical measurements.

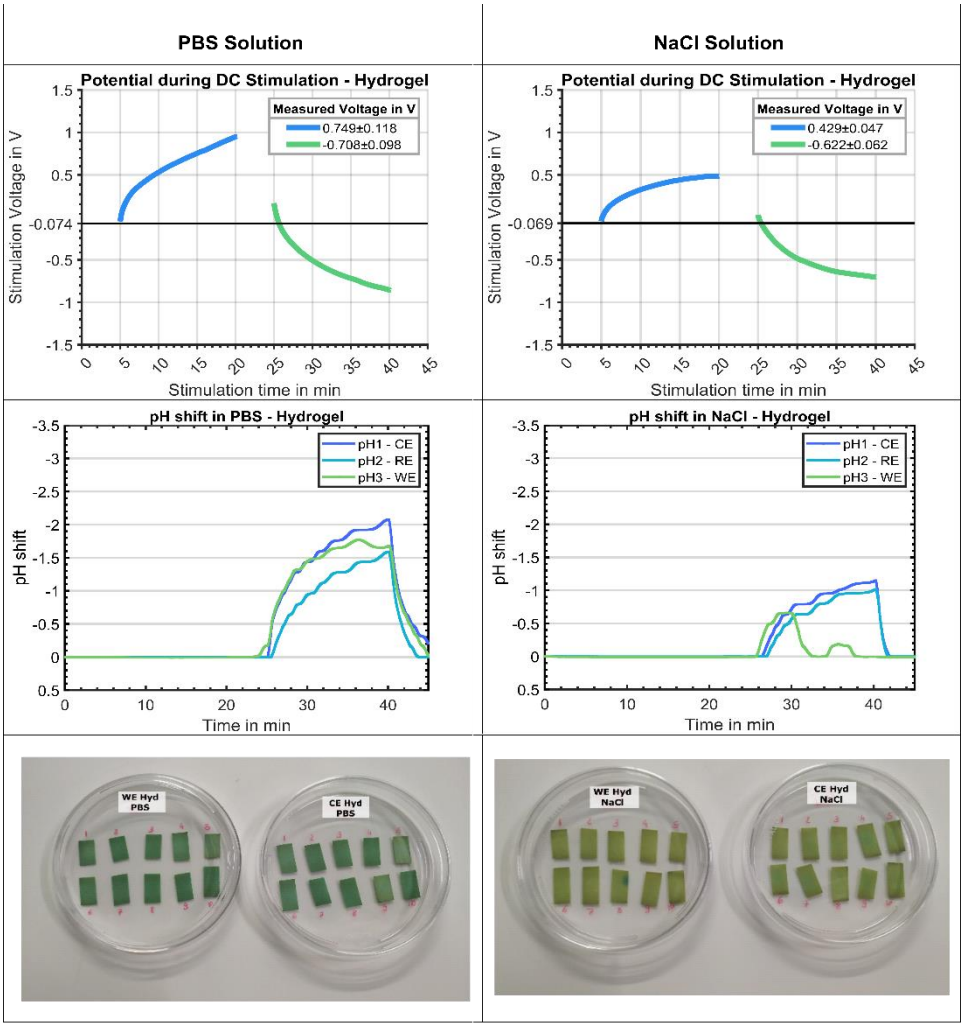

Figure 50: Potential and pH measurement during DC stimulation.(a) Potential during stimulation in PBS and NaCl mediums. (b) pH changes measured by pH sensors and pH readout. (c) pH measurements using pH paper.

6.6 Cytotoxicity Tests

The results obtained for the cytotoxicity tests are presented in the Supplementary material 12.3. After all the tests, no cytotoxicity was observable for any of the materials tested.

7 Discussion and conclusion

7.1 Electrodes characterization

The SIROF electrodes before PEDOT deposition were not identical, as can be observed in Figures 34 and 35. The difference between the electrodes can be due to some irregularities during the fabrication process, such as non-homogeneity during the sputtering of IrOx, damage of the surface during RIE, problems with the foil masks used during Mask alignment [90]. Despite some slight irregularities, the CV after PEDOT deposition showed a distinct difference between the wanted thicknesses as expected. More stability was visible in the electrodes coated with a thickness of 200 mC/cm^2 (Figure 36) than the ones with 400 mC/cm^2. Electrodes coated with a thicker layer, showed more variety and higher CSC values, as it was expected since for thicker layers of polymer, the charge storage capacity increases and the impedance decreases [91].

The electrodes coated with PDMAAp were cleaned on wafer level after the deposition of the hydrogel and showed some slight differences in the CV curves between the electrodes (Figure 37). The cleaning wafer method can also result in some electrodes with more impurities than others since 10 electrodes were cleaned at the same time. The CV performed to clean the wafer depends on the electrode design and surface. If there are differences on the surface of the electrode or more impurities, the impedance of the electrodes changes and the current is no longer divided equally through each wafer. Moreover, as the area of the electrode circumferences increases, there is a larger edge effect, and more current flows through these electrodes than the electrodes with smaller circumferences in the same row [78]. The CV of the 3 layers and 6 layers electrodes shows some differences between the electrodes that should have the same properties. The electrodes coated with 3 layers of PDMAAp have a bigger charge storage capacity than the electrodes with 6 layers of hydrogel (Figure 39). In the process of hydrogel coating, a thickness of hydrogel of approximately 5 µA is obtained when dipping the wafer 3 times [58]. Thicker layers of Hydrogel require longer time for the EDOT molecules to diffuse into the hydrogel network and reach the IrOx surface. Moreover, as the hydrogel volume increases, so does the impedance, which decreases current flow and subsequently the charge storage capacity. As expected, the CSC values are higher for PEDOT thicknesses of 400 mC/cm^2 in both hydrogel electrodes [92].

Comparing both type of electrodes, PEDOT/PSS with PDMAAp/PEDOT, it is possible to see that PEDOT electrodes have much higher values of charge storage capacity. This might be the result of how compact the PEDOT layer is on top of the IrOx electrodes, and how in the hydrogel network, the PEDOT is not as compact and does not have the same possibility of “trapping” the dopants in PEDOT’s

network. Therefore, fewer ions get into the PDMAAp/PEDOT layer, resulting in a lower charge storage capacity [92].

7.2 DC stimulation

The DC stimulation performed showed stability for all electrodes, except for some outliers. The stimulations in the PDMS channel had some difficulties associated, such as the preparation of the setup so that there would not be any leakage of the solution and the evaporation of PBS during some stimulations, leading to abnormalities in the stimulation potentials (Figure 40 and 43).

The stimulation with PEDOT electrodes showed that thicker PEDOT layers were more unstable than thicknesses of 200 mC/cm^2 (Figure 40). This is due to the fact that electrodes with a thicker layer, have a larger volume and during DC stimulations will be under more stress and can damage faster. The stress occurs from the absorption of ions in the polymer layer, which will make the polymers swell [91]. Mechanical stress can also occur during the preparation of electrodes and when setting up every experiment. The slight differences on the surface of the electrode before stimulation, results on conductivity differences, leading to one electrode being more oxidized/reduced after the stimulation than the other, which explains the differences between the CSC values of the WE and CE (Figure 42) [48].

The stimulation with hydrogel electrodes exhibited overall a very similar absolute average potential for all electrodes, considering the stable pairs during the stimulation (Figure 44). The CSC increased after DC stimulation, except for two outliers. It is evident the increase for the electrodes with 6 layers, that can be explained by the fact that since there are more layers of the hydrogel, the volume is bigger and more ions can be absorbed into the PDMAAp/PEDOT network [93].

The increase of the charge storage capacity for the electrodes with 3 layers is also seen; however, the values did not increase as much, and there is not the same similarity between electrodes as there is in the 6 layer ones (Figure 45).

The PDMAAp/PEDOT electrodes are able to DC stimulate for long periods of time with constant currents and achieving constant potentials, without showing any type of surface damage. The electrical properties of these electrodes demonstrated to be very similar to the PEDOT electrodes properties and can be increased by increasing the amount of PEDOT within the hydrogel network. Thicker CPs

coatings within a PDMAAp electrode can be more stable since the hydrogel has the necessary mechanical properties and high ionic permeability [92], [94].

7.3 pH measurements

The pH sensors were always stable during the calibrations, showing that they function correctly and are able to detect changes in the pH correctly without drifting (Figure 46). The voltage drop was determined for stimulations that are within the safe range (water window of platinum) for the electrodes, as the stimulation in the PDMS channel and the ±6 µA in the pH channel, and for those that exceed the safe rate (±10 µA in the pH channel). Since the voltage drop is small, and not enough to affect the stimulation potential during the measurements, any pH changes that would occur could be detected by the sensors.

The absolute average potential of the stimulation, was higher for the electrodes in PBS than in NaCl, as expected. NaCl has higher conductivity than PBS, therefore lower impedance, not requiring to achieve high potentials as the electrodes in PBS. The absolute average potentials for the stimulation with a current of ±6 µA are lower as the ones obtained for ±10 µA for the PEDOT and PDMAAp/PEDOT electrodes, which was expected since an increase on the current for the same resistance of the channel will require higher potentials (Figure 48). However, the IrOx electrodes reached really high potentials, and a big difference between the stimulation phases in the ±6 µA stimulation was seen, suggesting that these stimulations were not as stable as the ones with ±10 µA applied, possibly due to bad connections, or solution leakage.

Regarding the electrochemical pH measurements, pH changes were only detected during the anodic phases for the stimulation with ±10 µA applied, and the most significant changes were measured mainly in the CE (Figure 49). Explanations to these results can be changes in salt concentration within the diffusion layer as a result of the ionic stimulation, the way the potentiostat applies the potential, or even actual pH changes. pH paper was used to verify if there were indeed changes in the pH values throughout all the stimulations, and no slight pH decrease was seen (Figure 50).

A possible reason for the incorrect measure could be the changes in the salt concentration due to ionic stimulation. Both solutions, PBS and NaCl, have ions that will migrate away from the anode (Na^+) and react with the dopant PSS present on PEDOT, decreasing the phosphate and Cl^- concentrations, and subsequently decreasing the buffer capacity [74]. This could explain the pH changes in the CE when it is the anode; however, when the polarity was reversed, the same was not observed in the WE, excluding this hypothesis.

The pH sensors were stable and worked perfectly during pH calibrations, however, they might be affected when measuring changes next to electrodes during stimulation. The stimulation would be affecting the potential of the sensor, resulting in detecting false pH values. The potentiostat controls the current flow between the WE and CE in a galvanostatic mode and measures the potential difference between the Sense (S), which is shortened to the WE, and RE, which is shorted to the CE in a two-electrode setup. The potentiostat applies the current through the CE while trying to adjust the potential between RE and WE. This current flow can only be achieved if the CE changes its potential, which subsequently changes the RE potential and prevents the potential of the WE to be shifted. [95].

Electrode polarization of SIROF sensors can occur in the presence of high potentials. The CE is most likely polarizing the SIROF sensor when the current driven through it is ±10 µA, which can explain why the sensors are exhibiting the highest changes in the CE and measuring potential differences [88], [96]. Therefore, the sensors are measuring a potential difference besides the pH changes. A possible solution for this problem would be designing a new setup for differential pH measurements, where the potentials measured by the sensors would be subtracted, remaining only the pH change detected.

7.4 Cytotoxicity

None of the electrodes materials, either PEDOT, PDMAAp:PEDOT or simply PDMAAp, provoked cytotoxicity in cells. Some cytotoxicity was visible at the beginning of the experiments (first 24 h) for the hydrogel electrodes, however, after some hours this effect disappeared. This changes might have been due to the hydrogel absorbing part of the medium, leaving the cells without the necessary conditions to survive, leading a slight number of cell death and vitality. Moreover, the morphology of the cells was observed, and no changes were seen, concluding that both these materials have no toxic effect on cells.

8 Summary

In the realization of this thesis, several electrode designs were developed, fabricated, and characterized. The stability of the hydrogel electrodes, PDMAAp/PEDOT, was established and compared with PEDOT/PSS and IrOx electrodes. A channel was fabricated for the DC stimulation, and a new setup for electrotaxis experiments and pH measurements was created and fabricated. A circuit was designed to read the values measured with the pH sensors and fabricated. Moreover, new setups for cytotoxicity tests were fabricated. The following achievements were reached during this work:

- Development and fabrication of a batch of electrodes, as well as, coating of homogeneous hydrogel layers on wafers and development of a wafer-level cleaning process. DC stimulation was performed with different currents (±6, ±10 and ±20 μA) and different setups (PDMS and pH channels) for the same electrodes. All electrodes showed mechanical and electrical stability before PEDOT deposition, proving that the fabrication methods are successful.
- The electrodes developed were easy to handle and easy to coat with different thicknesses of PEDOT. The materials of electrodes were characterized during and after DC stimulation, which was performed with the same circumstances expected in a live-cell electrotaxis experiment and with extreme circumstances. The electrodes exhibited a stable stimulation potential for all the stimulations, and no relevant difference was seen between the designs or the materials of the electrodes. PDMAAp/PEDOT electrodes showed good electrical properties, which can be improved with higher thickness of PEDOT.
- pH sensors were implemented to determine pH changes during DC stimulation with different currents and electrode materials, and a channel was designed and fabricated for the pH measurements to be done as close as possible to the electrodes and within a fluidic channel to carefully monitor the changes in the electrode's surroundings. Significant pH changes were detected by the sensors, and pH paper was used to verify theses changes, which were not visible. The system pH readout, sensors, and stimulation were not working correctly. Therefore, the stimulation with high currents applied did not generate changes in the pH of the solution near the electrodes.
- The cytotoxicity of the polymers on the electrodes was tested to analyze their effects on cells, such as human keratinocytes and fibroblasts. No cytotoxicity and morphology changes were detected, concluding that these materials can be used without damaging the cells.

9 Outlook

The methods and processes used in the realization of this work proved that the hydrogel electrodes are mechanically and electrochemically stable, and further tests and research should be done. However, process optimizations are needed to improve the pH measurements system and to unsure further advances on the hydrogel electrodes.

Electrode optimization:

- Development an easier way to coat the electrodes wafer with hydrogel, that also allows selecting how thick the CP layer should be.
- Decide on an optimal design, since there is no significant difference between the designs studied in this work.
- Investigate the mechanical and swellability properties of the PDMAAp/PEDOT electrodes through bend testing and AFM measurements during stimulation.
- Develop a way of coating the electrodes with PEDOT also on wafer-level.

Improvement of pH measurements:

- Develop a differential pH readout system to detect real pH changes, independently on the current applied or on the potential measured.
- Develop and fabricate new pH sensors, more stable, and easier to handle without damaging them.

Further experiments:

- Stimulation of cells using the PDMAAp/PEDOT electrodes.
- Increase the thickness of PEDOT on the hydrogel electrodes to test how it can increase the electrical properties of the electrode.
- Long-term stimulation to determine the stability of electrodes and to prove the concept of stimulation in wound healing.

10 Bibliography

[1] B. Song, Y. Gu, J. Pu, B. Reid, Z. Zhao, and M. Zhao, "Application of direct current electric fields to cells and tissues in vitro and modulation of wound electric field in vivo," *Nat. Protoc.*, vol. 2, no. 6, pp. 1479–1489, 2007.

[2] B. Cortese, I. E. Palamà, S. D'Amone, and G. Gigli, "Influence of electrotaxis on cell behaviour," *Integr. Biol. (United Kingdom)*, vol. 6, no. 9, pp. 817–830, 2014.

[3] S. Zhao *et al.*, "ElectroTaxis-on-a-Chip (ETC): An integrated quantitative high-throughput screening platform for electrical field-directed cell migration," *Lab Chip*, vol. 14, no. 22, pp. 4398–4405, 2014.

[4] X. M. Shao and J. L. Feldman, "Micro-agar salt bridge in patch-clamp electrode holder stabilizes electrode potentials," *J. Neurosci. Methods*, vol. 159, no. 1, pp. 108–115, 2007.

[5] J. Li and F. Lin, "Microfluidic devices for studying chemotaxis and electrotaxis," *Trends Cell Biol.*, vol. 21, no. 8, pp. 489–497, 2011.

[6] R. Balint, N. J. Cassidy, and S. H. Cartmell, "Conductive polymers: Towards a smart biomaterial for tissue engineering," *Acta Biomater.*, vol. 10, no. 6, pp. 2341–2353, 2014.

[7] D. Alemu, H. Y. Wei, K. C. Ho, and C. W. Chu, "Highly conductive PEDOT:PSS electrode by simple film treatment with methanol for ITO-free polymer solar cells," *Energy Environ. Sci.*, vol. 5, no. 11, pp. 9662–9671, 2012.

[8] C. Boehler, M. Ieee, M. Asplund, and M. Ieee, "PEDOT as a high charge injection material for low-frequency stimulation," vol. 49, no. 0, pp. 2202–2205, 2018.

[9] Z. Shi, X. Gao, M. W. Ullah, S. Li, Q. Wang, and G. Yang, "Electroconductive natural polymer-based hydrogels," *Biomaterials*, vol. 111, pp. 40–54, 2016.

[10] A. S. Hoffman, "Hydrogels for biomedical applications," *Adv. Drug Deliv. Rev.*, vol. 64, no. 2–3, pp. 18–23, Dec. 2012.

[11] L. C. Kloth, "Electrical Stimulation Technologies for Wound Healing," *Adv. Wound Care*, vol. 3, no. 2, pp. 81–90, 2014.

[12] P. Martin and P. Martin, "Wound Healing — Aiming for Perfect Skin Regeneration," *Science (80-.).*, vol. 75, no. 1997, pp. 75–81, 2014.

[13] M. E. Mycielska and M. B. A. Djamgoz, "Cellular mechanisms of direct-current electric field effects: Galvanotaxis and metastatic disease," *J. Cell Sci.*, vol. 117, no. 9, pp. 1631–1639, 2004.

[14] A. Guo *et al.*, "Effects of physiological electric fields on migration of human dermal fibroblasts," *J. Invest. Dermatol.*, vol. 130, no. 9, pp. 2320–2327, 2010.

[15] R. Sanger, P. J. S. Smith, P. Nuccitelli, S. Ramlatchan, and R. Nuccitelli, "Imaging the electric field associated with mouse and human skin wounds," *Wound Repair Regen.*, vol. 16, no. 3, pp. 432–441, 2008.

[16] K. R. Robinson and M. A. Messerli, "Left/right, up/down: The role of endogenous electrical fields as directional signals in development, repair and invasion," *BioEssays*, vol. 25, no. 8, pp. 759–766, 2003.

[17] N. Gene, S. Property, R. Playing, and I. R. Williams, "Fibroblast Learn more about Fibroblast Fibroblasts Fibroblasts," 2019.

[18] S. Werner, T. Krieg, and H. Smola, "Keratinocyte-fibroblast interactions in wound healing," *J. Invest. Dermatol.*, vol. 127, no. 5, pp. 998–1008, 2007.

[19] J. Pu and M. Zhao, "Golgi polarization in a strong electric field," *J. Cell Sci.*, vol. 118, no. 6, pp. 1117–1128, 2005.

[20] J. Hunckler and A. de Mel, "A current affair: Electrotherapy in wound healing," *J. Multidiscip. Healthc.*, vol. 10, pp. 179–194, 2017.

[21] J. M. Reinke and H. Sorg, "Wound repair and regeneration," *Eur. Surg. Res.*, vol. 49, no. 1, pp. 35–43, 2012.

[22] M. Zhao *et al.*, "Electrical signals control wound healing through phosphatidylinositol-3-OH kinase-γ and PTEN," *Nature*, vol. 442, no. 7101, pp. 457–460, 2006.

[23] R. R. Isseroff and S. E. Dahle, "Electrical Stimulation Therapy and Wound Healing: Where Are We Now?," *Adv. Wound Care*, vol. 1, no. 6, pp. 238–243, 2012.

[24] J. A. L. Monaco and W. T. Lawrence, "Acute wound healing: An overview," *Clin. Plast. Surg.*, vol. 30, no. 1, pp. 1–12, 2003.

[25] V. Moulin, F. A. Auger, D. Garrel, and L. Germain, "Role of wound healing myofibroblasts on re-epithelialization of human skin," *Burns*, vol. 26, no. 1, pp. 3–12, 2000.

[26] I. Cell, "Learn more about Inflammatory Cell Cell Injury , Cellular Responses to In- jury , and Cell Death," 2009.

[27] H. Brem and M. Tomic-canic, "Cellular and Molecular Basis of Wound Healing in Diabetes," *J. Clin. Invest.*, vol. 117, no. 5, pp. 1219–1222, 2007.

[28] P. Carrier *et al.*, "Characterization of wound reepithelialization using a new human tissue-engineered corneal wound healing model," *Investig. Ophthalmol. Vis. Sci.*, vol. 49, no. 4, pp. 1376–1385, 2008.

[29] H. E. Desjardins-Park, D. S. Foster, and M. T. Longaker, “Fibroblasts and wound healing: an update " Increased comprehension of dermal fibroblast heterogeneity may yield both mechanistic insights into existing therapies and inspiration for novel therapeutics targeting specific cell populations in wound heal,” *Regen. Med.*, vol. 13, pp. 491–495, 2018.

[30] M. G. Woodbury, “Effect of Electrical Stimulation on Chronic Leg Ulcer Size and Appearance,” *Phys. Ther.*, no. January, 2003.

[31] P. E. Houghton *et al.*, “Electrical Stimulation Therapy Increases Rate of Healing of Pressure Ulcers in Community-Dwelling People With Spinal Cord Injury,” *Arch. Phys. Med. Rehabil.*, vol. 91, no. 5, pp. 669–678, 2010.

[32] M. R. Asadi, G. Torkaman, M. Hedayati, and M. Mofid, “Role of sensory and motor intensity of electrical stimulation on fibroblastic growth factor-2 expression, inflammation, vascularization, and mechanical strength of full-thickness wounds,” *J. Rehabil. Res. Dev.*, vol. 50, no. 4, pp. 489–498, 2013.

[33] P. Anna, J. Taradaj, and C. Kucio, “PL,” no. March, 2012.

[34] K. C. Balakatounis and A. G. Angoules, “Balakatounis_2008_EM polje.pdf,” no. Lic, pp. 283–291, 2008.

[35] J. I. Hoare, A. M. Rajnicek, C. D. McCaig, R. N. Barker, and H. M. Wilson, “Electric fields are novel determinants of human macrophage functions,” *J. Leukoc. Biol.*, vol. 99, no. 6, pp. 1141–1151, 2016.

[36] M. Rouabhia, H. Park, S. Meng, H. Derbali, and Z. Zhang, “Electrical stimulation promotes wound healing by enhancing dermal fibroblast activity and promoting myofibroblast transdifferentiation.,” *PLoS One*, vol. 8, no. 8, 2013.

[37] C. W. Huang, J. Y. Cheng, M. H. Yen, and T. H. Young, “Electrotaxis of lung cancer cells in a multiple-electric-field chip,” *Biosens. Bioelectron.*, vol. 24, no. 12, pp. 3510–3516, 2009.

[38] C. A. Erickson and R. Nuccitelli, “Embryonic fibroblast motility and orientation can be influenced by physiological electric fields,” *J. Cell Biol.*, vol. 98, no. 1, pp. 296–307, 1984.

[39] N. Li Jeon, H. Baskaran, S. K. W. Dertinger, G. M. Whitesides, L. Van De Water, and M. Toner, “Neutrophil chemotaxis in linear and complex gradients of interleukin-8 formed in a microfabricated device,” *Nat. Biotechnol.*, vol. 20, no. 8, pp. 826–830, 2002.

[40] N. Özkucur, S. Perike, H. H. Epperlein, and R. H. W. Funk, “Endogenous ion dynamics in cell motility and tissue regeneration,” *J. Phys. Conf. Ser.*, vol. 329, no. 1, 2011.

[41] R. Lemaire *et al.*, “Effects of Physiological Electric Fields on Migration of Human Dermal,” vol. 130, no. 6, pp. 1514–1523, 2011.

[42] F. X. Hart and J. R. Palisano, “The Application of Electric Fields in Biology and Medicine,” *Intech*, vol. i, no. Electrical Field, p. 13, 2016.

[43] A. Schopf, C. Boehler, and M. Asplund, “Analytical methods to determine electrochemical factors in electrotaxis setups and their implications for experimental design,” *Bioelectrochemistry*, vol. 109, pp. 41–48, 2016.

[44] F. Lin *et al.*, “Lymphocyte Electrotaxis in vitro and in vivo,” *Cell*, vol. 181, no. 4, pp. 2465–2471, 2009.

[45] S. F. Cogan, “Neural stimulation and recording electrodes,” *Annu. Rev. Biomed. Eng.*, vol. 10, pp. 275–309, 2008.

[46] S. Ud-Din *et al.*, “Angiogenesis is induced and wound size is reduced by electrical stimulation in an acute wound healing model in human skin,” *PLoS One*, vol. 10, no. 4, pp. 1–22, 2015.

[47] S. Ud-Din and A. Bayat, “Electrical Stimulation and Cutaneous Wound Healing: A Review of Clinical Evidence,” *Healthcare*, vol. 2, no. 4, pp. 445–467, 2014.

[48] D. R. Merrill, M. Bikson, and J. G. R. Jefferys, “Electrical stimulation of excitable tissue: Design of efficacious and safe protocols,” *J. Neurosci. Methods*, vol. 141, no. 2, pp. 171–198, 2005.

[49] A. Jackson, C. T. Moritz, J. Mavoori, T. H. Lucas, and E. E. Fetz, “The neurochip BCI: Towards a neural prosthesis for upper limb function,” *IEEE Trans. Neural Syst. Rehabil. Eng.*, vol. 14, no. 2, pp. 187–190, 2006.

[50] Y. Li and D. J. Mogul, “Electrical control of epileptic seizures,” *J. Clin. Neurophysiol.*, vol. 24, no. 2, pp. 197–204, 2007.

[51] D. Benninger and M. Schüpbach, “Deep brain stimulation,” *Ther. Umschau*, vol. 75, no. 7, pp. 425–431, 2018.

[52] R. E. Friedrich, H. A. Scheuer, and A. Gröbe, “Neural Stimulation and Recording Electrodes,” *In Vivo (Brooklyn).*, vol. 26, no. 6, pp. 1103–1107, 2012.

[53] C. Boehler, F. Oberueber, T. Stieglitz, and M. Asplund, “Iridium Oxide (IrOx) serves as adhesion promoter for conducting polymers on neural microelectrodes,” *Int. IEEE/EMBS Conf. Neural Eng. NER*, vol. 2015-July, no. 0, pp. 410–413, 2015.

[54] Y. Zhao, B. Lui, L. Pan, and G. Yu, “3D nanostructured conductive polymer hydrogels for high-performance electrochemical devices,” *Pharmazie*, vol. 34, no. 3, pp. 164–166, 1979.

[55] R. Ravichandran, S. Sundarrajan, J. R. Venugopal, S. Mukherjee, and S. Ramakrishna, "Applications of conducting polymers and their issues in biomedical engineering," *J. R. Soc. Interface*, vol. 7, no. SUPPL. 5, 2010.

[56] R. Dungani, M. N. Islam, H. P. S. Abdul Khalil, Y. Davoudpour, and A. Rumidatul, "Hydrogels in sensing applications," *BioResources*, vol. 9, no. 1, pp. 455–471, 2014.

[57] J. L. Bredas and G. B. Street, "Polarons, Bipolarons, and Solitons in Conducting Polymers," *Acc. Chem. Res.*, vol. 18, no. 10, pp. 309–315, 1985.

[58] C. Kleber, "Development and Characterization of a Plasma-Needle for Biomedical Applications," 2019.

[59] L. Ghasemi-Mobarakeh *et al.*, "Application of conductive polymers, scaffolds and electrical stimulation for nerve tissue engineering," *J. Tissue Eng. Regen. Med.*, vol. 5, no. 4, pp. e17–e35, Apr. 2011.

[60] P. A. Calvo, J. Rodríguez, H. Grande, D. Mecerreyes, and J. A. Pomposo, "Chemical oxidative polymerization of pyrrole in the presence of m-hydroxybenzoic acid- and m-hydroxycinnamic acid-related compounds," *Synth. Met.*, vol. 126, no. 1, pp. 111–116, 2002.

[61] N. K. Guimard, N. Gomez, and C. E. Schmidt, "Conducting polymers in biomedical engineering," *Prog. Polym. Sci.*, vol. 32, no. 8–9, pp. 876–921, 2007.

[62] G. G. Wallace, M. Smyth, and H. Zhao, "Conducting electroactive polymer-based biosensors," *TrAC - Trends Anal. Chem.*, vol. 18, no. 4, pp. 245–251, 1999.

[63] M. Trojanowicz, "Application of Conducting Polymers in Chemical Analysis," *Microchim. Acta*, vol. 143, no. 2–3, pp. 75–91, 2003.

[64] B. D. Malhotra, A. Chaubey, and S. P. Singh, "Prospects of conducting polymers in biosensors," *Anal. Chim. Acta*, vol. 578, no. 1, pp. 59–74, 2006.

[65] A. Guiseppi-Elie, "Electroconductive hydrogels: Synthesis, characterization and biomedical applications," *Biomaterials*, vol. 31, no. 10, pp. 2701–2716, 2010.

[66] C. Kleber, M. Bruns, K. Lienkamp, J. Rühe, and M. Asplund, "An interpenetrating, microstructurable and covalently attached conducting polymer hydrogel for neural interfaces," *Acta Biomater.*, vol. 58, pp. 365–375, 2017.

[67] S. K. M. Ul-islam, M. Wajid, and U. Yeji, "Synthesis and characterization of a novel bacterial cellulose – composite for use in biomedical applications," *Cellulose*, vol. 22, no. 4, pp. 2141–2148, 2015.

[68] O. Prucker, T. Brandstetter, and J. Rühe, “Surface-attached hydrogel coatings via C,H-insertion crosslinking for biomedical and bioanalytical applications (Review),” *Biointerphases*, vol. 13, no. 1, p. 010801, 2018.

[69] R. A. Green, S. Baek, L. A. Poole-Warren, and P. J. Martens, “Conducting polymer-hydrogels for medical electrode applications,” *Sci. Technol. Adv. Mater.*, vol. 11, no. 1, 2010.

[70] E. T. Urbansky and M. R. Schock, “Understanding, Deriving, and Computing Buffer Capacity,” *J. Chem. Educ.*, vol. 77, no. 12, p. 1640, 2009.

[71] P. Spitzer, R. Eberhardt, I. Schmidt, and U. Sudmeier, “Improved traceability of pH measurements,” *Anal. Bioanal. Chem.*, vol. 356, no. 3–4, pp. 178–181, 2004.

[72] R. G. Bates, “The Modern Meaning of pH,” *C R C Crit. Rev. Anal. Chem.*, vol. 10, no. 3, pp. 247–278, 1981.

[73] F. G. K. Baucke *et al.*, “MEASUREMENT OF pH . DEFINITION , STANDARDS , AND PROCEDURES (IUPAC Recommendations 2002),” *Pure Appl. Chem.*, vol. 74, no. 11, pp. 2169–2200, 2002.

[74] P. Kurzweil, Metal oxides and ion-exchanging surfaces as pH sensors in liquids: State-of-the-art and outlook, vol. 9, no. 6. 2009.

[75] J. Black, “Measuring pH: Indicators, Paper, and Meters,” *Carolina Biol. Supply Co.*, pp. 1–2, 2017.

[76] T. F. Scientific, “pH (colorimetric) 984349 3,” pp. 1–2.

[77] S. F. Cogan, J. Ehrlich, and T. D. Plante, “The effect of electrode geometry on electrochemical properties measured in saline,” *2014 36th Annu. Int. Conf. IEEE Eng. Med. Biol. Soc. EMBC 2014*, pp. 6850–6853, 2014.

[78] H. Park, P. Takmakov, and H. Lee, “Electrochemical evaluations of fractal microelectrodes for energy efficient neurostimulation,” *Sci. Rep.*, vol. 8, no. 1, pp. 1–11, 2018.

[79] M. Dürr, “Development of a novel setup for live cell imaging during electrotaxis experiments utilizing rotating coherent scattering (ROCS) microscopy.”

[80] G. Fytas, M. Gianneli, R. Roskamp, and U. Jonas, “Dynamics of Swollen Gel layers Anchored to Solid Surfaces,” *Br. J. Psychiatry*, vol. 111, no. 479, pp. 1009–1010, 2007.

[81] R. Toomey, D. Freidank, and J. Rühe, “Swelling behavior of thin, surface-attached polymer networks,” *Macromolecules*, vol. 37, no. 3, pp. 882–887, 2004.

[82] J. Bobacka, A. Lewenstam, A. Ivaska, and A. Fin, "Electrochemical impedance spectroscopy of oxidized poly(3,4-ethylenedioxythiophene) film electrodes in aqueous solutions," vol. 489, pp. 17–27, 2000.

[83] L. Groenedaal, F. Jonas, D. Freitag, H. Pielartzik, and J. R. Reynolds, "Poly(3,4-ethylenedioxythiophene) and Its Derivatives: Past, Present, and Future," in *Advanced Materials*, Hoboken, NJ, USA: John Wiley & Sons, Inc., 2015, pp. 145–170.

[84] S. G. Im and K. K. Gleason, "Systematic control of the electrical conductivity of poly(3,4-ethylenedioxythiophene) via oxidative chemical vapor deposition," *Macromolecules*, vol. 40, no. 18, pp. 6552–6556, 2007.

[85] S. Gláb, A. Hulanicki, G. Edwall, F. Folke, I. Ingman, and W. F. Koch, "Metal-Metal Oxide and Metal Oxide Electrodes as pH Sensors," *Crit. Rev. Anal. Chem.*, vol. 21, no. 1, pp. 29–47, 1989.

[86] J. Leal, "Development of a thin-film pH sensor for," *Master Thesis*.

[87] T. Stieglitz, H. Beutel, and J. U. Meyer, "'Microflex' - A new assembling technique for interconnects," *J. Intell. Mater. Syst. Struct.*, vol. 11, no. 6, pp. 417–425, 2000.

[88] S. B. Rieger, J. Pfau, T. Stieglitz, M. Asplund, and J. S. Ordonez, "Concept and development of an electronic framework intended for electrode and surrounding environment characterization in vivo," *Sensors (Switzerland)*, vol. 17, no. 1, 2017.

[89] V. V. Abhyankar, M. Wu, C. Y. Koh, and A. V. Hatch, "A reversibly sealed, easy access, modular (SEAM) microfluidic architecture to establish in vitro tissue interfaces," *PLoS One*, vol. 11, no. 5, pp. 1–20, 2016.

[90] S. H. Lee, J. H. Jung, Y. M. Chae, J. K. F. Suh, and J. Y. Kang, "Fabrication and characterization of implantable and flexible nerve cuff electrodes with Pt, Ir and IrO x films deposited by RF sputtering," *J. Micromechanics Microengineering*, vol. 20, no. 3, 2010.

[91] C. Boehler and M. Asplund, "A detailed insight into drug delivery from PEDOT based on analytical methods: Effects and side effects," *J. Biomed. Mater. Res. - Part A*, vol. 103, no. 3, pp. 1200–1207, 2015.

[92] D. N. Heo *et al.*, "Multifunctional hydrogel coatings on the surface of neural cuff electrode for improving electrode-nerve tissue interfaces," *Acta Biomater.*, vol. 39, pp. 25–33, 2016.

[93] C. Kleber, K. Lienkamp, J. Rühe, and M. Asplund, "Electrochemically Controlled Drug Release from a Conducting Polymer Hydrogel (PDMAAp/PEDOT) for Local Therapy and Bioelectronics," *Adv. Healthc. Mater.*, vol. 8, no. 10, pp. 1–11, 2019.

[94] C. Kleber, M. Bruns, K. Lienkamp, J. Rühe, and M. Asplund, “An interpenetrating, microstructurable and covalently attached conducting polymer hydrogel for neural interfaces,” *Acta Biomater.*, vol. 58, pp. 365–375, 2017.

[95] M. Autolab B.V, “Autolab application note EC08. Basic overview of the working principle of a potentiostat/galvanostat (PGSTAT),” pp. 1–3, 2011.

[96] D. Street, “Sputtered Iridium Oxide,” no. April, pp. 1–2, 2008.

11 Annex

11.1 Electrodes fabrication

In the following sections, it will be mentioned the most important parameters to fabricate the electrodes.

Polyimide coating

I. **PI Selection:** 2.5 ml U-Varnish-S/ thickness = 5 µm.
II. **Dehydration bake:** hotplate at 125 °C for 5 min.
III. **Spin coating PI:** 2.5 ml U-Varnish-S/ 500 RPM (8 s) → 3500 RPM (30 s).
IV. **Soft bake:** hotplate at 120 °C for 2 min.
V. **PI bake:** oven at 450 °C for 3 h.

Resist coating and structuring

I. **AZ Selection:** AZ1518 / thickness = 1.8 µm.
II. **Dehydration bake:** hotplate at 125 °C for 5 min.
III. **LOR coating:** 1.5 ml LOR 5A / 800 RPM (5 s) → 2000 RPM (30 s)
IV. **Soft bake:** hotplate at 100 °C for 1 min.
V. **Resist coating PI:** 2 ml AZ1518 / 4000 RPM (30 s).
VI. **Soft bake:** hotplate at 100 °C for 50 s.
VII. **Exposure:** Proximity contact / Flat alignment mode / 2.8 s.
VIII. **Development:** run twice Program P in TMAH (AZ726 MIF, Microchemicals GmbH, Ulm, Germany).

Pt Sputtering

I. RF 300 W / 4 cycles: 1:15 min on – 10 min pause / thickness = 300 nm.

Lift-off

I. **DMSO** bath overnight or at least 12 h (TechniStripR Micro D350, Microchemicals GmbH, Ulm, Germany).

II. **DMSO** + **ultrasound** (50 % power) for 10 min.

III. **Isopropanol** + ultrasound (100 % power) for 5 min.

IV. QDR

V. Rinse-Dry

IrOx Sputtering

I. **Ir layer** / RF 100 W / 1:00 min / thickness = 100 nm.

II. **IrOx layer** / O_2 flow 15 sccm / 2 cycles: 4:10 min on – 10 min pause / thickness = 800 nm.

Resist coating and RIE

I. **AZ Selection:** AZ9260 / thickness = 24 µm.

II. **Resist coating:** 5 ml AZ9260 / 16000 RPM (30 s).

III. **Soft bake:** hotplate at 100 °C / on pins for 2 min / on the plate for 3 min

IV. **Rehydration:** 3 hours at 70 % relative humidity.

V. **Exposure:** Soft contact / Flat alignment mode / 3 cycles: 12 s – 30 s pause.

VI. **Development:** K400:H_2O (1:3) for 4 min / rinse with H_2O / dry.

VII. **RIE:** O_2 flow / 15 min at 200 W – 30 min at 100 W

11.2 Buffer preparation

The buffers prepared for the pH sensors calibration were divided into acidic and alkaline solutions The neutral solution used was 0.01 M PBS (P-3818, Sigma Aldrich Corp., St. Louis, Missouri, USA), which pH value is 7.4. The composition and respective pH of the prepared buffers for 500 mL of solution is listed in Table 8 .

Table 8: Composition of buffers solutions

Type of solution	**pH**	**Vol. of Solution 1**	**Vol. of Solution 2**	**Vol. of DI water**	**Measured pH**
Acidic	2	125 mL of 0.2 M KCl	32.5 mL of 0.2 M HCl	342.5 mL	1.80
	5.8	250 mL of 0.1 M KH_2PO_4	18 mL of 0.1 M NaOH	232 mL	5.75
Alkaline	9	477.5 mL of 0.1 M $Na2HPO_4$	22.5 mL of 0.1 M HCl	-	9.46
	12	250 mL of 0.05 M $Na2HPO_4$	134.5 mL 0.1M NaOH	115.5 mL	11.96

11.3 pH measurement Hardware

The layout of the PCB design for the pH readout used for the pH sensors calibration and pH measurements during DC stimulation is shown in Figure 51. The specifications for the PCB fabrication are listed in Table 9.

Table 9: PCB fabrication specifications

Dimension	**148.00 mm x 62.00 mm**
Trackwidth	≥ 100 µm
Minimum drills	≥ 0.2 mm
Material	FRA 1.55 mm, 35 µm Cu
Surface finish	Hot-Air-Leveling, Lead-free

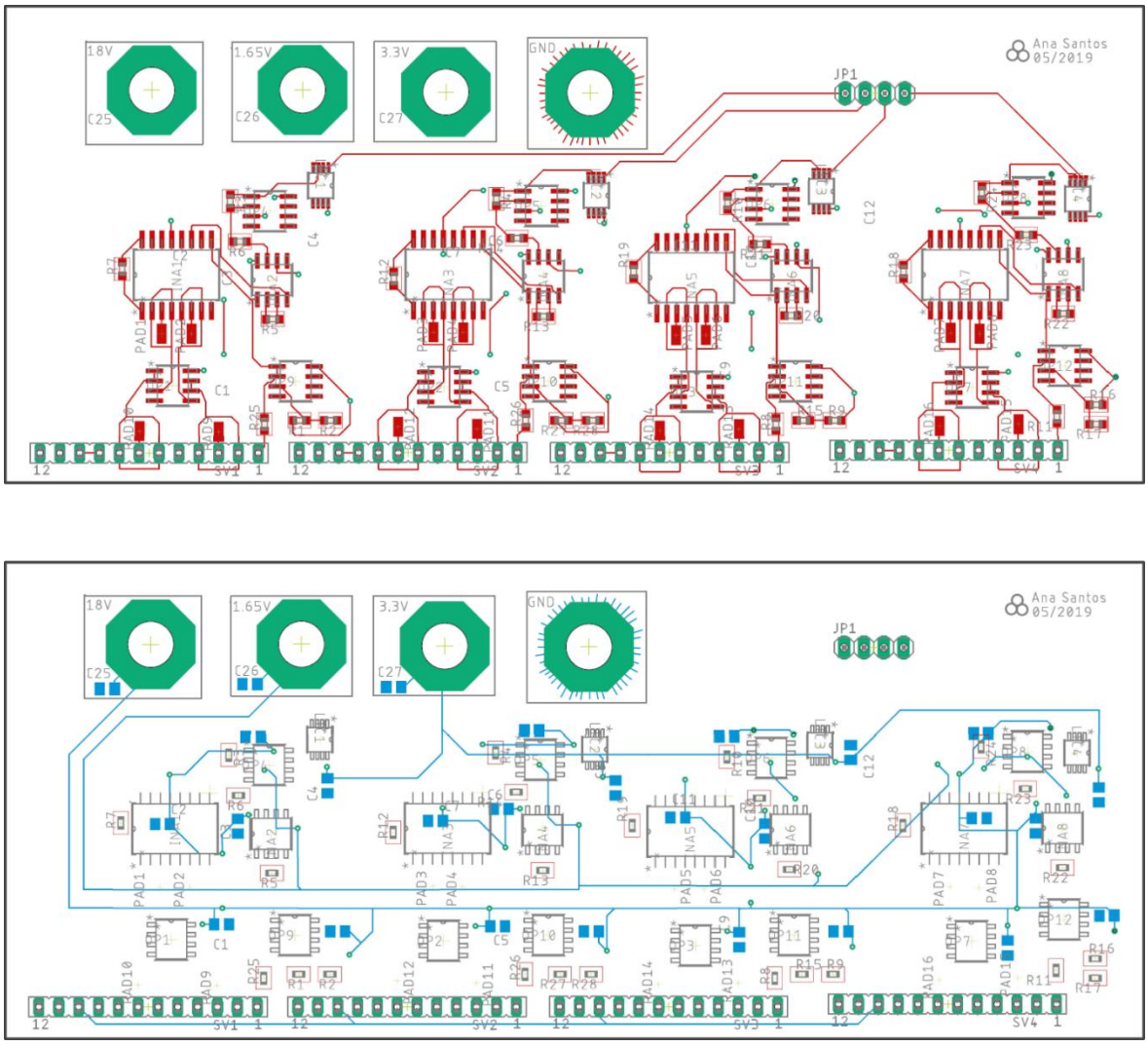

Figure 51: PCB design: top layer in red and bottom layer in blue.

12 Supplementary material

In this section, it is described how the cytotoxicity experiments were prepared and performed, as well as the results obtained.

12.1 Materials and Methods

The media used is present in Table 10. The cells used are immortalized Human epidermal Keratinocytes (iHEK) and primary human dermal Fibroblasts (hDF). The human epidermal Keratinocytes and Human dermal Fibroblasts have been received by the Department of Oral Biotechnology of the University Hospital of Freiburg. Both types of cells were isolated from skin biopsies of healthy patients with their permission and its approval by the ethical committee (Ethics *votum* number: EK-Freiburg; 411/08_121010, Medical Center, University Hospital of Freiburg) at the department of Oral Biotechnology at the University Hospital of Freiburg. Primary keratinocytes from epidermal tissue were established as described in Tomakidi et al., 1997. Primary human epidermal keratinocytes were immortalized according to the protocol published by Halbert et al. (1992), using amphotropic recombinant retroviruses. They were stored until usage in liquid nitrogen (Stickstofftank Asplund).

Table 10: Mediums used for the cytotoxicity tests

Dulbecco's modified Eagle medium (DMEM)	DMEM (Thermo Scientific), 10% FCS, 2 mM L-alanyl-L-glutamine (Thermo Scientific, Schwerte), 0.1 mg/ml kanamycin (Sigma Aldrich, Steinheim)
Keratinocyte growth medium (KGM_2)	KGM medium (Promocell, Heidelberg), supplements provided by the manufacturer, 0.1mg/ml kanamycin, 0.1 mg/ml neomycin (Sigma Aldrich, Steinheim)

12.1.1 Extracts preparation

Extracts have been carried out according to DIN ISO 10993-5. For all cell types and electrode samples, the respective serum-free medium has been used for extracts preparation (DMEM for fibroblasts and KGM_2 for keratinocytes). The extracts were incubated for 48 h in 37 °C and 5% CO_2 and were stored (max. 1 week) in -8 °C, light protected until usage.

12.1.2 Live/dead staining

The live/dead staining is used for rapid quantification of viable cells by differentially staining of live and dead cells with fluorescent dyes. In this assay, it is used the green fluorescent nucleic dye SYTO 16 (Sigma-Aldrich, Taufkirchen, Germany) for the labeling of living cells and Propidium Iodide (PI) (Sigma-Aldrich, Taufkirchen, Germany) for the staining of dead cells. The cell-permeant Syto 16 has a very low intrinsic fluorescence until binding to DNA or RNA, but the exact binding mode is yet unclear. Binding to nucleic acids enhances the fluorescence in a larger manner (>30-fold). The Excitation (max) and Emission (max) are: 488/518 nm (DNA), 494/525 nm (RNA) and can be used in double staining together with PI for detecting dead cells. PI is a membrane impermeant red fluorescent dye not able to traverse the intact membrane of viable cells. Cell death, regardless of the mechanisms of death like programmed (apoptosis) or induced cell death, is accompanied by plasma membrane permeability/leakage. PI is able to permeate the destroyed cell membrane and intercalates to double-stranded DNA, which fluorescence is then increased 20-30-fold. The excitation (max) and emission (max) are: 493/636 nm (DNA).

12.1.3 AlamarBlue assay

The alamarBlue Assay (Bio-Rad Laboratories GmbH, Munich,Germany) is a quantitative assay for cell viability and cell toxicity testing. This assay contains the non-toxic, weakly fluorescent, highly sensitive, cell-permeant dye resazurin, which serve as a RedOx reaction indicator. RedOx reactions occur in viable cells during cell metabolic processes (i.e., glycolysis) with $NADH/H^+$ or other enzymes (mitochondrial, cytosolic, microsomal) as reducing agent (Figure 52, a). With the addition of resazurin in the growth medium, this blue colored indicator permeates the cell membrane and is reduced in the cytosol to the pink colored and fluorescent resorufin (Figure 52, b). Resorufin is able to diffuse out of the cells and concentrates in the growth medium. The medium supernatant can be quantitatively evaluated by measuring the relative fluorescent units (RFU) using a *plate reader* with an excitation/emission spectrum of $560_{Ex}/590_{Em}$.

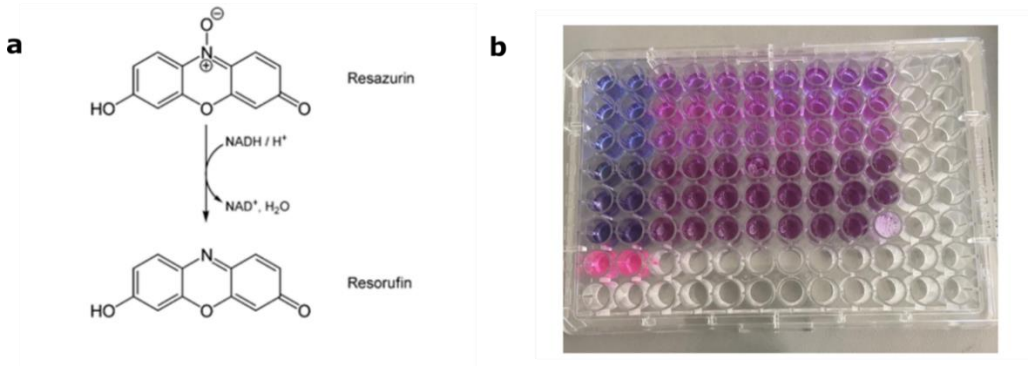

Figure 52: AlamarBlue test. a) RedOx reaction; b) AlamarBlue assay.

12.1.4 Phase Contrast Microscopy

Cell toxicity comes along with cell morphological changes. Atypical cell morphology represents significant cell reactivity towards useful compounds. Therefore a cell morphological verification is helpful as an additional examination of cell cytotoxic effects. These morphological changes will not automatically display a cytotoxic effect (except apoptotic vesicles inside of the cellular body or observation of dead cells), but significant cell reactivity (i.e., loss of focal adhesion contacts) may play an important role in following experiments and should always be performed in combination with other cell toxicity tests. Phase-contrast images of 3 biological replicates of immortalized human epidermal keratinocytes and human dermal fibroblasts were examined before performing AlamarBlue assay and live/dead staining incubated with different extracts (see chapter 12.3) for 3 different time points (24 h, 48 h, and 72 h). For each time point and cell type images of negative control samples (cells were grown in specific growth medium) has been recorded as well. Phase Contrast Microscopy was performed with the BZ-II Analyzer (Keyence) and a 20x objective at the Department of Oral Biotechnology of the university hospital Freiburg (representative Images for both cell types/conditions and time points are shown in Supplementary material, 12.3. Results). The scale bar (white) represents 100µm.

12.2 Experimental

Two different types of cells were tested for the cytotoxicity of the deposited conductive polymers on the electrodes: immortalized Human epidermal Keratinocytes and primary human dermal Fibroblasts. The tests performed are described in Table 11. After the Direct Seeding, it was performed live/dead

staining; following the Extracts, the cell morphology was verified through phase contrast, then it was performed AlamarBlue assay and finally the live/dead staining.

Table 11: Parameters for the Directing Seeding and Extracts

Parameters	**Direct Seeding**	**Extracts (48h incubated)**
Cell types	Keratinocytes	Keratinocytes and Fibroblasts
Timepoints of evaluation	24 and 48 h	24, 48 and 72 h
Eluates	PEDOT, Hydrogel and PEDOT + Hydrogel	Hydrogel and PEDOT + Hydrogel

12.2.1 Live/dead staining

The live/dead staining was performed once by directly seeded cells on the samples for 2-time points (24 h and 48 h) and by incubation of extracts (see extracts fabrication chapter 12.1.1) for 3 different time points (24 h, 48 h, and 72 h). All experiments have been performed in 3 independent biological replicates. Direct seeding has been performed with IHEK (immortalized human epidermal keratinocytes) and extracts test for DFs (human dermal fibroblast) and IHEKs.

For the direct seeding of the samples, the electrodes (PEDOT, hydrogel, and hydrogel + PEDOT) were deposited in 6 well plates and were seeded with 150,000 cells in 2 ml of growth medium (KGM_2 for Keratinocytes, see table 9) per well. After the specific time points (24 h and 48 h of incubation in 37 °C and 5 % CO_2) the medium has been removed and filled with 2 ml of growth medium containing Syto16 (1 µM) and PI (500 nM) and incubated for 30 minutes (dark, 37 °C and 5 % CO_2) before microscopy. For each sample, time point and biological replicate 2x 100 cells have been counted. The amount of dead/ live cells has been plotted in a bar graph (section 12.3), giving the percentage of living cells and the standard deviation.

For the extracts incubated cells, IHEK and DF have been seeded in 96- well plates. For each time point (24 h, 48 h, and 72 h) and extracts, samples 7.000 IHEK and 10.000 DF has been seeded in 200 µl growth medium per well in duplicates. The cells have been put back in the incubator for 24 h to let them adhere. After 24 h the medium was removed and refilled with 200 µl of the respective extract. Extracts change has been done after 48 h. For each time point, negative controls (cells cultivated in growth medium) has been prepared in duplicates.

12.2.2 AlamarBlue assay

The AlamarBlue Assay has been performed with IHEK and DF incubated with 2 different types of extracts (Hydrogel, PEDOT+Hydrogel) for 3 different time points (24 h, 48 h, and 72 h) in duplicates in 3 independent biological replicates. For each time point, a freshly prepared 10 % AlamarBlue solution in the respective extracts (also used for the blank reduction later) has been filled in the wells. The cells were incubated for 4 hours with the AlamarBlue reagent at 37 °C and 5°C CO_2 in the dark before the supernatant was collected and stored light protected in 8 °C until all timepoints have been reached (max 3 days). As a positive control (which serves as a 100% reduction of resazurin), a 10 % AlamarBlue solution in growth medium has been autoclaved and stored in the fridge until plate reading. As a "dead cell" control, for each time point and cell type AlamarBlue staining has been performed after incubating the cells in 4 % Triton-x solution for 10 minutes. After collecting all AlamarBlue stained supernatants for each time point, the relative fluorescent units (RFU) has been measured in duplicates with an excitation/emission spectrum of $560_{Ex}/590_{Em.}$ The data has been normalized to the respective negative control (NC) set as 100 % (cells grown in serum-free medium), for each time point. The normalized cell viability has been plotted in a bar graph with the standard deviation.

12.3 Results

Electrodes coated with PEDOT, Hydrogel, and Hydrogel+PEDOT were tested for cytotoxicity. The cell vitality decreases with the toxicity; for a vitality percentage under 70 %, there is toxicity. The direct seeding test with live/dead staining using keratinocytes did not show toxicity for any of the electrodes coatings (Figure 53).

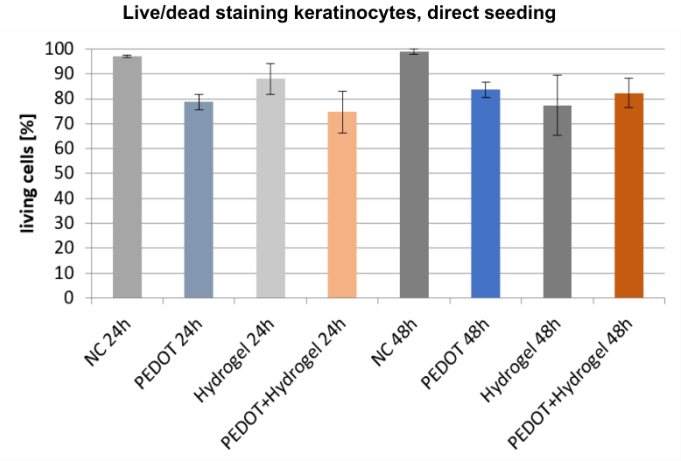

Figure 53: Cytotoxicity test using keratinocytes - direct seeding.

In the test using keratinocytes by incubation of extracts, it is possible to see slight toxicity for the Hydrogel + PEDOT electrodes after 24 h, which was overcome after 48 h. The electrodes coated only with Hydrogel did not show any toxicity for all time points (Figure 54).

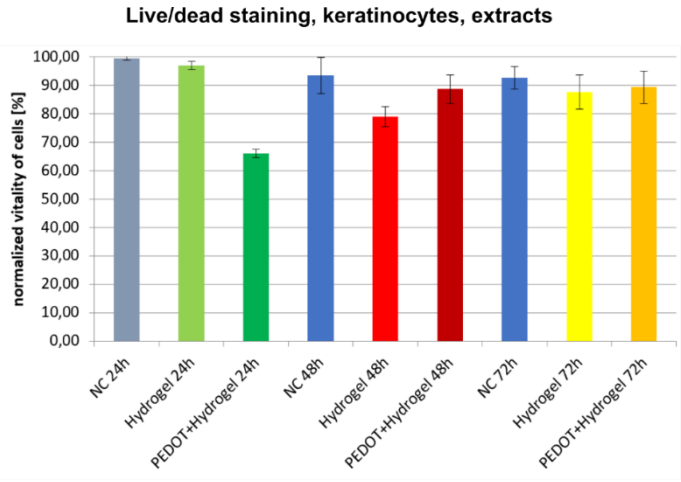

Figure 54: Cytotoxicity test using keratinocytes - extracts.

The live/dead staining with incubating extracts using the fibroblasts cells did not show any toxicity at all time points for the Hydrogel + PEDOT electrodes; however, for the Hydrogel electrodes, after 72 h there was slight cell reactivity (Figure 55).

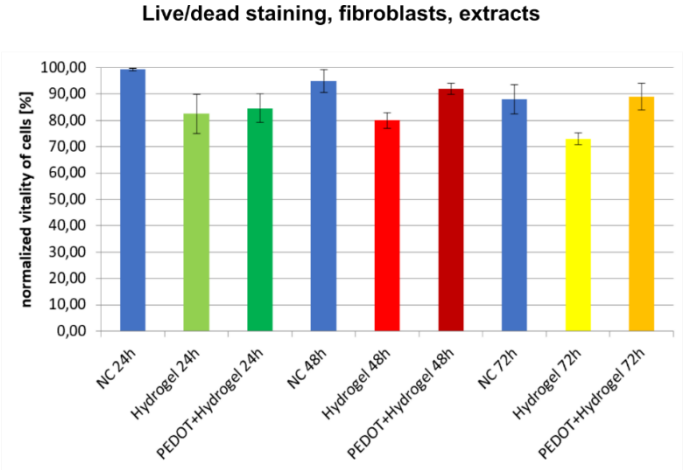

Figure 55: Cytotoxicity test using fibroblasts - extracts.

The tests performed using AlamarBlue showed no toxicity either for the keratinocytes nor for the fibroblasts. Using the keratinocytes is visible, an increase of relative Fluorescence units for the Hydrogel + PEDOT electrodes after 24 h and 48 h (Figure 56). With the fibroblasts, it is visible a decrease in the relative Fluorescence with the hydrogel electrodes after 24 h (Figure 57).

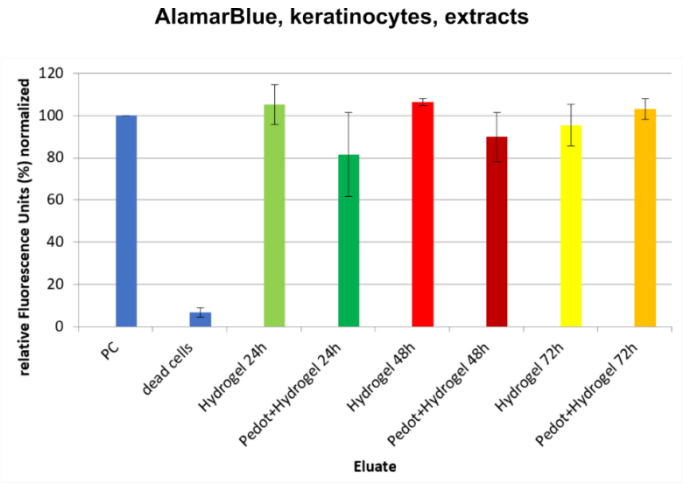

Figure 56: Cytotoxicity test using keratinocytes - extracts with AlamarBlue.

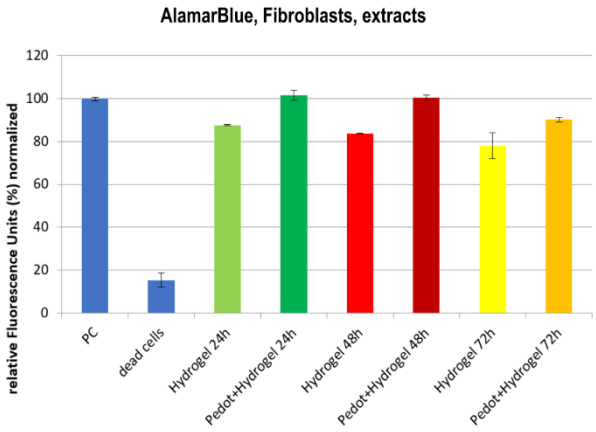

Figure 57: Cytotoxicity test using fibroblasts - extracts with AlamarBlue.

12.3.1 Phase-contrast result

The morphology of the cells did not change with the Hydrogel and Hydrogel + PEDOT electrodes, which demonstrated some cell reactivity. The morphology of the keratinocytes and fibroblasts was verified after 24, 48, and 72 h (Figure 58 and 59).

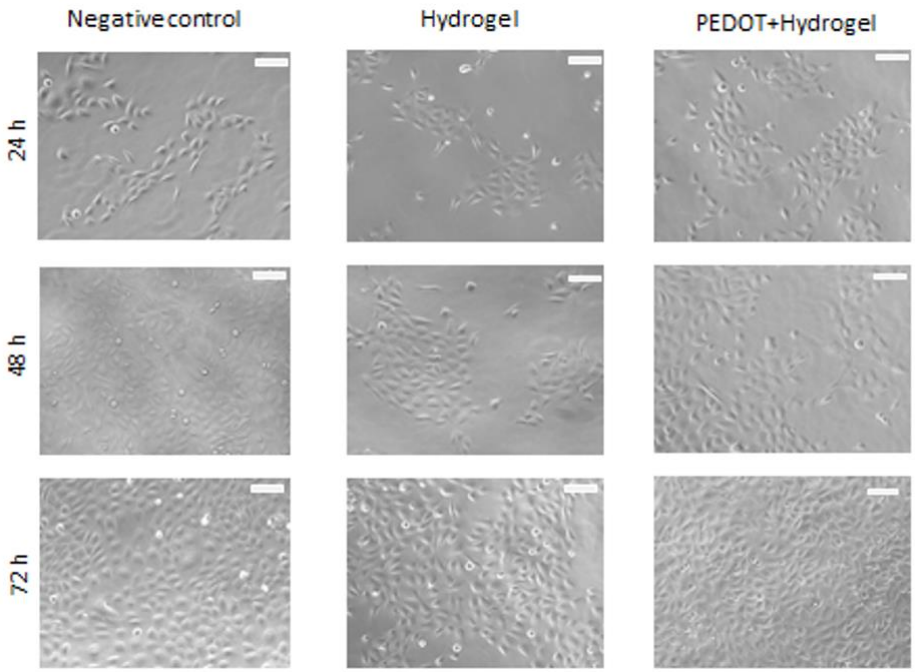

Figure 58: Phase contrast result of keratinocytes.

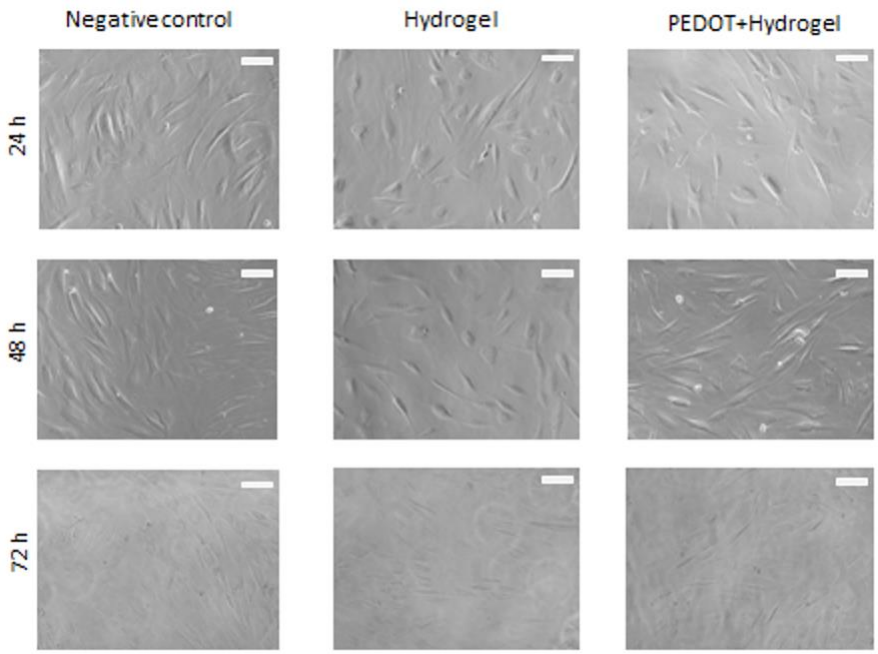

Figure 59: Phase contrast results with fibroblasts.